Towards a Reduced-Scaling Method for Calculating Coupled Cluster Response Properties

Ashutosh Kumar

Dissertation submitted to the Faculty of the

Virginia Polytechnic Institute and State University

in partial fulfillment of the requirements for the degree of

Doctor of Philosophy

in

Chemistry

T. Daniel Crawford, Chair

Eduard Valeyev

Diego Troya

Alan Esker

May 9, 2018

Blacksburg, Virginia

Keywords: Coupled Cluster, Reduced-Scaling, Response Properties

Towards a Reduced-Scaling Method For Calculating Coupled Cluster Response Properties

Ashutosh Kumar

(ABSTRACT)

One of the central problems limiting the application of accurate *ab initio* methods to large molecular systems is their high computational costs, i.e., their computing and storage requirements exhibit polynomial scaling with the size of the system. For example, the coupled cluster singles and doubles method with the perturbative inclusion of triples: the CCSD(T) model, which is considered as the "gold standard" of quantum chemistry scales as $\mathcal{O}(N^7)$ in its canonical formulation, where N is a measure of the system size. However, the steep scaling associated with these methods is unphysical since the property of dynamic electron correlation or dispersion (for insulators) is local in nature and decay as R^{-6} power of distance. Different reduced-scaling techniques which attempt to exploit this inherent sparsity in the wavefunction have been used in conjunction with the coupled cluster theory to calculate

ground-state properties of molecular systems with hundreds of heavy atoms in reasonable computational time. However, efforts towards extension of these methods for describing response properties which are related to the derivative of the wavefunction with respect to external electric or/and magnetic fields, like polarizabilities, optical rotations, etc., have been fairly limited and conventional reduced-scaling algorithms have been shown to yield large and often erratic deviations from the full canonical results for these properties. In this work, we identify the reasons behind the unsatisfactory performance of the pair natural orbital (PNO) based reduced-scaling approach for calculating linear response properties at the coupled cluster level of theory and propose novel modifications, which we refer to as PNO++, (A. Kumar and T. D. Crawford, 2018, *manuscript in preparation*) that can provide the necessary accuracy at significantly lower computational costs. The motivation behind the PNO++ approach comes from our works on the (frozen) virtual natural orbitals (FVNO), which can be seen as a precursor to the concept of PNOs (A. Kumar and T. D. Crawford, *J. Phys. Chem. A*, 2017, **121(3)**, pp 708-716) and the improved FVNO++ method (A. Kumar and T. D. Crawford, 2018, *manuscript in preparation*). The essence of these modified schemes (FVNO++ and PNO++) lie in finding suitable field perturbed one electron densities to construct "perturbation aware" virtual spaces which, by construction, are much more compact for calculating response properties, making them ideal for applications to large molecular systems.

This work was supported by a grant (CHE-1465149) from the U.S. National Science Foundation. Advanced Research Computing Center at Virginia Tech provided the necessary computational resources and technical support for all the calculations reported here.

Contents

List of Figures

List of Tables

Chapter 1

Introduction

1.1 Chirality

Lord Kelvin was the first person to use the word 'chiral' in his lecture at Oxford University in 1894: "I call any geometrical figure, or group of points, 'chiral', and say that it has chirality if its image in a plane mirror, ideally realized, cannot be brought to coincide with itself"[37]. There are different ways in which a molecule could be chiral. The most common example being the presence of a chiral center like a carbon or nitrogen atom with four different substituents. Axial chirality, usually possessed by molecules with cumulated double bonds like allenes and chirality planes found in compounds like paracyclophanes are some other popular examples.

A chiral molecule and its mirror image are known as enantiomers. Although the enantiomers

have idential physical properties like boiling and melting points, their interactions with a chiral environment can be quite different. For example, while the (R) enantiomer of the compound limonene smells like lemons and oranges, the (S) enantiomer on the other hand smells like turpentine. Thus, the interaction of the (S) enantiomer with the chiral molecules constituting the olfactory receptors responsible for the sensation of smell is totally different from its fellow enantiomer. The enantiomers also interact differently with the left- and right-hand circularly polarized (LCP and RCP) light in processes of absorption, refraction, etc. A chiral molecule posesses the properties of circular dichroism (CD) and circular birefringence, i.e. it has different absorption coefficents and refractive indices for the LCP and RCP light respectively. As a result of circular birefringence, the plane of polarization of a plane-polarized light in a chiral medium gets rotated/shifted by an amount known as the optical rotation of the medium. An enantiomeric pair of chiral molecules has equal magnitudes of optical rotation but in opposite directions.

Since almost every part of the human body is composed of chiral molecules, its unsurprising that more than 60% of the pharmaceutical drugs are chiral as well. One of the most important aspect of the drug-design research is to be able to define the absolute configuration (AC) of these drug molecules in order to study their behaviour in biological systems as many biological activities are only associated with one specific AC. A very tragic example in this regard is that of the drug thalidomide, which was originally prescribed to pregnant women in Europe in 1950s to cure morning sickness but resulted in birth-defects in thousands of infants. It was found through a study done on rodents that the (R) enantiomer of thalidomide

is indeed a sedative but the (S) enantiomer is a teratogen[13]. Furthemore, these enantiomers were found to rapidly interconvert in vivo in humans because of which separating these two forms before use doesn't help at all.

The first step in experimental determination of AC either involves the separation of a racemic mixture (equal concentrations of both the enantiomers) into individual enantiomers using chiral resolution methods like chiral column chromatography or a selective synthesis of a given enantiomer using the process of asymmetric synthesis. X-ray crystallography would then be the most popular procedure to determine AC directly, provided one can crystallize the molecule first, which usually requires the presence of heavy atom(s). Alternatively, one can measure the distinct responses of the enantiomers in absorption using chiroptical spectroscopic techniques like electronic and vibrational CD (ECD and VCD) or can measure the optical rotation of the chiral compounds in both liquid and gas phase using polarimetry and cavity ring down spectrometry techniques[] respectively. These measurement are usually followed by a comparison against some suitable reference chiral substrate. In this regard, accurate *ab initio* methods can help validate these experimental measurements. Furthermore, designing an asymmteric synthesis might not be straightforward for many chiral systems, especially for the ones with large number of stereocenters. In such cases, theory can even take the lead and predict the corresponding AC. In other words, theoretical calculations of these chiroptical properties could serve as a very useful computational tool for modern organic chemists. In particular, accurate optical rotation calculations are highly desired as the experimental techniques for measuring this property are fairly stable and robust in both

gas and liquid phases.

1.2 *Ab Initio* Optical Rotation Calculations

Rosenfeld developed a quantum mechanical recipe for calculating optical rotations in the year 1929[69]. He showed that in the presence of an external electromagnetic field, the induced dipole moment in a molecule can be written as:

$$\langle \vec{\mu} \rangle = \boldsymbol{\alpha} \vec{E} + \frac{1}{\omega} \mathbf{G}' \frac{\partial \vec{B}}{\partial t} \tag{1.1}$$

where $\vec{E}$ and $\vec{B}$ are the time dependent electric and magnetic field vectors respectively, ω is the frequency of the field, α is the electric dipole polarizability tensor and the $\mathbf{G}'$ tensor, also known as the Rosenfeld tensor is associated with the property of optical rotation. Invoking the time-dependent Schrödinger's equation in conjunction with perturbation theory, expanding the expectation value of the electric dipole operator in orders of perturbation and identifying the term linear in $\vec{E}$ and $\frac{\partial \vec{B}}{\partial t}$, for exact states, the $\boldsymbol{\alpha}$ and $\mathbf{G}'$ tensors look like,

$$\begin{aligned} \boldsymbol{\alpha}(\omega) &= -\frac{2}{\hbar} \sum_{n \neq 0} \frac{\omega_{no} \langle \psi_o | \vec{\mu} | \psi_n \rangle \langle \psi_n | \vec{\mu} | \psi_o \rangle}{{\omega_{no}}^2 - \omega^2} \\ \mathbf{G}'(\omega) &= -\frac{2}{\hbar} \mathrm{Im} \sum_{n \neq 0} \frac{\omega \langle \psi_o | \vec{\mu} | \psi_n \rangle \langle \psi_n | \vec{m} | \psi_o \rangle}{{\omega_{no}}^2 - \omega^2}. \end{aligned} \tag{1.2}$$

Here, $\vec{\mu}$ and $\vec{m}$ are electric and magnetic dipole operators, $\vec{\mu} = \sum_i q_i \vec{r_i}$ and $\vec{m} = \sum_i \frac{q_i}{2m_i} \vec{r_i} \times \vec{p_i}$, ω is the frequency of light, ω_{no} is the excitation energy of the state ψ_n. Im means the imag-

inary part of the equation and the summation runs over all the excited states ψ_n. Specific rotation, $[\alpha]_\omega$ is related to the trace of the Rosenfeld tensor normalized by pathlength and concentration and is usually reported in the units of deg $dm^{-1}(g/mL)^{-1}$,[13]

$$[\alpha]_\omega = \frac{(72.0 \times 10^6)\hbar^2 N_A\, \omega}{c^2 {m_e}^2 M} \times \left[\frac{1}{3} Tr(\mathbf{G}')\right] \tag{1.3}$$

Here, $\mathbf{G}'$ and ω are in atomic units, c is the speed of light (m/s), m_e is the mass of electron (kg), M is the molecular mass (amu) and N_A is Avogadro's number. Calculating the $\mathbf{G}'$ tensor using equation (1.2) requires explicit calculations of a large number of excited states which is of course computationally prohibitive. A more practical approach is to invoke the response formalism [39, 40], which casts these tensors as response functions,

$$\begin{aligned} \boldsymbol{\alpha}(\omega) &= -\langle\langle \vec{\mu}; \vec{\mu} \rangle\rangle \\ \mathbf{G}'(\omega) &= \mathrm{Im}\langle\langle \vec{\mu}; \vec{m} \rangle\rangle. \end{aligned} \tag{1.4}$$

The response theory focuses on the perturbation of the ground state wavefunction in the presence of an external field, avoiding explicit calculations of excited states. Polavarapu was the first to use this theory to calculate *ab initio* specific rotations using the time dependent Hartree Fock (TDHF) method [64]. The signs of the calculated values matched with that of the experiment for most of his structures, while their magnitudes differed generally by a factor of two. Inspired by Polavarapu's work, Cheeseman et al. [10, 86] included correlation effects in these calculations by using TD-DFT theory. Using large basis sets with diffuse functions like aug-cc-pVDZ and aug-cc-pVTZ,[20, 38, 92] they were able to match

the experimental values very closely, with a deviation of 20-25 degrees for a set of 28 chiral molecules. Ruud *et al.* extended the calculations to the coupled cluster (CC) level using coupled cluster response theory developed by Koch and Jørgensen[40], and obtained very promising results[72]. Unsurprisingly, these simulations have been used to determine the AC of a large number of chiral molecules over the years[42]. However, for a truly robust and reliable description of these response properties, one needs to take into account, a number of challenges associated with such simulations.

1.2.1 Challenges

One of the major challenges faced by the CCLR theory is that of gauge and origin invariance. The origin dependence while using length-gauge representation is a consequence of the non-variational nature of the coupled cluster wavefunction. Unlike HF and DFT methods, properties such as optical rotation computed via CCLR are not origin independent even at the complete basis set limit, and the dependence cannot be resolved using GIAOs.6 The modified velocity gauge formalism for the electric dipole operator has been developed to help address this issue. The velocity-gauge formalism, p, L , allows for the trace of the property tensor to be origin invariant. Here p and L are the electronic momentum and angular momentum operators, respectively, and , represents the response function evaluated at frequency . However, without a complete basis set, using the velocity gauge formalism results in unphysical behavior at zero frequency. To achieve the appropriate behavior, the value for the velocity gauge representation at the static limit (at zero frequency) is subtracted from

the original expression, as shown in Equation 1.1. 13 p, L p, L p, L 0 (1.1) Alternatively, the underlying response theory can be reformulated to incorporate orbital rotation parameters explicitly to achieve origin invariance.14,15

Since, most of the optical rotation measurements are carried out in liquid phase or solutions, response theory needs to be combined with accurate solvation models in order to match these experimental measurements. While a quantum mechanical description of both the solute and solvent molecules would be ideal, however, for the sake of computational practicality, most solvation models try to reduce the degrees of freedom of the solvent molecules without compromising the quality of description of the solvent-solute and the solvent-solvent interactions.

In this regard, molecular mechanics (MM) based models, broadly known as QM/MM methods, usually represent the solvent in the form of a classical potential by replacing them with point charges, polarizabilities, etc.,[] which polarizes the charge distribution of the solute resuting in a modification of the solute's potential which again back-polarizes the charge distribution of the solvent and so on. Thus, the final one-electron solvent potential is obtained in a self-consistent procedure and is added to the solute's Hamiltonian which is then followed by response calculations. The fluctuating charge model (FQ)[], the drude oscillator model[] and effective fragmentation potential (EFP)[] are a few examples.

Quantum continuum solvation models on the other hand place the solute in a cavity surrounded by a continuous dielectric medium representing the solvent. A majority of these continuum models use the concept of apparent surface charges[], where polarization charges

are introduced on the surface of the cavity, to capture the response of the medium to the charge distribution of the solute which is again, solved in a self-consistent manner as described above. The polarizable continuum model (PCM) [] and conductor-like screening model (COSMO) [] are some popular examples.

One of the earliest works employing a solvation model for studying specific rotations is that of Mennucci and co-workers in 2002[52], where they used DFT and PCM for calculating specific rotations of a set of seven chiral compounds in the presence of seven different solvents. While they obtained promising results for cyclohexane, acetone, methanol and acetonitrile, the model performed rather poorly for carbon tetrachloride, benzene, and chloroform due to the failure of the PCM in capturing the dominant nonelectrostatic solute-solvent interactions in the latter. A few years later, Pecul *et al.* [] used the same model (DFT-PCM) to study the effect of solvent on the electronic circular dichroism spectra and obtained promising results for valence-only transitions. However, this approach failed to describe the Rydberg transitions and specific solute-solvent interactions like hydrogen bonding accurately.

A direct way of accounting for the dynamic solvent effects is to use an explicit *ab initio* solvation model where both solute and solvent are treated quantum mechanically and final specific rotations are obtained by averaging their values over a series of configurations usually generated through molecular dynamics (MD) simulations. Beratan and co-workers used this model with DFT to calculate specific rotations of methyloxirane in water[] and benzene[] and were able to match the experimental values qualitatively. Barone *et al.*[] were also able to reproduce the experimental optical rotatory curve of methyloxirane (qualitatively) in wa-

ter by using a DFT/FQ/PCM approach. However, it remains to be seen if these models perform equally well in other solvents and with more accurate theories like coupled cluster as DFT has been shown to agree with gas-phase experimental data of methyloxirane only fortuitously[].

Kongsted and co-workers were the first to use a solvation model within the context of coupled cluster response theory, where they placed the solute in a sperical cavity surrounded by a dielectric medium. However, this approach could not match experimental measurements even qualitatively and gave a wrong sign of the specific rotation for (*S*)-methyloxirane in cyclohexane at 355 nm, even after incorporating accurate electron correlation theories[]. Similar behavior was observed with PCM as well, as demonstrated by Caricato[].

Another solvation model that deserves a mention here is the frozen density embedding scheme, introduced by Wesolowski and Warshel[]. In this model, *ab initio* electronic densities (or potentials) describing the environment (or solvent) can be obtained (or decoupled) from a DFT calculation on the full system. The potential can then be added to the Hamiltonian of the solute, followed by either a DFT (DFT-in-DFT) or a wavefunction (WFT-in-DFT) calculation[]. Neugebauer was the first to use the DFT-in-DFT FDE model to study the response properties of solvated molecular clusters[]. Crawford and co-workers[] applied the more accurate (but more expensive) WFT-in-DFT FDE model with coupled cluster theory to study chiroptical properties of several "micro-solvated" structures of (*P*)-dimethylallene in water. However, the FDE potentials resulted in very small perturbations in the solute's electronic distribution compared to an explicit calculation. Furthermore, it failed to repro-

duce the correct sign of the specific rotations of some of the structures. The reason behind the errors was attributed to the failure of the FDE model in capturing the response of the solvent to external field, which can have significant contributions for these properties.

Other challenges: Basis set, scaling of CC calculations, Conformational averaging, Vibrational corrections, temperature effects, etc.

1.2.1.1 Current Work

The only robust way of accounting for solvent effects seems to be including the solvent molecules explicitly in the QM calculations. Furthermore, CC theory because it is more reliable, accurate and systematicaly improvable compared to DFT. An obvious way to make these compuations practical is to seek the help of CC reduced-scaling techniques like the pair natural orbitals (PNO) approach[57, 58] which has been really successful in describing energetics of large molecular systems. However, work towards the extension of these methods to calculate chiroptical properties has been fairly limited[25, 28, 43, 51, 70, 71]. McAlexander and Crawford in their recent work[50] demonstrated that the regular PNO approach while calculating CC response properties suffers from slow convergence towards the full canonical result.

The main focus of this work is identifying the reasons behind the sub-optimal peformance of such approaches for optical rotations. Subsequently, we propose novel modifications which can improve the performance of these schemes significantly. The necessary equations required to calculate dynamic polarizabilities and specific rotations within the CC linear response

formalism are derived in Chapter 2. Chapter 3 investigates the performance of the natural orbitals (FVNO scheme) for CC dynamic polarizabilites. A new scheme called FVNO++ is developed in Chapter 4 which reduces the errors associated with the regular FVNO scheme significantly for both polarizabilities and rotations. Chapter 5 extends the FVNO++ (a reduced-prefactor) approach to the reduced-scaling domain by implementing what we call as the PNO++ method. Finally, concluding remarks are given in Chapter 6.

Chapter 2

Theoretical Background

This chapter focuses on covering the necessary theoretical background for deriving the coupled cluster (CC) response functions. As a prelude to the CC response theory, the formalism for obtaining ground state CC energies is discussed after a brief description of Hartree-Fock and Configuration Interaction models. The next section derives the simplified gradient expressions of the CC energy and subsequently parametrizes the left hand CC wavefunction.

2.1 Hartree-Fock Theory

Central to the field of quantum mechanics is the equation proposed by Erwin Schrödinger in 1926 or the Schrödinger's equation [75]. One of the biggest factors contributing to the rich diversity of quantum chemical theories is the fact that Schrödinger's equation (SE) is exactly solvable for only one electron systems like hydrogen atom. As such, numerous approxima-

tions have been proposed over the years to solve this equation for many electron systems. The Hartree-Fock (HF) theory[87] is one of the simplest approaches in this regard under the Born-Oppenheimer approximation[8]. This model attempts to transform the many body problem of SE into a one body problem where each electron only interacts with a mean field created by the other electrons. For an N-electron system, the HF wavefunction is a Slater determinant (obeys Pauli's antisymmetry principle naturally) composed of N spin orbitals, i.e. the one electron solutions of the HF equation. Following is a brief outline of the HF procedure: A Lagrangian is constructed with the HF energy (the expectation value of the Slater determinant) coupled with the constraint of the spin orbitals always remaining orthonormal to each other. The Lagrangian, thus, can be seen as a functional of the spin orbitals. In the next step, the variational principle is employed to set the first order change in the Lagrangian with respect to spin orbitals to zero. Finally, one obtains a non-linear eigenvalue equation where the spin orbitals are the eigenfunctions of the Fock operator which itself depends on the spin orbitals themselves. Thus, the equation is solved in a self-consistent manner usually in conjunction with the linear combination of atomic orbital (LCAO) approach, where the spin orbitals are expressed as a linear combination of basis functions and the coefficients are determined from the solving a generalized eigenvalue equation. The eigenvectors with the lowest N eigenvalues are the occupied orbitals, usually denoted by symbols $i, j, k, l, ...$ If a basis set of size K is employed, the remaining $K - N$ orbitals are termed as unoccupied or virtual orbitals usually denoted by symbols $a, b, c, d, ...$

Even with this mean field approach, one can extract almost 95-98% of the total electronic energy. The remaining energy, also known as the correlation energy, however, is very essential if one wants to attain "chemical accuracy", ex. 1kcal/mol for interaction energies. In spite of this, the simple yet robust structure of the HF procedure makes it one of the most popular reference wavefunctions for more complicated and accurate theoretical models.

2.2 Configuration Interaction Method

Configuration interaction (CI) method[82] attempts to solve the time independent Schrödinger's (TISE) by recasting it into a matrix eigenvalue problem,

$$HC = EC \tag{2.1}$$

where H is the matrix representation of the Hamiltonian, C is the coefficient matrix whose columns are the eigenvectors of the Hamiltonian and E is the diagonal matrix containing the eigenvalues or electronic energies (The lowest energy corresponds to the ground state wavefunction). If the vector space used to represent the Hamiltonian is complete, the CI approach, then popularly known as the Full CI method gives exact wavefunctions and electronic energies. Specifically, this model uses a vector space composed of substituted or excited Slater determinants which can form a complete space in the limit of an infinite one electron basis. Furthermore, this vector space also has the desired properties of antisymmetry and orthogonality. Indeed the Full CI wavefunction is a linear combination of all possible Slater determinants for a given basis set,

$$|\Psi\rangle = c_o|0\rangle + \sum_{ia} c_i^a|\Psi_i^a\rangle + \sum_{i>j,a>b} c_{ij}^{ab}|\Psi_{ij}^{ab}\rangle + \sum_{i>j>k,a>b>c} c_{ijk}^{abc}|\Psi_{ijk}^{abc}\rangle + ... \tag{2.2}$$

where $|0\rangle$ is the reference wavefunction (usuallly HF), $|\Phi_i^a\rangle$ refers to a singly excited determinant where an occupied orbital i of the reference wavefunction is replaced by a virtual orbital a and so on.

However, the Full CI method is computationally very expensive and scales factorially with system size. Unsurprsingly, it is mostly used in benchmark calculations of small molecules. In practice, truncated CI methods like CISD, CISDT where the vector space is restricted to include up to doubly and triply excited determinants is used. Unlike the exact wavefunction, truncated CI wavefunctions, however, do not posess the property of size-extensivity i.e. the CIS[D/T] energy doesn't scale linearly with the number of electrons in the asymptotic limit. Another notable deficiency is the lack of size-consistency which means that within these approaches, the sum of the energies of non-interacting fragments (each calculated separately) is not equal to the energy of the supermolecule when all the fragments are included in the calculations. As a result, the accuracy of these methods decreases progressively as the size of the system increases.

2.3 Coupled Cluster Theory

Coupled cluster (CC) theory[16] is an alternative formulation of the TDSE which attempts to reproduce the Full CI wavefunction through an exponential parametrization of the wavefunction. The CC wavefunction can be obtained by the operation of cluster operators $\hat{T}$ acting on the reference Slater determinant.

$$|\Psi_{CC}\rangle = e^{\hat{T}}|0\rangle, \tag{2.3}$$

where,

$$\hat{T} = \hat{T}_1 + \hat{T}_2 + \hat{T}_3 + ... \hat{T}_n. \tag{2.4}$$

Here $|0\rangle$ is the reference wavefunction, usually taken as the HF wavefunction. One of the most popular tools used for the derivation of the complicated CC equations is second-quantization[36]. The $\hat{T}_2$ operator in SQ form can be written as

$$\hat{T}_2 = \frac{1}{4}\sum_{ijab} t_{ij}^{ab}\{a_a^\dagger a_b^\dagger a_j a_i\}. \tag{2.5}$$

where $a_a^\dagger$ (or $a_b^\dagger$) is called a creation operator as it creates a new particle state (virtual orbital) when it acts on a Slater determinant.

$$a_a^\dagger|\phi_b...\phi_d\rangle = |\phi_a\phi_b...\phi_d\rangle. \tag{2.6}$$

Here, $|\phi_a\phi_b...\phi_d\rangle$ is a shorthand notation (Dirac) for a Slater determinant with orbitals $a, b, ..d$. The a_i (or a_j) operator on other hand is called as annihilation operator as it removes a hole state (occupied orbital) when it acts on a Slater determinant.

$$a_i|\phi_i\phi_j...\phi_l\rangle = |\phi_j...\phi_l\rangle. \tag{2.7}$$

Thus, the action of the $\hat{T}_2$ operator on a Slater determinant creates a linear combination of all doubly excited determinants with corresponding coefficients t_{ij}^{ab} which can be seen as the contribution of virtual orbitals a and b to the pair correlation function f_{ij}, which correlates the motions of any two electrons associated with occupied orbitals i and j.

$$\begin{aligned} \hat{T}_2 &= \sum_{ij} f_{ij} \\ f_{ij} &= \frac{1}{4}\sum_{ab} t_{ij}^{ab}\{a_a^\dagger a_b^\dagger a_j a_i\} \end{aligned} \tag{2.8}$$

Similarly, the $\hat{T}_3$ operator correlates the motion of all triplets of electrons. The $\hat{T}_1$ operator on the other hand captures the "adjustment of the one-electron basis"[16] as the effect of other correlation operators is added to the wavefunction.

$$\hat{T}_1 = \sum_{ia} t_i^a\{a_a^\dagger a_i\} \tag{2.9}$$

In general, the structure of these cluster operators can be shown as,

$$\hat{T}_n = \left(\frac{1}{n!}\right)^2 \sum_{ij..ab..}^{n} t_{ij..}^{ab..}\{a_a^\dagger a_b^\dagger ...a_j a_i\} \tag{2.10}$$

Expanding the "exponential ansatz" of the CC wavefunction,

$$|\Psi_{CC}\rangle = (1 + (\hat{T}_1 + \hat{T}_2 + \hat{T}_3 + ...) + \frac{1}{2!}(\hat{T}_1 + \hat{T}_2 + \hat{T}_3 + ...)^2 + ...)|0\rangle \tag{2.11}$$

a linear combination of all possible Slater determinants is obtained, which in the basis set limit, should be an exact solution of the TISE just like the Full CI wavefunction.

$$\hat{H}e^{\hat{T}}|0\rangle = E_{cc}\, e^{\hat{T}}|0\rangle \tag{2.12}$$

The Hamiltonian is also expressed in second-quantized form [16]:

$$\hat{H} = \sum_{pq} h_{pq}\{a_p^\dagger a_q\} + \frac{1}{4}\sum_{pqrs}\langle pq||rs\rangle\{a_p^\dagger a_q^\dagger a_s a_r\} \tag{2.13}$$

where, $h_{pq} = \langle p|h|q\rangle$ and $\langle pq||rs\rangle = \langle pq|rs\rangle - \langle pq|sr\rangle$ are the one and two electron components of the Hamiltonian respectively. The CC equations for calculating the amplitudes and the energy can be obtained by multiplying equation (2.12) by the inverse of the exponential operator i.e. $e^{-\hat{T}}$ and projecting it against the reference and excited determinants.

$$\langle 0|e^{-\hat{T}}\hat{H}e^{\hat{T}}|0\rangle = E_{cc} \tag{2.14}$$

$$\langle \mu|e^{-\hat{T}}\hat{H}e^{\hat{T}}|0\rangle = 0. \tag{2.15}$$

Here μ can refer to any excited Slater determinant: singles, doubles etc. The similarity transformed Hamiltonian $e^{-\hat{T}}\hat{H}e^{\hat{T}}$, also written as $\bar{H}$ can be expressed in terms of commutators of the Hamiltonian with the cluster operators $\hat{T}$ by using the Campbell-Baker-Hausdorff formula[53].

$$e^{-\hat{T}}\hat{H}e^{\hat{T}} = \hat{H} + [\hat{H},\hat{T}] + \frac{1}{2!}[[\hat{H},\hat{T}],\hat{T}] + \frac{1}{3!}[[[\hat{H},\hat{T}],\hat{T}],\hat{T}] + \frac{1}{4!}[[[[\hat{H},\hat{T}],\hat{T}],\hat{T}],\hat{T}] + ... \quad (2.16)$$

The expansion truncates naturally at the four nested commutator term since the Hamiltonian is at most a two electron operator and the cluster operators commute among themselves[16]. Invoking Wick's theorem[91], the CC energy equation gets simplified as:

$$E_{cc} = E_o + \sum_{ia} f_{ia}t_i^a + \frac{1}{4}\sum_{aibj}\langle ij||ab\rangle t_{ij}^{ab} + \frac{1}{2}\sum_{aibj}\langle ij||ab\rangle t_i^a t_j^b. \quad (2.17)$$

The non-linear amplitude equations are solved iteratively until the change in energies falls below a convergence threshold. However, just like its CI counterpart, Full CC is computationally impractical and hence, truncated CC methods like CCSD: $\hat{T} = \hat{T}_1 + \hat{T}_2$, CCSDT: $\hat{T} = \hat{T}_1 + \hat{T}_2 + \hat{T}_3$, are used. The exponential structure of the CC wavefunction makes the truncated CC methods more efficient and accurate than the corresponding linear CI methods. For example, the CCSD wavefunction implicitly includes the triples and quadruples excitation contributions to its singles and doubles amplitude equations because of the products of cluster

operators like $\hat{T}_1\hat{T}_2$, $\left(\hat{T}_2\right)^2$ etc., unlike the CISD method, which can only include singles and doubles excitation contributions. Furthermore, CC energies have the desired properties of size-extensivity and size-consistency (provided the reference wavefunction is size-consistent). Unsurprisingly, the CCSD(T)[81] method, which approximates the triples using perturbation theory is considered to be the "gold standard" of quantum chemistry. However, CC methods just like their CI counterparts, are computationally expensive: CCSD, CCSD(T), CCSDT scale as $O(N^6)$, $O(N^7)$, $O(N^8)$ respectively, where N is the number of basis functions.

2.3.1 Coupled Cluster Analytic Gradients

The gradient of the CC energy (equation 2.14) with respect to any external perturbation X can be written as:

$$\frac{\partial E_{cc}}{\partial X} = \langle 0|\frac{\partial \bar{H}}{\partial X}|\Psi_o\rangle = \langle \Psi_o|\bar{H}^X + [\bar{H}, \frac{\partial \hat{T}}{\partial X}]|\Psi_o\rangle \tag{2.18}$$

where,

$$\bar{H}^X = e^{-\hat{T}}\frac{\partial \hat{H}}{\partial X}e^{\hat{T}}. \tag{2.19}$$

Invoking the resolution of identity (RI),

$$1 = |0\rangle\langle 0| + \sum_{ia}|\Psi_i^a\rangle\langle\Psi_i^a| + \frac{1}{4}\sum_{ijab}|\Psi_{ij}^{ab}\rangle\langle\Psi_{ij}^{ab}| + ... \tag{2.20}$$

equation (2.18) can be seen to involve the derivatives of the amplitudes i.e $\frac{\partial t_\mu}{\partial X}$

$$\frac{\partial E_{cc}}{\partial X} = \langle 0|\bar{H}^X|0\rangle + \sum_\mu \langle 0|\bar{H}|\mu\rangle \frac{\partial t_\mu}{\partial X} \tag{2.21}$$

Calculating gradients using this approach would require taking the derivative of the non-linear equations used to solve for the amplitudes, which could be computationally demanding. However, explicit gradient calculations of the amplitudes can be avoided altogether through an alternative formulation. Taking the derivative of the CC amplitude equations with respect to X,

$$0 = \langle \mu|\bar{H}^X + [\bar{H}, \frac{\partial \hat{T}}{\partial X}]|0\rangle. \tag{2.22}$$

and using the RI method again, the above equation can be simplified as

$$\sum_\nu \langle \mu|\bar{H} - E_{cc}|\nu\rangle \frac{\partial t_\nu}{\partial X} = -\langle \mu|\bar{H}^X|0\rangle \tag{2.23}$$

or,

$$\frac{\partial t_\mu}{\partial X} = -\sum_\nu \langle \mu|(\bar{H} - E_{cc})^{-1}|\nu\rangle\langle \nu|\bar{H}^X|0\rangle \tag{2.24}$$

Plugging this gradient expression back into equation (2.21), we obtain the following expression,

$$\frac{\partial E_{cc}}{\partial X} = \langle 0|\bar{H}^X|0\rangle - \sum_{\mu}\langle 0|\bar{H}|\mu\rangle \sum_{\nu}\langle \mu|(\bar{H} - E_{cc})^{-1}|\nu\rangle\langle\nu|\bar{H}^X|0\rangle. \tag{2.25}$$

The second term of the RHS of the above equation involves an inverted $\bar{H}$ matrix which needs to be avoided at all costs as the dimensions of this matrix can be very large. As such, a linear operator $\hat{\Lambda}$ is defined in the following manner.

$$\langle 0|\hat{\Lambda}|\mu\rangle = -\sum_{\nu}\langle 0|\bar{H}|\nu\rangle\langle\nu|(\bar{H} - E_{cc})^{-1}|\mu\rangle. \tag{2.26}$$

or,

$$\sum_{\mu}\langle 0|\hat{\Lambda}|\mu\rangle\langle\mu|(\bar{H} - E_{cc})|\nu\rangle = -\langle 0|\bar{H}|\nu\rangle. \tag{2.27}$$

It can be easily seen from above equations that $\hat{\Lambda}$ is a linear de-excitation operator,

$$\hat{\Lambda} = \hat{\Lambda}_1 + \hat{\Lambda}_2 + \hat{\Lambda}_3 + ..., \tag{2.28}$$

where $\hat{\Lambda}_1 = \sum_{ia}\lambda_a^i\{a_i^\dagger a_a\}$, $\hat{\Lambda}_2 = \sum_{ijab}\lambda_{ab}^{ij}\{a_i^\dagger a_j^\dagger a_b a_a\}$ are the singles and doubles de-excitation operators respectively. The CC gradient expression can now be expressed in terms of the lambda operator,

$$\frac{\partial E_{cc}}{\partial X} = \langle 0|(1+\hat{\Lambda})\bar{H}^X|0\rangle = \langle 0|(1+\hat{\Lambda})e^{-\hat{T}}\frac{\partial \hat{H}}{\partial X}|\Psi_{cc}\rangle \tag{2.29}$$

and the governing equation for sloving the lambda amplitudes eq. (2.27) can be written in a more compact form as,

$$\langle 0|(1+\hat{\Lambda})(\bar{H}-E_{cc})|\mu\rangle = 0. \tag{2.30}$$

Thus, instead of taking the gradients of the non-linear T amplitude equations with respect to perturbations, we solve linear perturbation-independent $\hat{\Lambda}$ equations for calculating the CC energy gradient. Furthermore, CC gradients satisfy the generalized Hellman-Feynman equation[23] if $\langle 0|(1+\hat{\Lambda})e^{-\hat{T}}$ is defined to be the left hand wavefunction as due to the non-hermiticity of the $\bar{H}$ operator or the non-variational nature of the CC method, the left and right hand wavefunctions are not simple hermitian conjugates of each other.

2.3.2 General Response Theory

Response theory, as the name suggests, attempts to calculate molecular properties related to the response of the ground state wavefunction to an external perturbation. Within this formalism, the effect of an external electromagnetic field is incorporated into the Hamiltonian using the standard time-dependent perturbation theory:

$$\begin{aligned} H &= H_o + V(t) \\ V(t) &= \int_{-\infty}^{\infty} d\omega \;\; V(\omega)e^{(-i\omega+\alpha)t}, \end{aligned} \tag{2.31}$$

where H_o is the time independent or unperturbed Hamiltonian, $V(t)$ is the interaction operator with $V(\omega)$ as its Fourier transform and α is a real postive infinitesimal. The representation used for the $V(t)$ operator is an example of the adiabatically switched on perturbation[40] where the perturbation is assumed to be zero at $t = -\infty$. Thus, the molecule can be assumed to be in state Ψ_o, an eigenstate of H_o at $t = -\infty$. After the perturbation is switched on, the wavefunction becomes time dependent ($|\Psi_o(t)\rangle$) and evolves in time according to the time-dependent Schrödinger equation (TDSE).

$$i\frac{d}{dt}|\Psi_o(t)\rangle = (H_o + V^t)|\Psi_o(t)\rangle \tag{2.32}$$

Following the works of Olsen[59], the time dependent state $|\Psi_o(t)\rangle$ can be parametrized in terms of a phase factor ($\epsilon(t)$),

$$|\Psi_o(t)\rangle = |\bar{\Psi}_o\rangle e^{i\epsilon(t)} \tag{2.33}$$

where $|\bar{\Psi}_o\rangle$ is the phase isolated wavefunction which can be expanded in orders of perturbation (time dependence is assumed).

$$|\bar{\Psi}_o\rangle = |\Psi_o\rangle + |\Psi_o\rangle^{(1)} + |\Psi_o\rangle^{(2)} + ... \tag{2.34}$$

It should be noted that the phase factor cancels out when one takes an expectation value of an operator with the wavefunction of equation 2.33 and hence can be ignored in the following derivations. From the above equation, it can be seen that an expectation value of a time independent operator A can also be expanded in a similar fashion. The response functions are the Fourier transforms of these time dependent terms appearing in the expansion up to a given order.

$$\begin{aligned}\langle A\rangle(t) = \langle A\rangle + \int_{-\infty}^{\infty} d\omega_1 \langle\langle A; V^{\omega_1}\rangle\rangle_{\omega_1 + i\alpha} e^{-i(\omega_1 + i\alpha)t} \\ + \frac{1}{2}\int_{-\infty}^{\infty} d\omega_1 \int_{-\infty}^{\infty} d\omega_2 \ \langle\langle A; V^{\omega_1}; V^{\omega_2}\rangle\rangle_{\omega_1 + i\alpha, \omega_2 + i\alpha} e^{-i(\omega_1+\omega_2+2i\alpha)t} + ...\end{aligned} \tag{2.35}$$

where the linear response function (LRF), $\langle\langle A; V^{\omega_1}\rangle\rangle$ can be seen as the first order change in the expectation value of the time independent operator A with respect to perturbation. The first order perturbed wavefunction $|\Psi_o\rangle^{(1)}$ can be obtained using Ehrenfest's theorem and combined with the above equation to construct the LRF, which for exact states looks like,

$$\langle\langle A; V^{\omega_1}\rangle\rangle = \sum_k \left[\frac{\langle\Psi_o|A|\Psi_k\rangle\langle\Psi_k|V^{\omega_1}|\Psi_o\rangle}{\omega_1 - \omega_k} - \frac{\langle\Psi_o|V^{\omega_1}|\Psi_k\rangle\langle\Psi_k|A|\Psi_o\rangle}{\omega_1 + \omega_k} \right] \tag{2.36}$$

where ω_k is the excitation energy between the states Ψ_o and Ψ_k and the summation runs over all the solutions of the time independent Schrödinger equation, Ψ_k. However, calculating response functions using the above equation (also known as the sum of states equation) is very computationally expensive as it involves explicit calculations of all the excited states.

2.3.3 Coupled Cluster Response Theory

Coupled cluster response theory was proposed by Koch and Jørgensen in 1990[40] as a recipe for accurate calculations of response properties like dynamic (hyper)polarizabilities, optical rotations, etc. It avoids the sum of states approach through a suitable parametrization of the CC wavefunction. In this formalism, the right and left hand CC wavefunction evolve in time through time dependent $\hat{T}$ and $\hat{\Lambda}$ amplitudes,[40]

$$|\Psi_{cc}(t)\rangle = e^{\hat{T}(t)}|0\rangle e^{i\epsilon(t)} \tag{2.37}$$

$$\langle\Lambda(t)| = \{\langle 0| + \sum_{\mu} \lambda_{\mu}(t)\langle\mu|e^{-\hat{T}(t)}\}e^{-i\epsilon(t)} \tag{2.38}$$

where $e^{\pm i\epsilon(t)}$ is a time dependent phase factor. The governing equation for the time evolution of these amplitudes is the time-dependent Schrödinger equation.

$$i\frac{d}{dt}|\Psi_{cc}(t)\rangle = (H_o + V(t))|\Psi_{cc}(t)\rangle \tag{2.39}$$

$$\frac{d}{dt}\langle\Lambda(t)| = i\langle\Lambda(t)|(H_o + V(t)) \tag{2.40}$$

On multiplying eq. (2.39) by $e^{-\hat{T}(t)}$ on both sides and projecting it against the excited determinants $\langle\mu|$, the time derivative expression of the t_μ amplitudes can be obtained.

$$\frac{dt_\mu}{dt} = -i\langle\mu|e^{-\hat{T}(t)}(H_o + V(t))e^{\hat{T}(t)}|0\rangle \tag{2.41}$$

Similarly, multiplying eq.(2.40) by $e^{i\epsilon(t)}$ and invoking the RI, the time derivative equation of the λ_μ amplitudes can be derived.

$$\frac{d\lambda_\mu}{dt} = i\langle\tilde{\Lambda}(t)|[H_o + V(t), \tau_\mu]|\widetilde{\Psi}_{cc}(t)\rangle \tag{2.42}$$

where $\sim$ denotes the usual expressions without the phase factor $e^{\pm i\epsilon(t)}$. The amplitudes are then expanded in orders of the perturbation which is followed by a Fourier transformation.

$$\begin{aligned} t_\mu(t) &= t_\mu^{(0)} + t_\mu^{(1)} + t_\mu^{(2)} + ... \\ &= t_\mu^{(0)} + \int_{-\infty}^{\infty} d\omega_1 X_\mu^{(1)}(\omega_1 + i\alpha)e^{(-i\omega_1+\alpha)t} + ... \end{aligned} \tag{2.43}$$

$$\begin{aligned} \lambda_\mu(t) &= \lambda_\mu^{(0)} + \lambda_\mu^{(1)} + \lambda_\mu^{(2)} + ... \\ &= \lambda_\mu^{(0)} + \int_{-\infty}^{\infty} d\omega_1 Y_\mu^{(1)}(\omega_1 + i\alpha)e^{(-i\omega_1+\alpha)t} + ... \end{aligned} \tag{2.44}$$

Using 2.41-2.44, the equations for solving the Fourier transforms $X_\mu^{(1)}$ and $Y_\mu^{(1)}$ can be derived,

$$\begin{aligned} \sum_\nu \left((\omega_1 + i\alpha)\boldsymbol{I} - \boldsymbol{A}\right)_{\mu\nu} X_\nu^{(1)} &= -\langle\mu|\bar{V}^{\omega_1}|0\rangle \\ \sum_\nu Y_\nu^{(1)}\left((\omega_1 + i\alpha)\boldsymbol{I} + \boldsymbol{A}\right)_{\nu\mu} &= -\eta_\mu^{(1)} - \sum_\gamma F_{\mu\gamma} X_\gamma^{(1)}. \end{aligned} \tag{2.45}$$

Here $\boldsymbol{I}$ is the identity matrix and $\boldsymbol{A}$ is the (unsymmetric) CC Jacobian,

$$A_{\mu\nu} = \langle \mu | [\bar{H}_o, \tau_\nu] | 0 \rangle \tag{2.46}$$

where overbar on an operator denotes similarity transformation with the ground state T operator, ex. $\bar{H}_o = e^{-T\hat{(0)}} \hat{A} e^{T\hat{(0)}}$. The $\boldsymbol{\eta}^{(1)}$ vector and the symmetric $\boldsymbol{F}$ matrix are defined as,

$$\begin{aligned} F_{\mu\nu} &= \langle (1 + \hat{\Lambda}) | [[\bar{H}_o, \tau_\mu], \tau_\nu] | 0 \rangle \\ \eta_\mu^{(1)} &= \langle (1 + \hat{\Lambda}) | [\overline{V}^{\omega_1}, \tau_\mu] | 0 \rangle. \end{aligned} \tag{2.47}$$

For a CC wavefunction, time-dependent expectation value of a time-independent operator A is defined as[62],

$$\begin{aligned} \langle A \rangle_{CC}(t) =& Re[\langle \Lambda(t) | A | CC(t) \rangle] \\ &= \frac{1}{2} (\langle \Lambda(t) | A | CC(t) \rangle + \langle \Lambda(t) | A | CC(t) \rangle^*) \end{aligned} \tag{2.48}$$

since both $\hat{T}$ and $\hat{\Lambda}$ amplitudes can be complex quantities but the expectation values should always be real. To identify CC response functions, the quantity $\langle \Lambda(t) | A | CC(t) \rangle$ is expanded in orders of perturbation[62].

$$\begin{aligned}\langle\Lambda(t)|A|CC(t)\rangle &= \langle\Lambda(t)|A|CC(t)\rangle^{(0)} + \langle\Lambda(t)|A|CC(t)\rangle^{(1)} + \langle\Lambda(t)|A|CC(t)\rangle^{(2)} + ... \\ &= \langle\Lambda|A|CC\rangle + \int_{-\infty}^{\infty} d\omega_1 \; F^{A;V^{\omega_1}}_{\omega_1+i\alpha} e^{-i(\omega_1+i\alpha)t} \\ &+ \frac{1}{2}\int_{-\infty}^{\infty} d\omega_1 \int_{-\infty}^{\infty} d\omega_2 \; F^{A;V^{\omega_1};V^{\omega_2}}_{\omega_1+i\alpha,\omega_2+i\alpha} e^{-i(\omega_1+\omega_2+2i\alpha)t} + ...\end{aligned} \tag{2.49}$$

From eqns 2.48 and 2.49 and using the relation $F^{V^{\omega_1};A}_{-\omega_1} = F^{A;V^{\omega_1}}_{\omega_1}$, the CC-LRF can be identified as,

$$\langle\langle A; V^{\omega_1}\rangle\rangle_{\omega_1+i\alpha} = \frac{1}{2}(F^{A;V^{\omega_1}}_{\omega_1+i\alpha} + (F^{V^{\omega_1};A}_{\omega_1+i\alpha})^*). \tag{2.50}$$

or,

$$\langle\langle A; B\rangle\rangle_{\omega_1} = \frac{1}{2}\hat{P}(A,B)[\langle 0|\ [\hat{Y}^B_{\omega_1}, \bar{A}]|0\rangle + \langle 0|\ (1+\hat{\Lambda})|[\bar{A}, \hat{X}^B_{\omega_1}]|0\rangle] \tag{2.51}$$

where $V^{\omega_1} = B$, $\hat{P}(A,B)$ simultaneously interchanges operators A and B and takes the complex conjugate of the expression, and $\hat{X}^B_{\omega_1}$ and $\hat{Y}^B_{\omega_1}$ are the first-order right and left hand perturbed amplitudes corresponding to operator B respectively. An alternative formulation of the CC-LRF avoids calculating $\hat{Y}_{\omega_1}$ amplitudes by solving an extra set of $\hat{X}_{-\omega_1}$ amplitudes,

$$\langle\langle A; B\rangle\rangle_{\omega_1} = \frac{1}{2}\hat{C}^{\pm\omega_1}\hat{P}'[A(-\omega_1), B(+\omega_1)]\left[\langle 0|(1+\hat{\Lambda})\left([\bar{A}, \hat{X}^B_{\omega_1}] + \frac{1}{2}[[\bar{H}_o, \hat{X}^A_{-\omega_1}], \hat{X}^B_{\omega_1}]\right)|0\rangle\right] \tag{2.52}$$

where $\hat{C}$ is a symmetrizer that simultaneously interchanges the sign of the field frequency

and takes the complex conjugate of the expression, and $\hat{P}'$ symmetrizes the expression with respect to the operators A and B.

The LRFs can also be defined as second-order derivatives of a time-averaged quasi-energy with respect to external perturbations A and B. This formalism is specially useful for deriving LRFs for approximate coupled cluster theories like CC2, CC3 etc.

Chapter 3

Frozen Virtual Natural Orbitals for Coupled-Cluster Linear-Response Theory

3.1 Introduction

In the construction of many-body electronic wave functions, the scaling of a given method with the number of molecular orbitals (MOs) plays a pivotal role in the ultimate cost of

the calculation. For many-body methods such as coupled cluster (CC),[17, 27, 80] which, in its canonical formulation, displays a high-order polynomial dependence on the number of MOs, numerous mechanisms have been explored over the last half century for reducing the size of the virtual-MO space. Among the earliest of these was Löwdin's[48] introduction in 1955 of the concept of "natural orbitals" (NOs) — orbitals for which the one-electron density matrix is diagonal. Löwdin demonstrated that NOs yield faster convergence of the configuration interaction (CI) wave function expansion than Hartree-Fock MOs. Some years later, Bender and Davidson[7] used natural orbitals in conjunction with CI (NO-CI) calculations to construct and analyze the most important configurations contributing to the correlated wave functions for a series of closed- and open-shell first-row diatomic hydrides. This work motivated Barr and Davidson a year later[4] to utilize only the virtual natural orbitals, obtained by diagonalization of the virtual-virtual block of the one-electron density matrix, for NO-CI calculations on the Ne atom.

The concept of pair natural orbitals (PNOs – originally called "pseudonatural orbitals") was developed by Edmiston and Krauss[21], by Meyer[56], and by Ahlrichs and co-workers[2]. In the PNO approach, the virtual-virtual MO block of the one-electron density is constructed and diagonalized independently for each occupied MO pair, leading to separate non-orthogonal virtual spaces. Although this approach leads to rapid convergence of the correlation energy with respect to the size of the virtual space, it was little used following initial investigations until it was resurrected in recent years by Neese and co-workers with great success in the context of reduced-scaling electron correlation methods[58, 68].

Following these pioneering efforts, NOs have been exploited in numerous applications to construct compact CI[1, 22, 82], multiconfigurational self-consistent-field (MCSCF)[35], and CC wave functions[18, 19, 46, 84, 88, 89]. In many of these studies, the virtual-MO block of the one-electron density is first obtained from a simpler model, such as second-order many-body perturbation theory (MBPT) calculation, and then diagonalized to yield the virtual-NO space. The space is then truncated based on an occupation-number-related criterion and fixed for the subsequent correlated-wave-function calculation. In addition, the final energy is commonly corrected using the second-order Møller-Plesset perturbation theory (MP2) correlation energy contributions arising from the external virtual space. These studies have indicated that, for energetics and related properties, even aggressive truncation of the virtual-NO space often has only a small impact on the resulting property as compared to full-space computations. For example, Landau *et al.*[46] found that, for NOs combined with the equation-of-motion coupled-cluster method for ionized states (EOM-IP-CC), reduction of the virtual space by up to 70% yielded truncation errors within ca. 1 kcal/mol for ionization energies of organic compounds and non-parallelity errors in potential surfaces of weakly bound complexes.

While the above studies have demonstrated clearly the usefulness of NOs for aggressively truncating the virtual space when computing correlation energies, more complex properties have yet to be considered. As shown in a number of recent reports[25, 43, 50, 51, 70, 71], properties that are related to the linear- or higher-order response of the wave function to external electric and magnetic fields, for example, exhibit much greater sensitivity to the

quality of the wave function than simple energetics. In particular, local correlation methods have been shown[43, 50, 51, 70, 71] to require significantly larger domains for properties such as polarizabilities than for ground-state energies. Furthermore, the many-body expansion — which has yielded impressive convergence for energetics and dipole moments for clusters of weakly interacting molecules (such as a solute embedded in an explicit solvent) — converges erratically, at best, for spectroscopic response properties due to its strong basis-set dependence.[49] In order to account for this, the ability to reduce the dimensionality of the virtual space becomes paramount. Thus, the focus of the present work is on the extension of the NO approach to linear-response properties, especially the case of frequency-dependent dipole polarizabilities.

3.2 Theoretical Background

3.2.1 Frozen Virtual Natural Orbitals

The MP2 unrelaxed one-electron density matrix can be written in terms of spin orbitals as:

$$\gamma_{pq} = \langle \Psi^{(1)} | \{ a_p^\dagger a_q \} | \Psi^{(1)} \rangle, \tag{3.1}$$

where $|\Psi^{(1)}\rangle$ is the first order correction to the Hartree-Fock wave function,

$$|\Psi^{(1)}\rangle = \frac{1}{4}\sum_{ijab} t_{ij}^{ab}|\Phi_{ij}^{ab}\rangle \tag{3.2}$$

and

$$t_{ij}^{ab} = \frac{\langle ij||ab\rangle}{\epsilon_i + \epsilon_j - \epsilon_a - \epsilon_b}. \tag{3.3}$$

Here, $\langle ij||ab\rangle$ is an antisymmetrized two-electron integral in Dirac's notation and $\epsilon_i, \epsilon_a...$ refer to the Hartree-Fock molecular orbital energies. We use the indices $i, j, k, ...$ to indicate occupied orbitals while $a, b, c, ...$ denote virtual orbitals. $|\Phi_{ij}^{ab}\rangle$ refers to a doubly-excited determinant where occupied orbitals i and j are replaced by virtuals a and b respectively. The brackets around the second-quantized operators in Eq. (3.1) indicate normal ordering with respect to the reference wave function.

In the MP2 based NO method, the virtual-virtual block of γ_{pq} is constructed,

$$\gamma_{ab} = \frac{1}{2}\sum_{ijc} t_{ij}^{ac} t_{ij}^{bc}, \tag{3.4}$$

and then diagonalized,

$$\boldsymbol{\gamma V} = \boldsymbol{nV}. \tag{3.5}$$

The eigenvectors, $\boldsymbol{V}$, are the virtual natural orbitals (NOs), and the eigenvalues, $\boldsymbol{n}$, are the associated occupation numbers. As noted earlier, the wave function amplitudes contain significantly greater sparsity when represented in the NO basis than the original canonical

MO basis; orbitals with lower occupation numbers yield $\hat{T}_2$ amplitudes with smaller magnitudes and concomitantly smaller contributions to the correlation energy. Thus, orbitals with occupation numbers below a selected threshold can be removed without introduction of significant errors, leading to reduced computational cost. The Hartree-Fock virtual molecular orbitals and associated integrals are then transformed to this truncated NO basis, followed by semicanonicalization of the virtual-virtual block of the Fock matrix, for subsequent computations using higher-order correlation methods such as CC theory. In most cases, the final correlation energy in the truncated virtual space is corrected using the MP2 energy in the external (non-truncated) NO space to minimize the resulting errors, as described below.

3.2.2 Coupled Cluster Response Theory

Dynamic response functions representing higher-order properties such as polarizabilities and hyperpolarizabilities, optical activity tensors, magnetizabilities, etc. can be obtained by expanding the expectation value of an appropriate time-independent operator in perturbational orders with respect to a time-dependent external field. The CC form of response theory has been routinely used for many years for accurate calculations of such properties.[31] The CC linear response function for property operators $\boldsymbol{A}$ and $\boldsymbol{B}$, for example, can be written as

$$\langle\langle \boldsymbol{A}; \boldsymbol{B} \rangle\rangle_{\omega} = \frac{1}{2}\hat{C}^{\pm\omega}\hat{P}[A(-\omega), B(+\omega)] \left[\langle \Psi_0 | (1 + \hat{\Lambda}) \left([\bar{A}, \hat{X}^B_{\omega}] + \frac{1}{2}[[\bar{H}, \hat{X}^A_{-\omega}], \hat{X}^B_{\omega}] \right) | \Psi_0 \rangle \right] \tag{3.6}$$

where Ψ_0 is the reference wavefunction, $\hat{\Lambda}$ is a de-excitation operator used to parametrize the CC left hand wavefunction, ω is the frequency of the external field, $\hat{C}$ is a symmetrizer that simultaneously interchanges the sign of the field frequency and takes the complex conjugate of the expression, and $\hat{P}$ symmetrizes the expression with respect to the operators $\boldsymbol{A}$ and $\boldsymbol{B}$. Operators with an overbar have been similarity transformed with the ground state cluster operators, $\hat{T}$, e.g. $\bar{H} = e^{-\hat{T}}\hat{H}e^{\hat{T}}$. The first-order (right-hand) perturbed wave function is represented by $\hat{X}^B_\omega$, whose amplitudes can be obtained by solving a set of appropriate linear equations, e.g.,

$$\langle \Phi^{ab\ldots}_{ij\ldots} | (\bar{H} - \omega) | \hat{X}^B_\omega | \Psi_0 \rangle = -\langle \Phi^{ab\ldots}_{ij\ldots} | \bar{B} | \Psi_0 \rangle. \tag{3.7}$$

In the case of dynamic polarizabilities, for example, both $\boldsymbol{A}$ and $\boldsymbol{B}$ are cartesian components of the electric dipole operator, $\boldsymbol{\mu} = -\boldsymbol{r}$, and the isotropic polarizability α_ω is related to the trace of the polarizability tensor such that Eq. (3.6) reduces to the following form (for real wavefunctions),

$$\alpha_\omega = \frac{1}{3}\mathrm{Tr}\left[\langle \Psi_0 | (1+\hat{\Lambda})\left(\left[\bar{\mu}, (\hat{X}^\mu_\omega + \hat{X}^\mu_{-\omega})\right] + \left[\left[\bar{H}, \hat{X}^\mu_{-\omega}\right], \hat{X}^\mu_\omega\right]\right) | \Psi_0 \rangle\right] \tag{3.8}$$

For dynamic polarizabilities computed using the coupled cluster singles and doubles (CCSD) method, for example, six sets of perturbed amplitudes, $\hat{X}_1(X^a_i)$ and $\hat{X}_2(X^{ab}_{ij})$, must be com-

puted, one for each cartesian component of $\boldsymbol{\mu}$ at both positive and negative frequencies.

3.3 Computational Details

The primary molecular test cases of this work is hydrogen peroxide, H_2O_2, though additional tests are reported for related species such as (*P*)-dimethylallene and (*S*)-methyloxirane, as well as those same molecules interacting with one or more water molecules. All molecular structures were optimized using the B3LYP functional[6, 47, 85] in the aug-cc-pVDZ (aDZ) basis[20, 38, 92]. (Coordinates of all structures are provided in Tables 6.1-6.5 of the Supporting Information.) Frequency-dependent polarizabilities were computed at the coupled cluster singles and doubles (CCSD) level of theory[66] using a linear-response formulation[11]. While the aDZ basis set was used for most test calculations, the larger aug-cc-pVTZ (aTZ) and aug-cc-pVQZ (aQZ) basis sets were also employed for selected analyses[38]. All orbitals were active in the correlated models utilized here, and all coupled-cluster calculations were carried out using the PSI4 open-source quantum chemistry package[90]. In all calculations in which virtual orbitals are truncated, the same orbital space is used in the solution of the unperturbed and perturbed amplitudes equations, just as is required for locally correlated property calculations[14]. We note that the size-extensivity of the polarizability is unaffected by the truncation of the virtual space.

3.4 Results and Discussion

It is well known that deletion of higher-energy canonical Hartree-Fock MOs (CMOs) typically leads to significant errors in the recovery of electron correlation energies, whereas, by design, the truncation of virtual NOs with low occupation numbers results in little loss of accuracy.[46, 88, 89] For example, Fig. 3.1 plots the error in the CCSD correlation energy

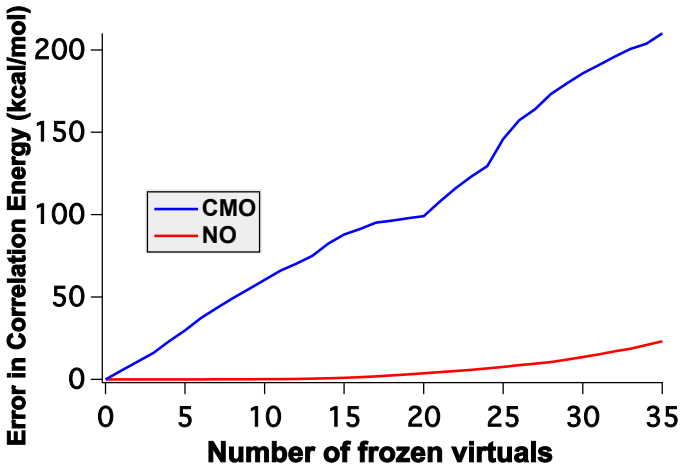

Figure 3.1: Error in the CCSD energy of H_2O_2 in kcal/mol as a function of the number of frozen virtual orbitals in both CMO and NO bases.

of H_2O_2 in the aDZ basis as a function of the number of frozen virtual CMOs (removed starting from the highest energy orbitals) or NOs (starting from the lowest occupation numbers). Clearly the correlation energy is very sensitive towards the removal of CMOs, with the error increasing by more than 4 kcal/mol after the deletion of even one virtual orbital. On the other hand, removal of low occupation-number NOs introduces errors of only ca. 2.5

kcal/mol even when up to 33% of the virtual space (18 of 55 orbitals) is truncated. The errors in the NO basis can be further minimized by employing an MP2 energy correction,

$$E_{\text{corr}}^{\text{MP2}} = \frac{1}{4}\sum_{ij}\sum_{ab\in\text{ext}}\frac{|\langle ij||ab\rangle|^2}{\epsilon_i+\epsilon_j-\epsilon_a-\epsilon_b}. \tag{3.9}$$

where the summation over virtual orbitals is limited to NOs in the external, truncated space. Fig. 3.2 plots the error in the CCSD correlation energy for the same system as above in the

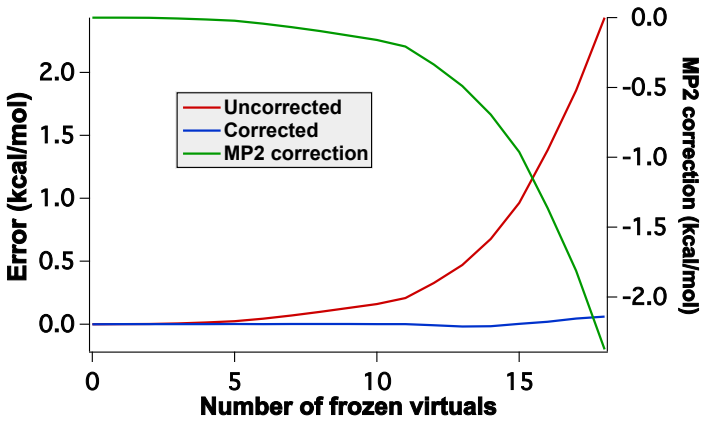

Figure 3.2: Error in CCSD energy of H_2O_2 in the NO bases, with and without MP2 corrections and MP2 correction as a function of the number of frozen virtual orbitals.

NO basis, with and without this correction (left-hand vertical axis), as well as the correction itself (right-hand axis). After employing the correction, the error in the correlation energy falls to less than 0.1 kcal/mol when 1/3 of the virtual space is eliminated. Similar results are

obtained for aTZ and aQZ basis sets, where the truncation errors are less than 1 kcal/mol even after the removal of 50% of the virtual space. We note that the MP2 energy correction is significant (on the order of mE_h or several kcal/mol) even for small compounds such as H_2O_2. The correction scales linearly with the number of electrons and thus is a critical component for the success of the frozen virtual NO approach for larger molecules.

3.4.1 Frozen Virtual Orbitals and Response Properties

What is the impact of freezing virtual orbitals — whether CMO or NO — on higher-order properties? Fig. 3.3 plots errors in dynamic polarizabilites (computed at a wavelength of

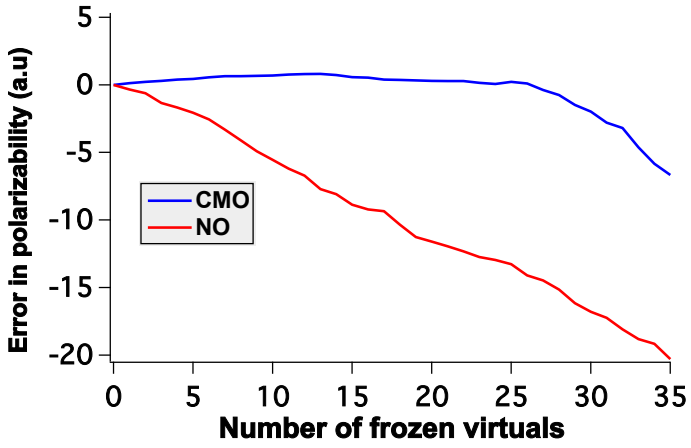

Figure 3.3: Errors in the CCSD/aDZ dynamic polarizability (589 nm) of H_2O_2 in in both CMO and NO bases as a function of number of virtual orbitals removed .

589 nm) as a function of the number of virtual orbitals deleted at the CCSD/aDZ level of

theory for the same H_2O_2 test case as above. Comparison to Fig. 3.1 reveals precisely the opposite behavior for polarizabilities as for correlation energies, *viz.*, truncation of the CMO virtual space induces much smaller errors than does that of the NO virtual space. For the latter, errors increase approximately linearly with the number of frozen virtual NOs. On the other hand, for the CMO basis, the error increases slowly to a maximum of 1.9% when 13 virtual orbitals are removed and then decreases to only -0.3% when as many as 27 orbitals (ca. 50% of the virtual space) are frozen. This trend is not unique to H_2O_2 or the aDZ basis set. As shown in Fig. 6.1 of the Supporting Information, the same behavior is observed for other molecules such as dimethylallene, methyloxirane, and such compounds interacting with explicit solvent molecules. In addition, Figs. 6.2 and 6.3 report the same trends for H_2O_2 with the larger aTZ and aQZ basis sets.

What is the source of this unexpected behavior? It is well known that diffuse basis sets are essential for the accurate descriptions of a variety of response properties, such as dipole polarizabilities.[92] Fig. 3.4 plots the spatial extent — $\langle r^2 \rangle$ — for each virtual CMO or NO in the same ordering as they are deleted in Fig. 3.3. The Figure clearly shows that the earliest NOs to be removed (the ones with the lowest occupation numbers) are the most diffuse, *i.e.*, they should contribute substantially to the description of the dynamic polarizability. On the other hand, the first CMOs to be frozen (those with the highest orbital energies) are also the most compact and thus contribute the least to this property. Given that highly diffuse basis functions typically contribute primarily to CMOs with low orbital energies — often below that of what is normally considered the true anti-bonding "LUMO" — the latter result is

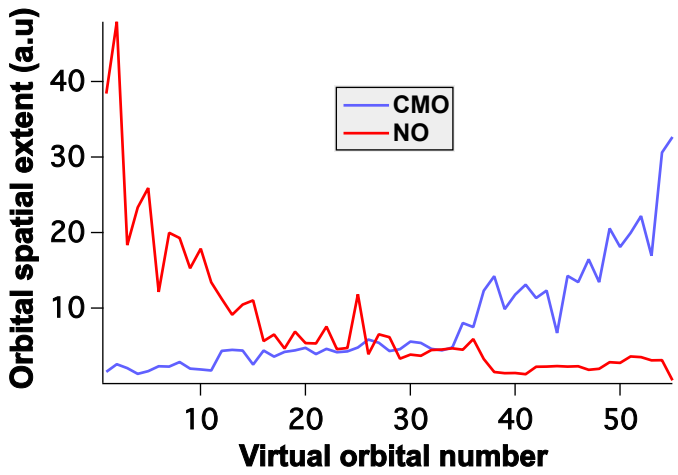

Figure 3.4: Spatial extent ($\langle r^2 \rangle$) of virtual orbitals of H_2O_2 in both CMO and NO bases. Orbitals are ordered left-to-right by decreasing energy (CMOs) or increasing occupation number (NOs).

not surprising; these diffuse CMOs appear to the far right of Fig. 3.4 and are thus never deleted, leading to the good behavior of the CMO truncation in Fig. 3.3. These same diffuse basis functions, however, contribute little to the description of dynamical correlation effects, and thus exhibit very low occupation numbers upon transformation to the NO virtual space. Thus, they are truncated first in the NO basis, yielding the large errors in the polarizability depicted in Fig. 3.3.

The above observations suggest that, for computing response properties such as dynamic polarizabilities, an alternative approach to truncation of the virtual space is to order the orbitals by increasing values of $\langle r^2 \rangle$ rather than by decreasing orbital energies (as is done for CMOs) or increasing occupation numbers (for NOs). Fig. 3.5 plots errors in the CCSD/aDZ

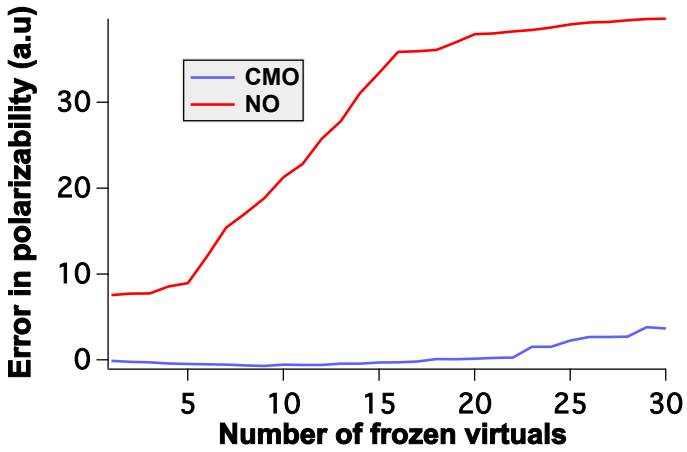

Figure 3.5: Spatial extent ($\langle r^2 \rangle$) of virtual orbitals of H_2O_2 in both CMO and NO bases. Orbitals are ordered left-to-right by decreasing energy (CMOs) or increasing occupation number (NOs).

dynamic polarizability of H_2O_2 as the virtual CMOs or NOs are removed in order of increasing spatial extent. While the errors are comparable to that observed in Fig. 3.3 for the CMO truncation, the behavior associated with removal of virtual NOs is significantly different. First, the polarizability errors exhibit two plateaus: one associated with diffuse NOs 2-5 and another with NOs 16-30, and removal of these NOs has little impact on the observed error. However, deletion of the virtual NO with the *smallest* spatial extent unexpectedly leads to a large initial error (ca. 7.5 a.u.), followed later by a linearly increasing error as virtual NOs 6-15 are removed. Clearly, spatial extent is not the only criterion by which we may predict the importance of a given virtual NO to the polarizability.

Another possible source of error is the lack of orbital response in the chosen formulation

of the coupled cluster linear response function.[41] In the infinite-lifetime approximation, frequency-dependent properties such as dipole polarizabilities exhibit first-order poles at the excitation frequencies. In the coupled cluster formulation described above, the orbital response to the external field is typically neglected so that these poles correspond solely to the response for the correlated wave function, and additional, spurious poles arising due to the Hartree-Fock reference determinant will not appear. (This approximation is typically justified based on the fact that much of the orbital-response effects are accounted for by the singles amplitudes[12]. In order to test whether the orbital relaxation significantly impacts the behavior of the computed polarizability as the virtual space is reduced, we have computed *static* ($\omega = 0.0$) polarizabilities using finite-differences (with a a central-difference formula with a differential field strength of 0.001 a.u.) The errors in the CCSD/aDZ static polarizability of H_2O_2 for both CMO and NO virtual spaces are reported in Fig. 3.6. Interestingly, with orbital relaxation included, the truncation of the NO space now becomes better behaved than the CMO space over a large domain of orbitals removed. Unfortunately, we cannot take advantage of this improvement in conjunction with Hartree-Fock orbitals without corrupting the pole structure of the response function. A Brueckner or orbital-optimized approach may prove superior in this regard, though further investigation is warranted.[41, 61]

3.4.2 Wave Function Truncation in the Virtual-Orbital Space

For additional insight into the above observations, we examine errors arising in dynamic polarizabilities as a function of truncation of specific wavefunction parameters in either the

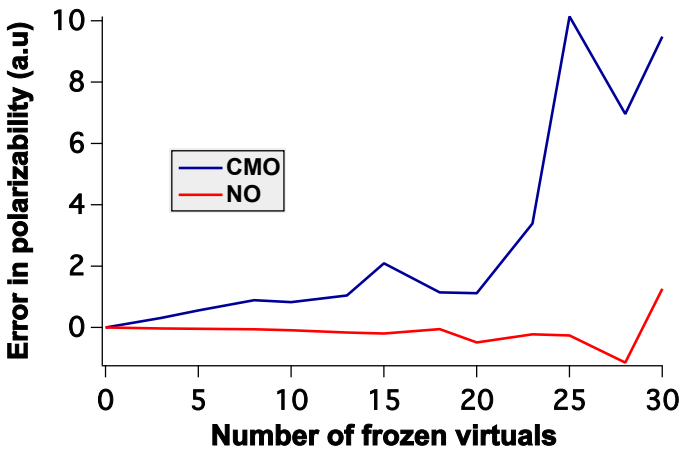

Figure 3.6: Errors in the CCSD/aDZ static polarizability (including orbital relaxation effects) of H_2O_2 in in both CMO and NO bases as a function of number of virtual orbitals removed.

CMO or NO basis. Fig. 3.7 plots the errors in CCSD/aDZ dynamic polarizabilities of H_2O_2 as a result of truncations of the unperturbed ground-state cluster amplitudes $\hat{T}$ and $\hat{\Lambda}$, as well as perturbed amplitudes, $\hat{X}^{\mu}_{\omega}$, represented in the CMO basis. Note that, in this analysis, only the specified amplitudes associated with the selected CMOs are forced to zero; the CMOs remain active for all other wave function components. From the Figure, it can be clearly seen that removing $\hat{T}_1$ alone does not introduce any significant error in the polarizability, whereas truncating $\hat{T}_2$ amplitudes results in substantial positive errors which increase almost linearly with the number of virtual CMOs. Not surprisingly, freezing both $\hat{T}_1$ and $\hat{T}_2$ amplitudes together have essentially the same effect as freezing $\hat{T}_2$ amplitudes alone. Alternatively, for the left-hand wave function, removing $\hat{\Lambda}_1$ and $\hat{\Lambda}_2$ amplitudes either

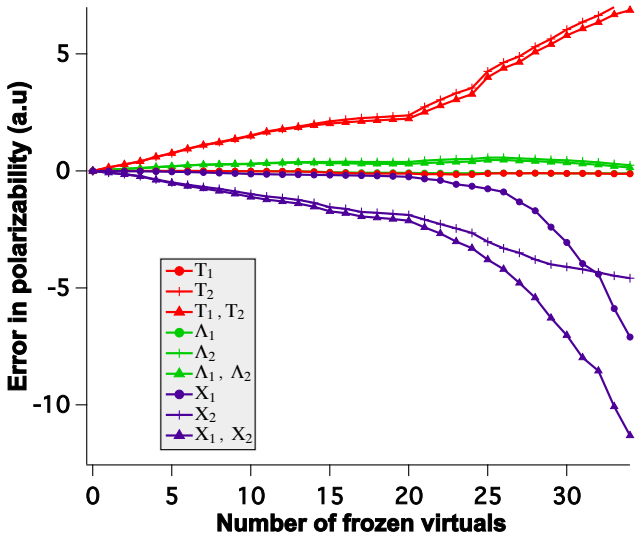

Figure 3.7: Errors introduced in CCSD/aDZ polarizabilities of H_2O_2 in the virtual CMO bases by the truncation of different classes of wave function amplitudes.

separately or pairwise seems to have negligible impact. In the case of the perturbed amplitudes, only small (negative) errors are introduced even after freezing all $\hat{X}_1$ amplitudes involving almost 23 virtual CMOs, but the error then rises sharply with further truncation. On the other hand, the negative errors due to truncation of $\hat{X}_2$ amplitudes are significant from the beginning and increase almost linearly. Thus the error due to removal of both $\hat{X}_1$ and $\hat{X}_2$ amplitudes belonging to the first 23 CMOs is due to elimination of $\hat{X}_2$ amplitudes alone, whereas beyond that limit, the total error corresponds to the sum of errors from $\hat{X}_1$ and $\hat{X}_2$ truncation.

A key observation is that, within the domain of the first 23 virtual CMOs, the positive

errors introduced by truncation of $\hat{T}_2$ are cancelled almost exactly by the negative errors arising from the truncation of $\hat{X}_2$. This is further illustrated in Fig. 3.8, which plots on

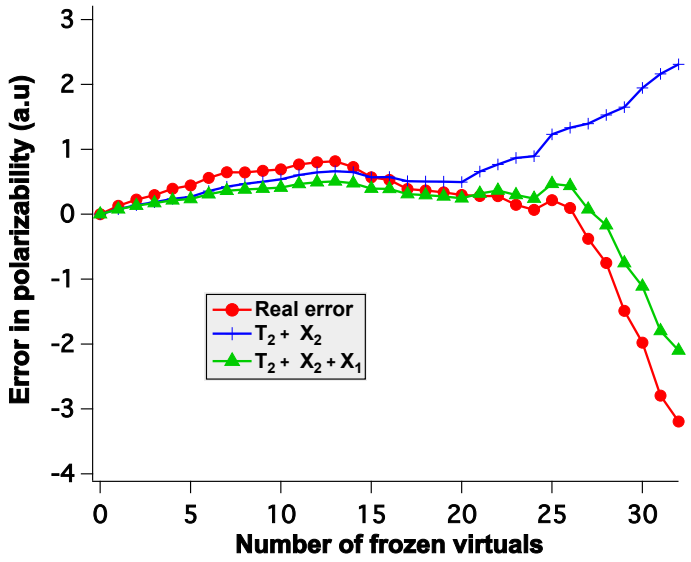

Figure 3.8: Errors introduced in CCSD/aDZ polarizabilities of H_2O_2 in the virtual CMO bases by the truncation of specific classes of wave function amplitudes as compared to the total errors obtained by freezing of virtual CMOs.

a narrow range the errors in the polarizability associated with truncating specific classes of $\hat{T}_2$ and $\hat{X}_2$ amplitudes against the total errors obtained by freezing CMOs entirely (for all amplitudes). Outside of this domain, errors associated with neglect of $\hat{X}_1$ amplitudes become dominant, leading to the accumulation of negative total errors observed in Fig. 3.3. Thus, the apparently robust performance of the truncation of the virtual CMO space arises, in fact, from offsetting errors.

Similarly to the above analysis for the virtual CMO space, Fig. 3.9 reports errors in the

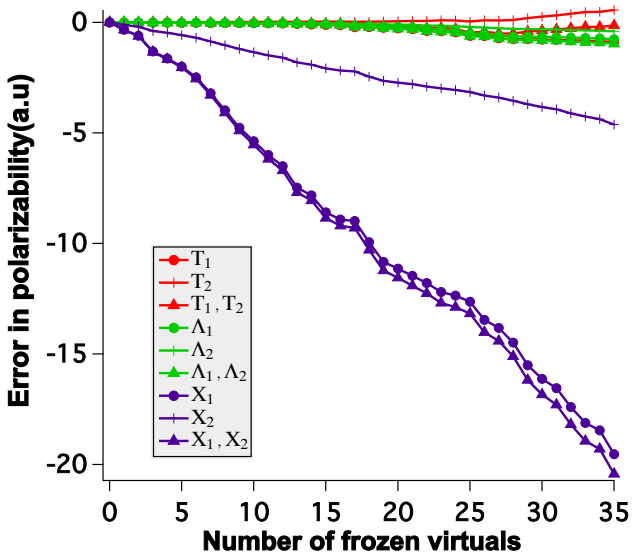

Figure 3.9: Errors introduced in CCSD/aDZ polarizabilities of H_2O_2 in the virtual NO bases by the truncation of different classes of wave function amplitudes.

CCSD/aDZ polarizability of H_2O_2 introduced by the neglect of various classes of wave function amplitudes associated with selected virtual NOs. We observe first that, unlike the CMO case, neglecting $\hat{T}_2$ amplitudes associated with particular virtual NOs has no significant effect on the error. This behavior is expected, because the $\hat{T}_2$ amplitudes are, by construction, sparse in the virtual NO basis such that orbitals with low occupation numbers are associated with $\hat{T}_2$ amplitudes of smaller magnitude. Furthermore, just as in the CMO case, the removal of $\hat{T}_1$, $\hat{\Lambda}_1$ and $\hat{\Lambda}_2$ amplitudes introduces only small errors, while the removal of selected $\hat{X}_2$ amplitudes based on NOs yields significant negative errors that increase linearly with the

number of virtual NOs truncated.

However, unlike the virtual CMO case, neglecting $\hat{X}_1$ amplitudes corresponding to specific virtual NOs introduces large negative errors in the polarizability even from the first NO removed, and the total error obtained by truncating both $\hat{X}_1$ and $\hat{X}_2$ amplitudes is almost the same as the error due to truncation of the $\hat{X}_1$ amplitudes alone. Indeed, the greatest contribution ($> 90\%$) to the total polarizability errors arises from the perturbed singles amplitudes.

The significance of the $\hat{X}_1$ amplitudes is evident upon analysis of their leading-order contribution to the polarizability [cf. Eq. (3.8)],

$$\alpha_\omega \leftarrow \frac{1}{3}\sum_{ia}\sum_{x}\mu_{ia}^{x}(X_{ia}^{x}(\omega) + X_{ia}^{x}(-\omega)), \tag{3.10}$$

where μ_{ia}^{x} is an element of the occupied-virtual block of the Cartesian component, x, of the electric-dipole moment integral matrix, and the inner sum runs over all such components. The singles themselves are obtained from the corresponding form of Eq. (3.7),

$$\langle\Psi_i^a|X_\omega^\mu|\Psi_0\rangle = -\sum_{\nu}\langle\Psi_i^a|(\bar{H}-\omega)^{-1}|\nu\rangle\langle\nu|\bar{\mu}|\Psi_0\rangle, \quad \nu \in \{\Psi_j^b, \Psi_{jk}^{cd}\}, \tag{3.11}$$

where $\bar{\mu}$ is the similarity transformed electric-dipole operator,

$$\bar{\mu} = \hat{\mu} + \left[\hat{\mu}, \hat{T}\right] + \frac{1}{2}\left[\left[\hat{\mu}, \hat{T}\right], \hat{T}\right]. \tag{3.12}$$

The corresponding leading-order contribution to the $\hat{X}_1$ amplitudes themselves is

$$X_{ia}^{\mu}(\omega) \leftarrow \frac{\mu_{ia}}{\overline{H}_{ii} - \overline{H}_{aa} + \omega}, \tag{3.13}$$

where the largest contribution to the diagonal elements of the similarity transformed Hamiltonian, $\bar{H}$, arises from the orbital energies (more precisely, the diagonal Fock matrix elements expressed in the CMO or NO basis), which are plotted in Fig. 3.10. While the values for the

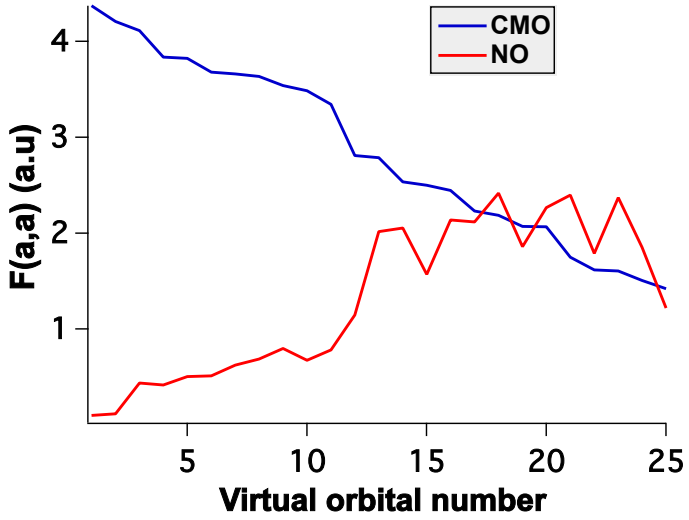

Figure 3.10: Virtual diagonal elements (a.u.) of the Fock matrix (F) in the CMO and NO bases.

virtual CMOs decrease steadily, their NO counterparts actually *increase* and display greater oscillation. Clearly, the diagonal elements of the Fock matrix for virtual NOs are significantly smaller in magnitude than the corresponding CMOs, which concomitantly increases the values of the $\hat{X}_1$ amplitudes associated with such NOs. This effect can be seen in Fig. 3.11 which plots the sum of the absolute values of $\hat{X}_1$ amplitudes for a given virtual orbital, i.e.

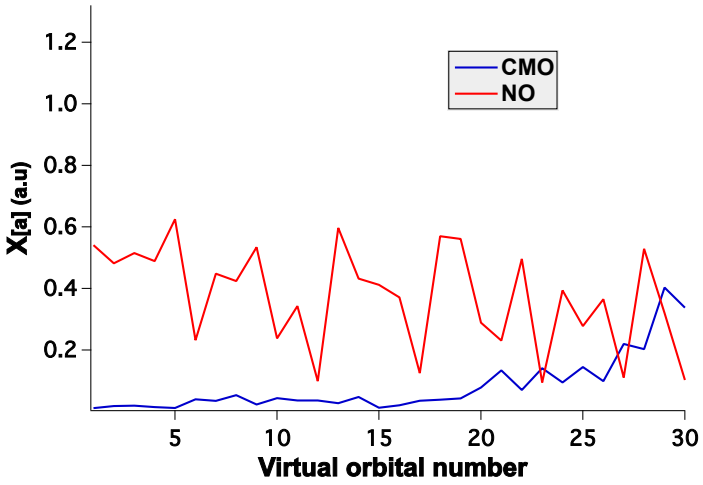

Figure 3.11: Sum of the absolute values of $\hat{X}_1$ amplitudes for a given virtual, $\sum_i |X_i^a|$, for perturbation μ_x and frequency 589 nm, plotted for each virtual NO or CMO.

$\sum_i |X_i^a|$, for both virtual CMOs and NOs. Thus, the sparsity of the $\hat{X}_1$ amplitudes present in the CMO basis is almost completely lost in the NO basis, which leads to the large errors in dynamic polarizabilities due to the truncation of $\hat{X}_1$ amplitudes in the NO basis observed earlier.

Furthermore, the dependence of the $\hat{X}_1$ amplitudes on both $\hat{T}_2$ and $\hat{X}_2$ plays a significant role in the overall *sign* of the polarizability error. This point is clearly illustrated in Fig. 3.12, which plots the 2-norm of the $\hat{X}_1$ vector as $\hat{T}_2$ or $\hat{X}_2$ amplitudes associated with a given

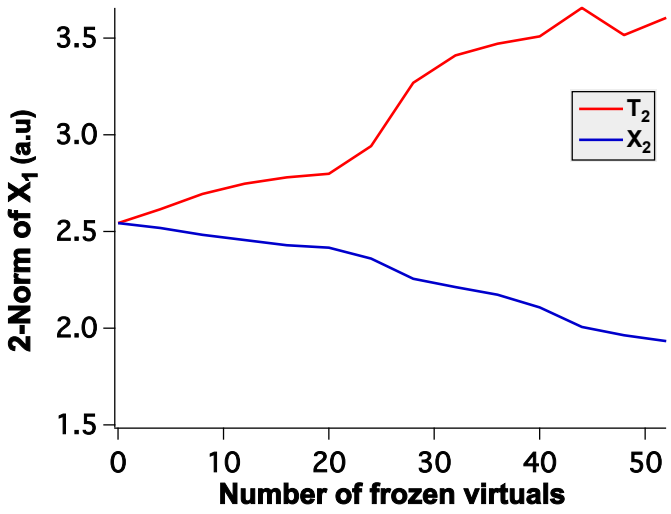

Figure 3.12: The 2-norm of the $\hat{X}_1$ amplitude vector in the CMO bases as a function of the truncation of classes of unperturbed $\hat{T}_2$ and perturbed $\hat{X}_2$ amplitudes.

virtual CMO are neglected (in the same manner as used in Figs. 3.7 and 3.8). As the $\hat{T}_2$ amplitudes associated with a given virtual orbital are removed, the norm of the $\hat{X}_1$ vector increases, leading to the positive errors in the polarizability observed in Fig. 3.7. On the other hand, removal of $\hat{X}_2$ amplitudes leads to a decrease in the norm of the $\hat{X}_1$ vector and the negative errors in the polarizability appearing in Fig. 3.7.

3.4.3 External-Space Corrections

As noted earlier, a key aspect of the strong performance of virtual NOs for correlation energies is the use of MP2-based corrections for the contributions of the truncated or "external" virtual space, as given in Eq. (3.9). When considering a similar correction for properties, however, we have explored three options: time-dependent Hartree-Fock (TDHF) and both static and dynamic CC2[12] corrections. In each case, we have used the same MP2-based virtual NO space and computed the correction as the difference between the full-virtual space polarizability and the truncated virtual-NO polarizability, with the CCSD/aDZ results for polarizabilties of H_2O_2 shown in Fig. 3.13. The CC2-based corrections recover nearly all of

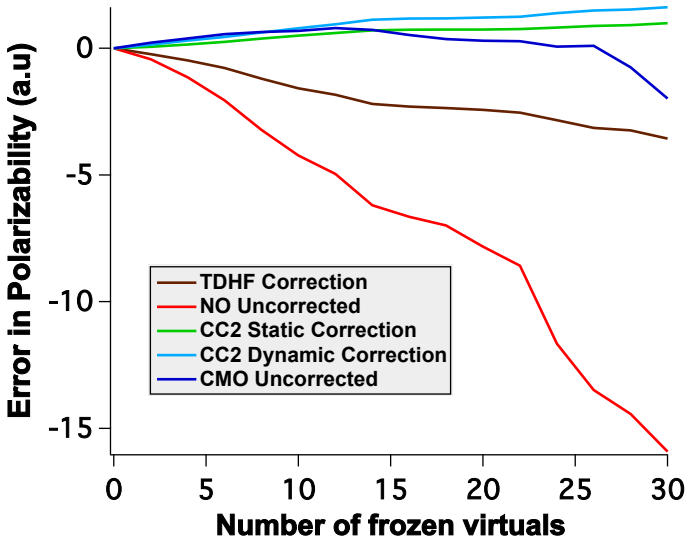

Figure 3.13: Correction schemes for the external truncated NO space for the CCSD/aDZ polarizabilities of H_2O_2.

the error associated with the uncorrected virtual NO space across a wide range of truncation, with the static correction actually yielding slightly smaller errors than its dynamic counterpart. The less expensive TDHF corrections offer significant improvement over the original virtual NO results, and recover most (ca. 85%) of the error until about 40% (21 orbitals) of the virtual space has been deleted, but they clearly produce overall larger errors than the correlated methods. In addition, the TDHF corrections are potentially problematic because the pole structure of the polarizability naturally follows that of the underlying Hartree-Fock perturbed orbitals rather than that of the correlated wave functions,[3, 30, 67] a criticism that would also hold for purely MP2-based corrections. On the other hand, the CC2-based corrections are significantly more expensive than TDHF, in part because of their iterative nature and the need to transform two-electron integrals involving three virtual orbitals (with the latter criticism again holding for an MP2-based correction).

3.4.4 Perturbed Natural Orbitals

Given that the purpose of the NOs is to "focus" the important components of the basis for the description of electron correlation effects into a compact space, without consideration of the importance of the basis set for other properties, an alternative approach might be to build a virtual space that explicitly takes such properties into account, such as the inclusion of the perturbed one-electron density in the definition of the space. Instead of diagonalizing the ground-state MP2 density, we diagonalize its gradient with respect to the external electric field, thereby incorporating the effects of the external perturbations. The

resulting "occupation numbers" obtained thus carry information about orbital occupancies in the perturbed states. The x^{th} Cartesian component of the perturbed density matrix can be written in terms of spin orbitals as

$$\gamma^x_{ab} = \frac{1}{2}\sum_{ijc} P_+(a,b)\left[\frac{t^{bc}_{ij}}{D^{ac}_{ij}}\left(P_-(a,c)\sum_d t^{ad}_{ij}\mu^x_{cd} - P_-(i,j)\sum_m t^{ac}_{im}\mu^x_{mj}\right)\right] \tag{3.14}$$

where P_+ and P_- are symmetric and anti-symmetric permutation operators, respectively, and the orbital-energy denominator $D^{ac}_{ij} = \epsilon_i + \epsilon_j - \epsilon_a - \epsilon_c$. (For computational convenience, orbital relaxation terms have been neglected.) To obtain the perturbed NOs and their corresponding eigenvalues, we take an average of the three cartesian components of the density and diagonalize the result. The eigenvalues consist of both positive and negative values as the perturbed density matrix is not positive definite, and thus we truncate the orbitals based on the absolute values of these eigenvalues. Fig. 3.14 compares the performance of these perturbed NOs with that of the CMOs and NOs, where the error in the CCSD/aDZ dynamic polarizability of H_2O_2 is plotted as a function of the number of virtual orbitals removed. While the perturbed NOs lower the truncation errors associated with conventional NOs, they still introduce significantly higher errors than the corresponding CMOs. The reason for this underperformance is related to the definition of the perturbed density, which naturally bears strong similarity to its unperturbed counterpart [cf. Eqs. (3.4) and (3.14)]. As a result, similar sparsity and orbital energy issues illustrated in Figs. 3.10 and 3.11 arise for the perturbed density just as for the original NOs, indicating that such an approach does

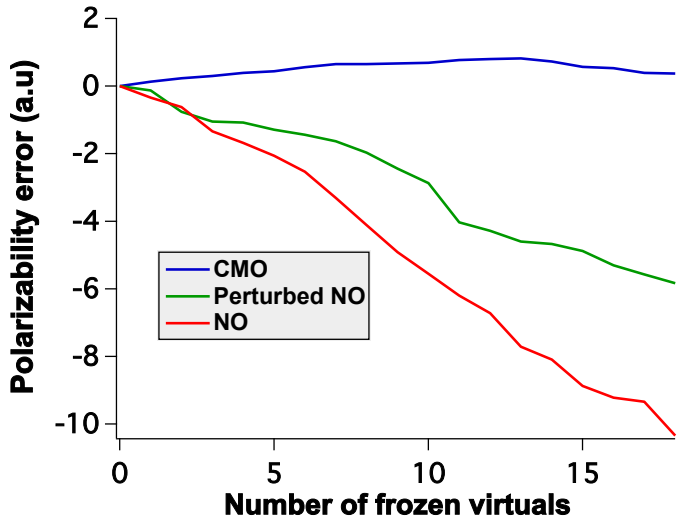

Figure 3.14: Errors introduced in CCSD/aDZ polarizabilities of H_2O_2 in the virtual CMO and NO bases, as well as the perturbed virtual NO basis as a function of number of virtual orbitals removed.

not resolve the problem.

3.4.5 The Dipole-Amplitude Criterion

The above results demonstrate that the CMO basis provides the best performance among the various virtual spaces considered here, albeit based on cancellation of errors. But what criterion should be used to determine the truncation level that provides optimal balance between computational cost (most compact virtual space) and accuracy? The CMO orbital energies are one possibility, but they have no direct connection to the properties in question. Another alternative is the "dipole amplitude", d_a, which is defined for each virtual CMO as

$$d_a \equiv \sum_x \sum_i \frac{(\mu_{ia}^x)^2}{\epsilon_i - \epsilon_a}. \tag{3.15}$$

This expression, which is trivially computed post-Hartree-Fock, is based on Eqs. (3.10) and (3.13), using the fact that the leading contributions to the diagonal elements of the similarity-transformed Hamiltonian are the orbital energies. As we are constructing a phenomenological truncation criterion, we have chosen to neglect the dependence on the field frequency. Fig. 3.15 plots the values of the dipole amplitude for each CMO, as well as the

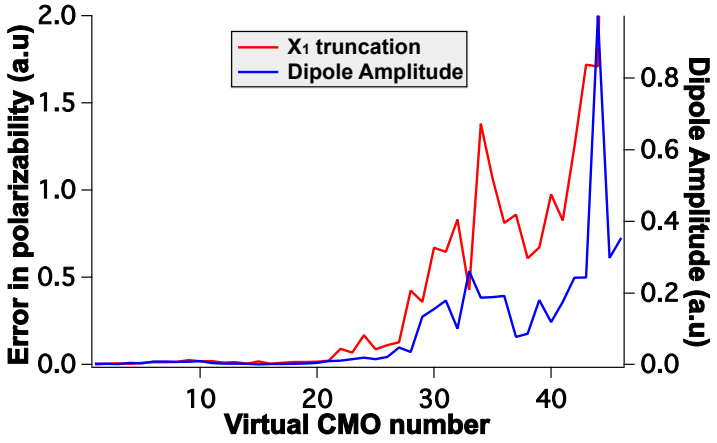

Figure 3.15: Absolute errors introduced in CCSD/aDZ polarizabilities of H_2O_2 due to truncation of $\hat{X}_1$ amplitudes and dipole amplitudes plotted as a function of different virtual CMOs.

corresponding error in the CCSD/aDZ dipole-polarizability of H_2O_2 introduced by deleting the $\hat{X}_1$ amplitude associated with a given virtual CMO. There is a clear correlation between

the two functions, and one can see that as both the error due to truncation of $\hat{X}_1$ and the value of the dipole amplitude increase sharply once we reach CMOs 27-28 — ca. 50% of the virtual space for this test case. Accordingly, one should stop the truncation of the virtual CMO space once the dipole amplitude values start rising sharply. While the optimal choice of such a threshold will be addressed systematically in subsequent work, our preliminary analyses using H_2O_2, methyloxirane, dimethylallene, and related compounds suggest a cutoff of ca. 3-3.5% (of the total dipole amplitude) yields minimal errors in the polarizability.

3.5 Conclusions

On the basis of the above findings, we conclude that, in the absence of orbital relaxation, virtual NOs are not suited for higher-order property calculations such as dynamic polarizabilities, and that the occupation number is not an acceptable criterion for estimating the importance of a virtual orbital for such calculations. Although the use of external space corrections based on CC2 polarizabilities reduces the observed truncation errors, they are too relatively costly to be practical for large molecular systems. Furthermore, the use of perturbed virtual NOs offers only slight improvement as compared to unperturbed virtual NOs. CMOs, on the other hand, provide a much more stable mechanism for reducing the size of the virtual space — with truncation of up to 50% of the orbitals yielding shifts of less than 2% as compared to full-space calculation – but the source of their success lies in a significant cancellation of errors. Although further systematic studies are needed, the dipole amplitude

appears to provide a useful threshold for an *a priori* truncation of the CMO virtual space.

Chapter 4

Perturbed Natural Orbitals for Coupled-Cluster Linear-Response Theory

4.1 Introduction

One of the central problems limiting the application of accurate *ab initio* methods like coupled-cluster (CC) theory to large molecular systems is their high computational cost, i.e., their computing and storage requirements exhibit polynomial scaling with the size of the system or equivalently with the number of one electron basis functions used in these calculations. Specifically, the size of the virtual space is of greater concern since they usually far

outnumber the occupied orbitals. Furthermore, the canonical virtual orbitals obtained from the Hartree-Fock (HF) procedure are non-local in nature and hence, the convergence of a determinantal expansion involving these orbitals is quite slow. However, Löwdin [48]showed that using "natural orbitals" (NOs) instead of the canonical HF orbitals can significantly accelerate the convergence of the configuration interaction (CI) wavefunction expansion. The NOs are the eigenvectors of the one electron reduced density matrix (1-RDM) associated with a wavefunction. The corresponding eigenvalues are commonly referred to as "occupation numbers"(ONs). Since Löwdin's pioneering work, NOs have found a lot of applications especially in techniques aimed at obtaining a compact representation of the virtual space for correlated calculations[18, 19, 46, 84, 88, 89]. Please refer to ref.[46] for an excellent overview on this subject. Within the context of the CC theory, the frozen virtual NO (FVNO) scheme, where the NOs are usually obtained from the 1-RDM of a less expensive correlated method such as the second-order Möller-Plesset (MP2) theory and the virtual space for subsequent CC calculations is truncated based on the values of the ONs has been used quite successfully to calculate correlation energies, ionization energies, etc. For example, Landau et al.[46] demonstrated that even after the removal of 70% of the virtual space, the errors in the ionization energies of the organic compounds under study were less than 1 kcal/mol. However, it has been well established from previous studies that response properties are usually much more sensitive to the truncation of the wavefunction than simple energetics[43, 70, 71, 51, 25, 50]. Recently, we investigated the applicability of such approaches for properties like dynamic polarizabilities using CC linear reponse theory

[40]. In contrast with the earlier studies[45], we got huge errors in polarizabilities which increased almost linearly with the number of truncated virtual orbitals. It was found that the ground-state MP2 density used to generate the NOs was unable to capture the response of the wavefunction to the external field. For example, the FVNO procedure threw out first the diffuse virtual orbitals, which are known to be very important to describe the low lying Rydberg type excited states (a common feature in majority of chiral compounds), resulting in large errors. This was not unsurprising since these diffuse orbitals have very low contributions to the correlation energy and hence possess very low occupation numbers. Consistent with the findings of Sundholm and co-workers[79], dropping higher energy canonical HF virtual orbitals led to very small errors in polarizabilities due to a) cancellation of errors resulting from the truncation of unperturbed and perturbed doubles amplitudes and b) the smaller magnitudes of the perturbed singles amplitudes associated with such orbitals. We also constructed a first-order perturbed MP2 density by taking the gradient of the ground state MP2 density with respect to the electric field, hoping that the ONs obtained from this density would be a better metric for estimating the importance of a virtual orbital for response properties but this approach only offered minor improvements over the regular FVNO method. Nevertheless, a suite of methods, conceptually not very different from our perturbed density approach have been proposed recently to calculate CC excitation energies. Baudin and co-workers used natural transition orbitals (NTOs) obtained from approximate CIS(D) transition densities in a scheme which they call CorNFLEx for calculating CC2 excitation energies of large solvated formamide clusters[5]. In similar works, Höfener and Klopper ob-

tained effective virtual spaces by combining MP2 ground state density with excited state densities constructed from CIS excitation vectors[34] while Mester *et al.* used MP2 and CIS(D) amplitudes to define their optimal virtual and occupied spaces[54, 55]. These successful works prompted us to take back a closer look at the reasons behind the failure of our perturbed density approach. Finally, we have developed a new method which we call as FVNO++ where a second-order perturbed density is constructed to capture the response of the wavefunction to the external electric and magnetic fields. In this paper, we take a closer look at this scheme and report its performance in calculating CC dynamic polarizabilities and specific rotations of a number of chiral molecules.

4.2 Theoretical Background

4.2.1 Coupled Cluster Response Theory

The response functions for calculating dynamic higher-order properties can be defined by the frequency dependent coefficients appearing in the expansion of the expectation value of an appropriate time-independent operator in orders of the perturbation[40].

$$\begin{aligned}\langle A\rangle(t) = \langle A\rangle + \int_{-\infty}^{\infty} d\omega_1 \langle\langle A; V^{\omega_1}\rangle\rangle_{\omega_1 + i\alpha} e^{-i(\omega_1 + i\alpha)t} \\ + \frac{1}{2}\int_{-\infty}^{\infty} d\omega_1 \int_{-\infty}^{\infty} d\omega_2 \, \langle\langle A; V^{\omega_1}; V^{\omega_2}\rangle\rangle_{\omega_1 + i\alpha, \omega_2 + i\alpha} e^{-i(\omega_1+\omega_2+2i\alpha)t} + ...\end{aligned} \tag{4.1}$$

Here $\langle A \rangle$ is the time independent expectation value and $\langle\langle A; V^{\omega_1} \rangle\rangle_{\omega_1 + i\alpha}$ is the linear response function (LRF) i.e. the first order change in the expectation value of A in a time-dependent field V at frequency ω_1. The third term in the expansion contains the quadratic response function and so on. The CC-LRF is defined as,

$$\langle\langle A; B \rangle\rangle_{\omega_1} = \frac{1}{2}\hat{P}(A,B)[\langle 0|\ [\hat{Y}^B_{\omega_1}, \bar{A}]|0\rangle + \langle 0|\ (1+\hat{\Lambda})|[\bar{A}, \hat{X}^B_{\omega_1}]|0\rangle] \tag{4.2}$$

where A and B are the one electron perturbation operators, $\hat{P}(A,B)$ simultaneously interchanges operators A and B and takes the complex conjugate of the expression, ω_1 is the frequency of the external field, $|0\rangle$ is the reference wavefunction, $\hat{\Lambda}$ is a linear de-excitation operator that parametrizes the CC left hand wavefunction to make sure that the CC gradients satisfy the generalized Hellman-Feynman theorem[40], overbar on operataor A denotes similarity transformation with the ground state T operator, $\bar{A} = e^{-\hat{T}}\hat{A}e^{\hat{T}}$ and $\hat{X}^B_{\omega_1}$ and $\hat{Y}^B_{\omega_1}$ are the excitation operators involving the first-order right and left hand perturbed amplitudes corresponding to operator B respectively. These amplitudes can be obtained by solving a linear system of equations,

$$\begin{aligned}
&\sum_{\nu}\langle\mu|\big[(\bar{H}-\omega I), \tau_\nu\big]|0\ \rangle X^B_\nu = -\langle\mu|\bar{B}|0\rangle \\
&\sum_{\nu} Y^B_\nu\langle\nu|\big[(\bar{H}+\omega I), \tau_\mu\big]|0\rangle\ + \langle 0|(1+\hat{\Lambda})|\big[\big[\bar{H}, \tau_\nu\big], \tau_\mu\big]|0\rangle\ X^B_\nu = -\langle 0|(1+\hat{\Lambda})|\big[\bar{B}, \tau_\mu\big]|0\rangle.
\end{aligned} \tag{4.3}$$

Here τ_μ, τ_ν are the excitation operators which when acting on the reference wavefunction $|0\rangle$ create excited determinats $|\mu\rangle$ and $|\nu\rangle$ respectively. Also, the dependence of perturbed amplitudes on ω_1 is assumed. The right hand amplitudes are solved first after which they enter into the left hand amplitude equations as inhomogenous terms. It should be noted that these equations need to be solved for every cartesian component of the given perturbation operators. For example, calculation of optical rotation tensor using the length-gauge representation of the dipole operator would require solving a total of 12 linear equations, six each for both electric and magnetic dipole perturbation.

4.2.2 Perturbed Natural Orbitals

The CC-LRF (eq. 4.9) can also be formulated in terms of perturbed densities,

$$\langle\langle A;B\rangle\rangle_{\omega_1} = \frac{1}{2}\hat{P}(A,B)\big[\sum_{pq} A_{pq}[D_{pq}^{B^{\omega_1}}]^{(1)}\big] \tag{4.4}$$

where $[D^{B^{\omega_1}}]^{(1)}$ is the frequency dependent first-order perturbed one-electron density related to operator B. The structures of the virtual-virtual blocks of perturbed densities of different orders (for a given perturbation operator) can be easily identified in spin orbitals,

$$\begin{aligned}
D_{ab}^{(0)} &= \frac{1}{2}(\lambda_{ac}^{ij})^{(0)}(t_{ij}^{bc})^{(0)} \; + (\lambda_a^i)^{(0)}(t_i^b)^{(0)} \\
D_{ab}^{(1)} &= \frac{1}{2}[(\lambda_{ac}^{ij})^{(0)}(t_{ij}^{bc})^{(1)} \; + (\lambda_{ac}^{ij})^{(1)}(t_{ij}^{bc})^{(0)}] + [(\lambda_a^i)^{(0)}(t_i^b)^{(1)} \; + (\lambda_a^i)^{(1)}(t_i^b)^{(0)}] \\
D_{ab}^{(2)} &= \frac{1}{2}[(\lambda_{ac}^{ij})^{(1)}(t_{ij}^{bc})^{(1)} \; + (\lambda_{ac}^{ij})^{(0)}(t_{ij}^{bc})^{(2)}] \; + [(\lambda_a^i)^{(1)}(t_i^b)^{(1)} + (\lambda_a^i)^{(0)}(t_i^b)^{(2)}].
\end{aligned} \tag{4.5}$$

In the above equations, the indices i, j and a, b, c refer to occupied and virtual orbitals respectively and Einstein summation notation is used. The first order perturbed amplitudes $(\lambda_{ac}^{ij})^{(1)}$ and $(t_{ij}^{bc})^{(1)}$ are nothing but the $\hat{X}_{\omega_1}^B$ and $\hat{Y}_{\omega_1}^B$ amplitudes that we saw earlier.

Just as the ground state MP2 density can transfer its knowledge of the electron correlation effects to the one electron basis (virtual NOs) through diagonalization, the perturbed densities can be used in a similar way to construct a compact "perturbation aware" basis. In our earlier work, we constructed a guess first-order perturbed density associated with each cartesian component (x,y,z) of the perturbation operator (electric dipole in the case of polarizabilities) from MP2 amplitudes, took an average of the three densities and then diagonalized it to obtain our virtual space, but this approach offered only a minor improvement[45]. To investigate the reason behind the failure of this model, we constructed the virtual-virtual block of the full CCSD first-order perturbed density. All the diagonal elements of this density matrix were found to be zeros irrespective of the perturbation operator. The exact reason for this is not yet understood but clearly, the virtual NOs (VNOs) obtained from this (or guess) density do not carry any useful information. However, since the polarizabilities and specific rotations are of second-order in perturbation, we realized that second-order perturbed densities should in principle be a better metric for estimating the importance of a VNO for these properties. In this paper, we use an average of second-order guess densities corresponding to each cartesian component of an appropriate perturbation operator to define our virtual space for correlated response calculations. For a perturbation operator A, this guess density looks like:

$$[D^A_{ab}]^{(2)} = \frac{1}{2}[t^{ac}_{ij}(A)]^{(1)}[t^{bc}_{ij}(A)]^{(1)} + [t^a_i(A)]^{(1)}[t^b_i(A)]^{(1)}. \tag{4.6}$$

where

$$\begin{aligned} t^{ac}_{ij}(A)^{(1)} &= \frac{\bar{A}^{ac}_{ij}}{\overline{H}_{aa} + \overline{H}_{cc} - \overline{H}_{ii} - \overline{H}_{jj}}, \\ t^a_i(A)^{(1)} &= \frac{\bar{A}^a_i}{\overline{H}_{aa} - \overline{H}_{ii}}. \end{aligned} \tag{4.7}$$

and

$$\begin{aligned} \overline{A}^{ac}_{ij} &= P^{ac}_{ij}(t^{ec}_{ij}A^a_e - t^{ac}_{mj}A^m_i), \\ \overline{H}_{ii} &= f_{ii} + t^{ef}_{in}(2\langle in|ef\rangle - \langle in|fe\rangle), \\ \overline{H}_{aa} &= f_{aa} - t^{fa}_{mn}(2\langle mn|fa\rangle - \langle mn|af\rangle), \end{aligned} \tag{4.8}$$

where f refers to the Fock matrix. The above equations are derived by using the MP2 amplitudes for the similarity transformation, ignoring the terms involving second-order perturbed amplitudes and approximating the first-order perturbed λ amplitudes with the corresponding t amplitudes. The structure of the guess density chosen above becomes clearer if one looks at the equations for solving the first-order right-hand perturbed amplitudes (eq. 4.3) in terms of the inverse of the CC Jacobian,

$$\begin{aligned} t^{ac}_{ij}(A)^{(1)}(\omega_1) &= \sum_\mu -\langle\Phi^{ac}_{ij}|(\bar{H} - \omega_1 I)^{-1}|\mu\rangle\langle\mu|\bar{A}|0\rangle, \\ t^a_i(A)^{(1)}(\omega_1) &= \sum_\mu -\langle\Phi^a_i|(\bar{H} - \omega_1 I)^{-1}|\mu\rangle\langle\mu|\bar{A}|0\rangle \end{aligned} \tag{4.9}$$

It can be easily seen that the guesses for $t^{ac}_{ij}(A)^{(1)}$ and $t^a_i(A)^{(1)}$ amplitudes in this work have

been chosen by only considering the diagonal elements of the $(\bar{H} - \omega_1 I)^{-1}$ matrix, which can be justified due to the diagonally dominant nature of the $\bar{H}$ matrix. Furthermore, we keep ω_1 as zero as we want to use the same density matrix for a given property calculation at different frequencies. We also assume that removing ω_1 should not significantly change the sparsity pattern of the perturbed amplitudes.

Finally, the basic outline of this approach involves doing an MP2 calculation, generation of guess densities using MP2 amplitudes and perturbation operators, diagonalization of the virtual-virtual block of the guess density to obtain VNOs, truncation of VNOs with occupation numbers below a given threshold, diagonalization of the Fock matrix in the truncated VNO basis to obtain a semi-canonical basis, transformation of all the one and two electron integrals to this semi-canonical basis, followed by CCSD-LR calculations at given frequencies.

4.3 Computational Details

The main target of this work is large scale CC2[12]/CCSD calculations of specific rotations of solvated molecular clusters. However, first, we need to ensure that the FVNO++ approach has the right convergence behavior towards the full canonical result. In this regard, we carry out dynamic polarizabilities and specific rotation calculations on linear chiral systems like hydrogen peroxide and hydrogen dimer (P)-$(H_2)_n$ helices as they provide a convenient model for estimating the efficiency of these truncation schemes.

4.3.1 Polarizabilities

Polarizability calculations on these chiral molecules can mostly be as seen as a diagnostic tool for gaining an insight into the nature of specific rotation calculations as one truncates the virtual space. Even though the response functions of both the properties are quite similar, polarizabilities are much less sensitive to the wavefunction truncation. However, the results on polarizabilities obtained in this work can be extended to non-chiral systems as well. In all these calculations, the length-gauge (LG) representation of the electric dipole operator was used. The natural choice of the perturbed densities for such calculations would be $\sum_q \frac{1}{3}[D_{ab}^{\mu_q}]^{(2)}$, where $q \equiv [x, y, z]$.

4.3.2 Specific Rotations

All the specific rotation calculations in this work employ the LG representation. Even though LG specific rotations are dependent on the choice of origin for the CC2/CCSD-LR method, they are a good starting point for our analysis as they show a faster convergence towards the CBS (complete basis set) limit than the velocity gauge (VG) representation. Since these calculations involve both electric and magnetic dipole operators, we use, in addition to the electric dipole based densities, i.e. FVNO++ (μ), two other approaches of defining our virtual space. The first approach, FVNO++ ($\mu * L$) builds the density as a product of the first order amplitudes corresponding to the electric and magnetic perturbations (L). However, this makes the density matrix non positive -definite and both positive and negative

eigenvalues appear as a result. Nevertheless, we truncate these "VNOs" based on the absolute values of their "ONs". The second approach, FVNO++ (μ, L) builds two truncated VNO spaces (50% in this work) based on the densities of the electric and magnetic dipole operators individually and does a singular value decomposition on the union of the two spaces. Finally, just like before, the VNOs are truncated based on their singular values. We report the performance of all three approaches in this work. The primary basis set used in this work is aug-cc-pVDZ[20, 38, 92] and all the property calculations were carried out at 589 nm using using Psi4 and Psi4Numpy software packages.[60, 83] It should be noted that we have used the same virtual space for calculating both unperturbed and perturbed amplitudes as this ensures a match with results obtained from the finite-field procedures. The use of only perturbed densities for solving both unperturbed and perturbed amplitudes can be justified due to an inherent insensitiviy of these response properties to the values of the ground state amplitudes. For example, Table 4.1 shows that the values of specific rotations and polarizabilities obtained using the CCSD-LR(1) scheme which involves only one iteration of the CCSD $\hat{T}$ equation while approximating the λ_μ amplitudes with the corresponding t_μ amplitudes, are very close to the full canonical result (CCSD-LR).

4.4 Results and Discussion

We demonstrated the importance of diffuse virtual orbitals for calculating dynamic polarizabilities of hydrozen peroxide in our previous work. Thus, a better approach for calculating

Table 4.1: Comparison of the canonical CCSD-LR polarizabilities in atomic units (α) and specific rotations ($[\alpha]$) in deg $dm^{-1}(g/mL)^{-1}$ of different test cases calculated at 589 nm with that of the approximated CCSD-LR(1) scheme.

	CCSD-LR(1)		CCSD-LR	
Molecules	α	$[\alpha]$	α	$[\alpha]$
H_2O_2	14.2	-175.3	14.2	-185.5
$(H_2)_4$	19.6	1357.9	19.3	1322.9
$(H_2)_5$	24.1	1409.3	23.8	1380.6
$(H_2)_6$	28.7	1542.7	28.2	1508.8
$(H_2)_7$	33.0	1643.0	32.5	1606.3

response properties with natural orbitals would be to preserve these diffuse orbitals and apply the FVNO procedure to the "non-diffuse" virtual space only where the orbital spatial extent (OSE), $\langle\phi_a|r^2|\phi_a\rangle$, can be taken as a measure of the diffusivity of a virtual orbital (ϕ_a). Hence, we sorted the virtual canonical MOs according to their OSEs and chose an empirical cutoff that that led to the retention of the 26 most diffuse orbitals for the H_2O_2 molecule in the aDZ basis. The MP2 ground stare density matrix is then created and diagonalized in the remaining (29) virtual space and the VNOs with low ONs are removed one by one. We refer to this modified FVNO scheme as FVNO(M). Fig. 4.1 compares the performances of both the approaches for calculating CCSD dynamic polarizabilities and specific rotations

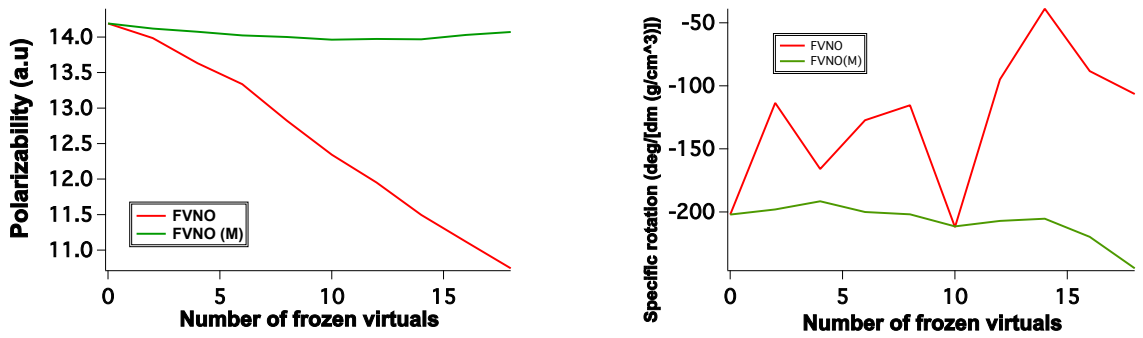

(a) (b)

Figure 4.1: CCSD/aDZ polarizabilities (a) and specific rotations (b) of H_2O_2 in both FVNO and FVNO(M) schemes as a function of the number of virtual orbitals removed.

of the H_2O_2/aDZ system at 589 nm. Unsurprisingly, the errors in the FVNO(M) scheme are minimal compared to the original scheme for both polarizabilities and specific rotations even after 18 (out of 29) "non-diffuse" VNOs are removed. Specifically, the specific rotations curves are much better behaved in the FVNO(M) approach. Similar trends can be observed for other excited state properties like excitation energies, oscillator strengths and rotational strengths as well. Figure 4.2 plots the EOM-CCSD excitation energies and rotational strengths for the lowest four excited states of the H_2O_2/aDZ system in both FVNO and FVNO(M) procedures as a function of the number of virtual orbitals removed. It can be easily observed that the FVNO(M) curve is very well-behaved for both the properties for all the four states and the errors in excitation energies are less than 0.1 eV even after removing as many as 18 virtual orbitals i.e. 33 % of the virtual space. The rotational strengths also see a drastic improvement in the FVNO(M) scheme, (especially the second lowest excited state). It should be noted that similar results can be expected for a majority of chiral molecules who

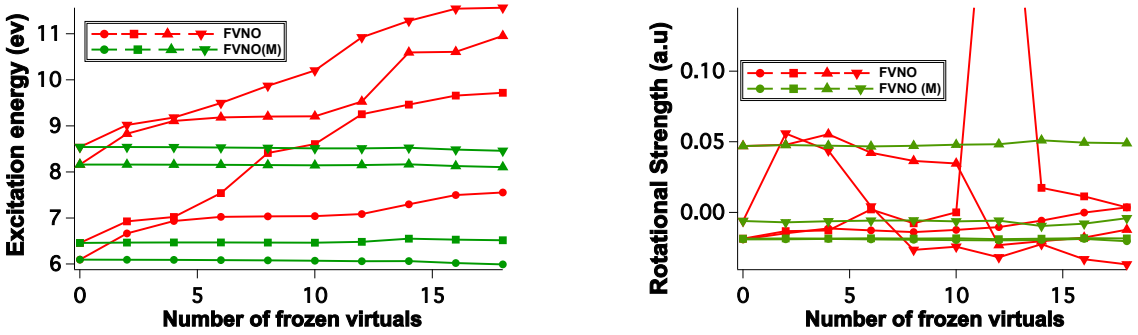

(a) (b)

Figure 4.2: EOM-CCSD/aDZ excitation energies (a) and rotational strengths (b) of the lowest four excited states of H_2O_2 in both FVNO and FVNO(M) schemes as a function of the number of virtual orbitals removed.

like hydrogen peroxide require diffuse orbitals for a better description of the Rydberg states. However, extension of this method to larger systems is not straightforward as OSEs are not a very robust crietrion for the selction of diffuse orbitals. Furthermore, not all diffuse orbitals are equally important for calculating these response properties. The FVNO++ scheme on the other hand has a very well-defined truncation criterion based on ONs and the structure of the perturbed density used in this approach closely resembles the response functions used to calculate these properties. Thus, the FVNO++ approach, by construction, should mimic the performance of the FVNO(M) scheme as seen above. Fig. 4.3 compares the performances of both FVNO and FVNO++(μ) approaches for calculating CCSD dynamic polarizabilities and specific rotations for the same system as above. The FVNO++ scheme indeed captures the contribution of VNOs to the response of the wavefunction in the right manner. As a result, the removal of VNOs with low ONs seems to have negligible effect on both polarizabilities and specific rotations. Specific rotations can be seen to be more sensitive than

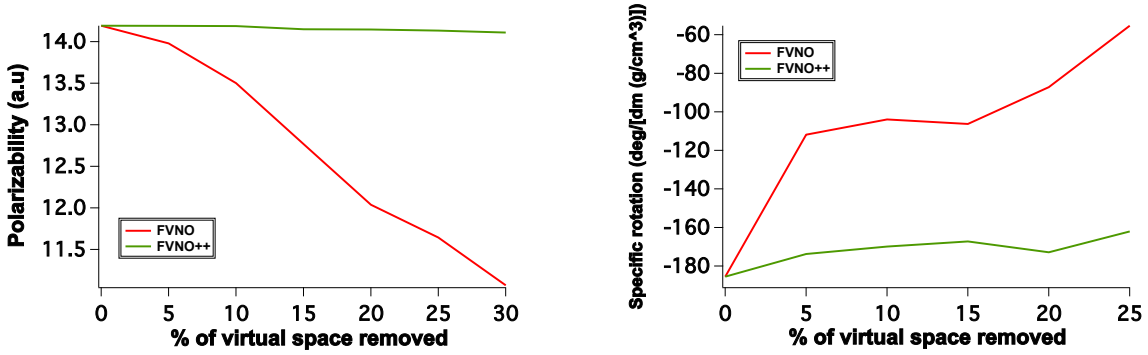

(a) (b)

Figure 4.3: CCSD/aDZ dynamic polarizabilities (a) and specific rotations (b) of H_2O_2 in both FVNO and FVNO++ schemes as a function of number of virtual orbitals removed.

polarizabilities with respect to truncation of orbitals in both the methods. However, the deviations with respect to the full canonical result in the FVNO++ approach are minimal compared to the FVNO scheme. Fig. 4.4 and Fig. 4.5 extends the comparison of the two schemes to the linear $(H_2)_n$ helices. As expected , the errors in the FVNO++ scheme for both polarizabilities and specific rotations are very small even after the removal of as much as 30% of the virtual space for all the four helices. For the $(H_2)_7$ system, the errors in the polarizability in the FVNO and FVNO++ methods are approximately 7% and 0.4% respectively after truncation 30% of VNOs. For the same system and truncation percentage, the FVNO method gives opposite signs of specific rotations while the FVNO++ approach yields errors within 5%. We also investigated if the truncation errors associated with the FVNO++ approach can be minimized by optimizing the guess densities. In this regard, we carry out one iteration of the CC2 response equations with MP2 amplitudes to obtain the perturbed amplitudes to build the guess density. Fig. 4.6 plots the polarizabilities obtained

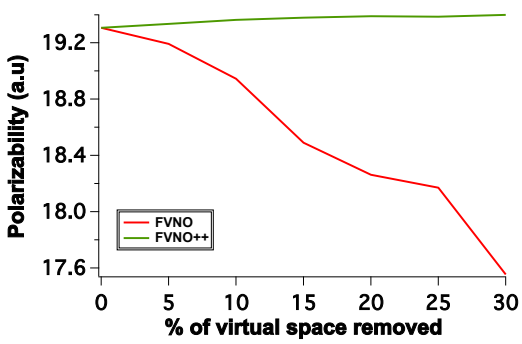

(a) $(H_2)_4$

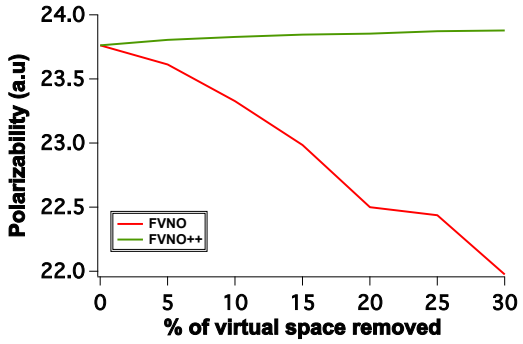

(b) $(H_2)_5$

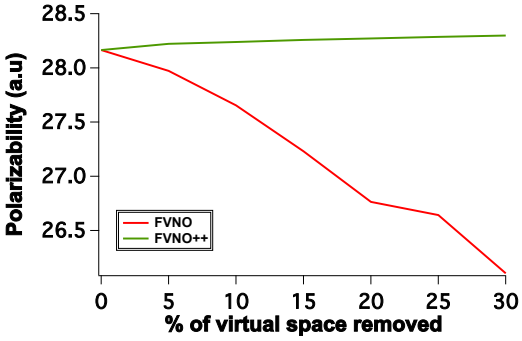

(c) $(H_2)_6$

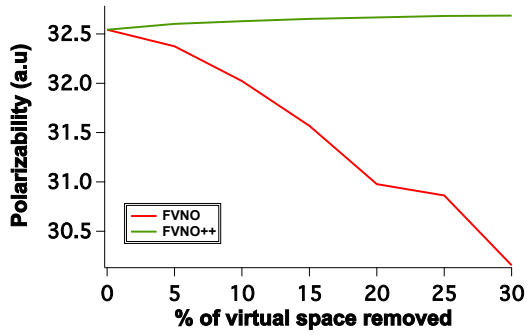

(d) $(H_2)_7$

Figure 4.4: CCSD/aDZ polarizabilities of $(H_2)_n$ helices, $n = 4 - 7$ in both FVNO and FVNO++ schemes as a function of percentage of virtual space removed.

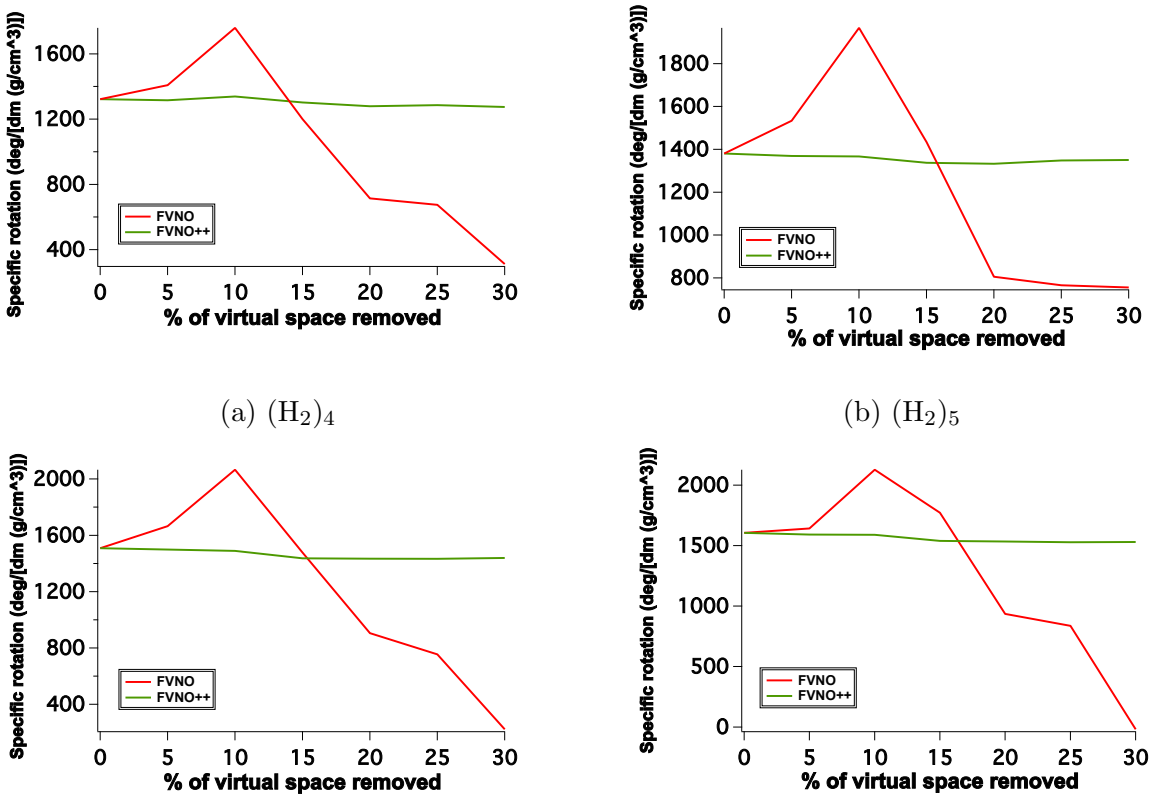

(a) $(H_2)_4$

(b) $(H_2)_5$

(c) $(H_2)_6$

(d) $(H_2)_7$

Figure 4.5: CCSD/aDZ specific rotations of $(H_2)_n$ helices, $n = 4-7$ in both FVNO and FVNO++ schemes as a function of percentage of virtual space removed.

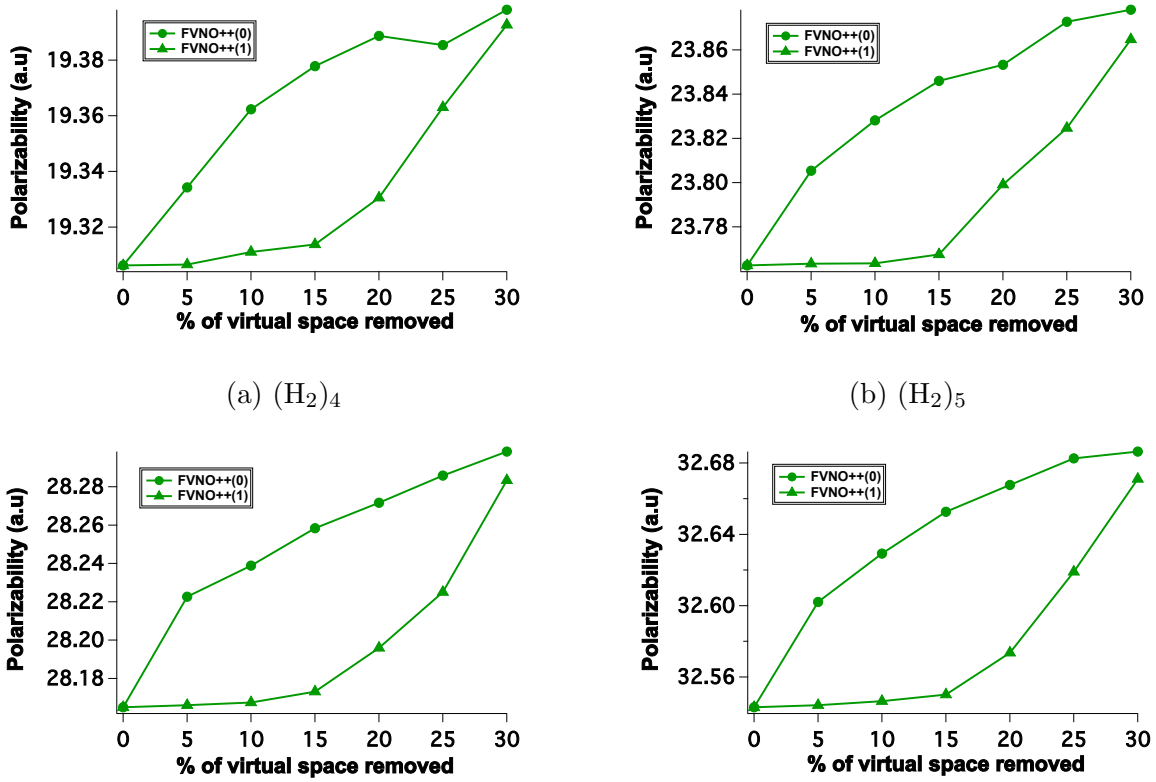

(a) $(H_2)_4$ (b) $(H_2)_5$

(c) $(H_2)_6$ (d) $(H_2)_7$

Figure 4.6: CCSD/aDZ polarizabilities of $(H_2)_n$ helices, $n = 4-7$ in both FVNO++(0) and FVNO++(1) schemes as a function of percentage of virtual space removed.

using this optimized density (FVNO++(1)) and compares them with the earlier approach (FVNO++(0)). It can be easily seen that the VNOs obtained from FVNO++(1) method are significantly more compact in the truncation range of up to 20%. However, the errors start increasing steeply there after and become comparable with that of the FVNO++(0) approach indicating that the aDZ basis set for these small systems is fairly compact. For specific rotations, (fig. 4.7) the results obtained using both the schemes are comparable up to a truncation of 10% after which the errors in the FVNO++(0) method start rising sharply.

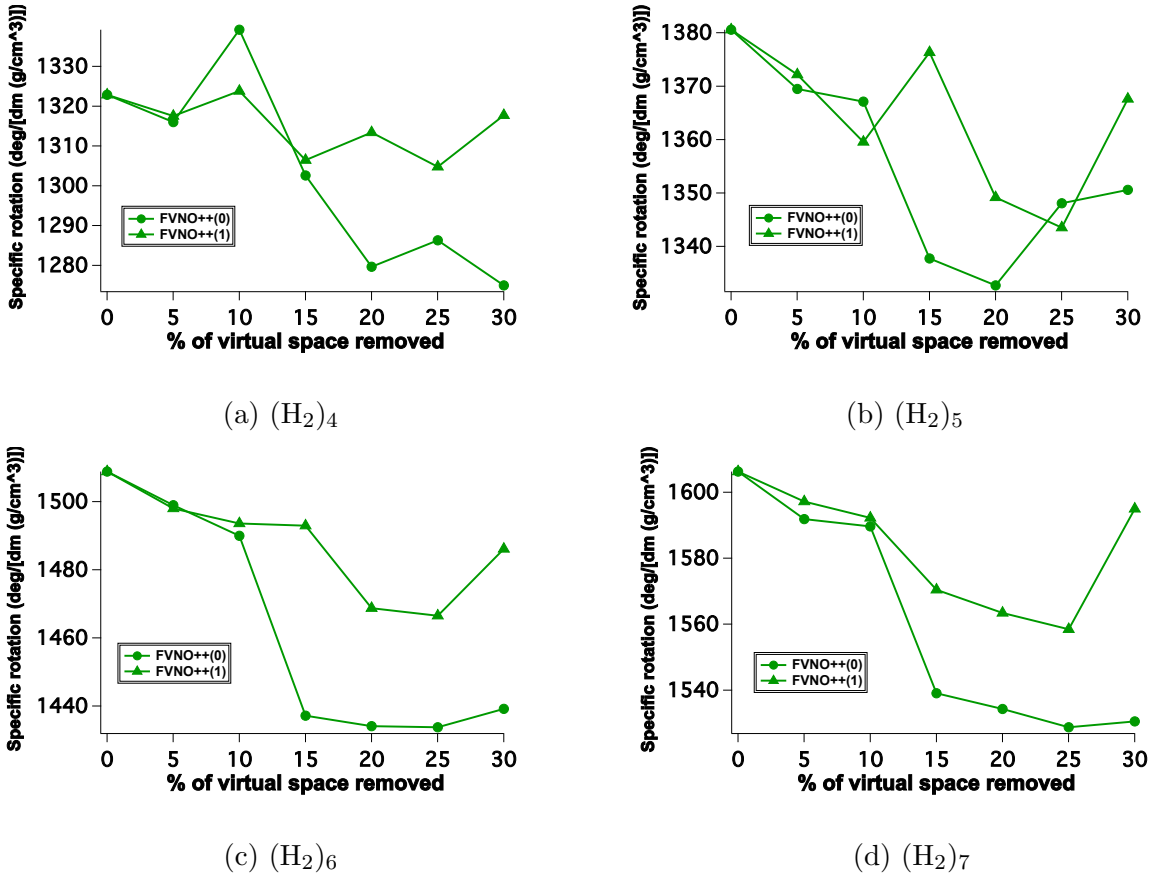

(a) $(H_2)_4$ (b) $(H_2)_5$

(c) $(H_2)_6$ (d) $(H_2)_7$

Figure 4.7: CCSD/aDZ specific rotations of $(H_2)_n$ helices, $n = 4-7$ in both FVNO++(0) and FVNO++(1) schemes as a function of percentage of virtual space removed.

For the $(H_2)_7$ molecule, the FVNO++(1) approach gave a maximum error of only 3% (earlier 5%) for the plotted truncation range.

As mentioned before, we also tested the performance of two new approaches, FVNO++ $(\mu * L)$ and FVNO++ (μ, L) for specific rotations for the $(H_2)_7$ molecule, see fig. 4.7. It can be seen that both the approaches start performing better than the FVNO++ (μ) approach after a truncation of 10% and yield similar results till about 20% of the virtual space is removed. However, the errors in the FVNO++ $(\mu * L)$ method increase steeply threafter. Even

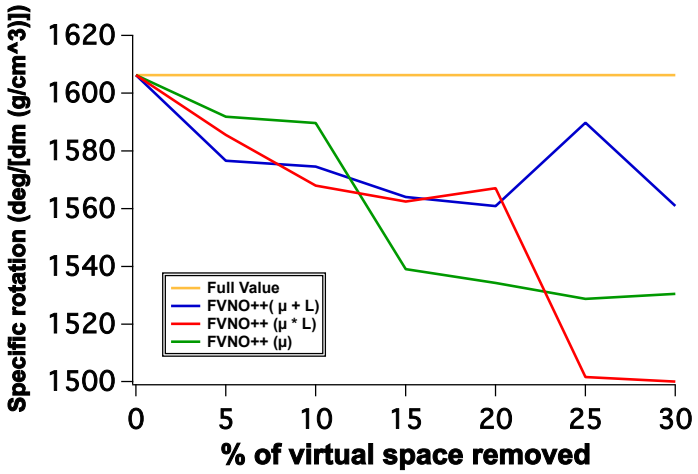

Figure 4.8: CCSD/aDZ specific rotations of $(H_2)_7$ molecule in both FVNO++ $(\mu * L)$ and FVNO++ (μ, L) schemes as a function of percentage of virtual space removed.

though the FVNO++ (μ, L) method yields the lowest errors out of all the three approaches, more calculations are needed in order to confirm this behavior.

4.5 Conclusions

We propose a novel modification of the FVNO scheme for calculating linear response properties at the CC level of theory. The new scheme, which we have named as FVNO++ constructs second-order perturbed densities to obtain "perturbation aware" VNOs whose ONs can be seen as a metric for estimating their importance in capturing the response of the wavefunction to the external perturbation. Based on pilot studies on small chiral molecules:

hydrogen peroxide and linear $(H_2)_n$ helices, we conclude that this approach offers a very compact virtual space for calculating both dynamic polarizabilities and specific rotations while maintaining very low truncation errors. However, more calculations are needed on two and three dimensional molecular systems to make the FVNO++ truncation scheme truly robust. We are currently in the process of implementing a RI-CC2 linear response code[26] which we intend to use in conjunction with the FVNO++ formalism to tackle large solvated clusters. Furthermore, we propose to extend this approach to the reduced-scaling domain based on pair natural orbitals[57, 58].

Chapter 5

Perturbed Pair Natural Orbitals for Coupled-Cluster Linear-Response Theory

5.1 Introduction

Accurate *ab initio* models like the coupled cluster theory have been used quite reliably to predict the chiroptical properties of molecules. However, they have been limited to very small system sizes due to the heavy computational expenses associated with such methods. For example, the coupled cluster singles and doubles method (CCSD) has a high polynomial scaling of $O(N^6)$, where N is some measure of the system size. This is clearly unphysical

as the phenomenon of dynamic electron-correlation, which these methods aim to capture, is local in nature[73]. This steep scaling can be attributed to the use of delocalized canonical Hartree-Fock MOs (CMOs) as the one electron basis for representing the wavefunction. Local correlation techniques try to exploit the intrinsic sparsity in correlated wavefunctions by unitarily localizing the occupied orbitals (LMOs) using methods like Boys-Foster, Pipek-Mezey[9] etc. and constructing excitation domains corresponding to each LMO. The sizes of these domains are usually very small compared to the full virtual space and become constant in the asymptotic limit, making these approaches reduced-scaling. Saebo and Pulay's introduction of projected atomic orbitals (PAO) as a representation of the virtual space stands as one of the earliest works in this regard[65, 73, 74]. As the name suggests, PAOs are formed by projecting out the occupied MO components from the AO basis. Since the PAOs are centered on atoms (just like AOs), an excitation domain for a given LMO can be constructed by including only those PAOs which are on or near the atoms associated with that LMO. Subsequently, domains corresponding to a pair of LMOs can be formed by taking a union of the PAO space of both the LMOs and so on. Werner, Schütz and co-workers [33, 76, 78] were the first to apply these concepts within the framework of CC theory. By employing truncated PAO domains coupled with other approximations like weak and distant pairs, they were able to achieve linear scaling while maintaining accurate description of ground-state properties like reaction enthalpies, thermodynamic constants etc.[29, 33, 65, 73, 74, 76, 78]. Crawford and King were the first to use PAOs with the equation of motion CCSD method to calculate excitation energies[15]. In a similar work, Korona and Werner[43] constructed

state specific PAO domains to minimize the average localization errors for their test set to only 0.06 eV. Schütz and co-workers extended this approach with density-fitted second order coupled cluster (CC2) [12] method to calculate excited state properties of large systems.[77] However, these approaches could require very large domian sizes depending on the character of the excited state, for example, excitations in a charge-transfer excited state could be fairly non-local. PAOs have also been used within the context of CC linear response theory to calculate higher-order response properties like (hyper)polarizabilities, chiroptical response etc. albeit on a much smaller scale. In 2004, Korona and Werner[43] used PAOs with local coupled cluster singles and doubles method (LCCSD) to calculate electric dipole moments and static polarizabilities where they got average errors of 1.61% and 0.48% (with respect to full canonical result) respectively. Further minimization of the errors required building bigger domains leading to a significant increase in computational expenses. In the same year, Russ and Crawford[70] used a modified domain building procedure within the PAO framework, where they augmented the ground state orbital domains on the basis of first-order orbital response coefficients obtained by solving the coupled-perturbed Hartree-Fock equations, to calculate CC static polarizabilities. A few years later, they extended this formalism to calculate dynamic polarizabilities and optical rotations[71]. While the localization errors for linear molecular structures were shown to be only a few percent of canonical results, three dimensional compounds required very large domains, especially for optical rotations. A similar conclusion was drawn when Friedrich and co-workers applied the incremental scheme, a fragmentation based local correlation technique to calculate CC

dynamic polarizabilities.[25] For a more detailed overview of the applications of PAO based methods in this field, please refer to ref[50]. Within the framework of local correlation, the pair natural orbitals (PNOs) introduced in 1970s by Edimnston and Krauss[21], Meyer[56], Ahlrichs, Kutzelnigg, Staemmler and co-workers[2] and orbital specific virtuals (OSVs) developed by Chan and co-workers in 2011 [93], are other popular alternatives to PAOs for a compact representation of the virtual space. In the local PNO (LPNO) approach, each pair of LMOs have their own virtual space which can be obtained by the diagonalization of the virtual-virtual block of an approximate 1-electron pair specific density. The OSV approach on the other hand involves diagonalization of a separate density for each LMO. Even though the PNOs were shown be to be quite useful as a wavefunction compression technique, they were initially abandoned due to the computational costs involved in the transformation of the two electron integrals, onlyto be revived later by Neese and co-workers in 2008 by making use of the density-fitting procedure [57, 58]. They also proposed a variant of the LPNO approach, a scheme which they call domain based LPNO (DLPNO), where the PNOs are expressed in terms of PAOs, to achieve near-linear scaling behavior in MP2 and CC calculations [68]. Following their pioneering works, the LPNO and the DLPNO methods have been used quite sucessfully to study ground state properties of molecular systems previously unreachable by canonical correlated methods. Hättig and co-workers were the first to extend this scheme to excited states by using state-specific PNOs generated from CIS(D) densities at CC2 level of theory[32] and recently with CCSD[24]. Valeev and co-workers[63] recently implemented a state-averaged L-PNO-CCSD simulation program by taking an av-

erage of the CIS(D) densities over a desired set of excited states. Similar works employing state-specific natural transition orbitals and natural orbitals for calculating excitation energies have also been reported[5, 34, 54, 55]. Our group implemented the LPNO scheme in conjunction with CC2 and CCSD linear response (LR) theory to calculate dynamic polarizabilities and specific rotations of different chiral molecules ranging from linear (H2)n helices to cagelike 1r-4r-norbornenone, where consistent with earlier studies, PNOs were found to be much more compact than the PAOs and OSVs for representing the wavefunction. However, the truncation errors in specific rotations for 3-dimensional structures were quite large and the convergence of both the properties towards the canonical result turned out to be very slow[50]. The failure of the regular LPNO-CC2/CCSD-LR approach for higher-order response properties could be attributed to the inability of the ground-state MP2 density to capture the response of the wavefunction, as shown in our earlier work with natural orbitals (NOs)[45]. However, we have recently demonstrated that the NOs obtained from "perturbation aware" densities are better suited for calculating these response properties.[44] In this paper, we extend this approach which we have named PNO++ by constructing second-order pair specific perturbed densities, and compare its performance with the regular method.

5.2 Theory

5.2.1 Coupled Cluster Response Theory

Coupled cluster (CC) response theory has been proven to be quite a reliable and accurate theoretical tool to calculate higher-order response properties. Within this formalism, one expands the time-dependent expectation value of a time-independent operator in different orders of the perturbation. The response functions can then be identified as fourier transforms (FT) of the time-dependent expansion terms up to a given order, ex. the linear response function (LRF) is the FT of terms appearing in the first order in the expansion. CC-LRF for time independent operators A and B can be written as,

$$\langle\langle A;B\rangle\rangle_{\omega_1} = \frac{1}{2}\hat{P}(A,B)[\langle 0|\ [\hat{Y}^B_{\omega_1},\bar{A}]|0\rangle + \langle 0|\ (1+\hat{\Lambda})|[\bar{A},\hat{X}^B_{\omega_1}]|0\rangle] \tag{5.1}$$

where $\hat{P}(A,B)$ is a symmetrizing operator which simultaneously interchanges operators A and B and takes the complex conjugate of the expression, ω_1 is the frequency of the external field, $|0\rangle$ is the reference wavefunction, $\hat{\Lambda}$ is a linear de-excitation operator that parametrizes the CC left hand wavefunction, overbar on operator A denotes a similarity transformation with the ground state T operator, $\bar{A} = e^{-\hat{T}}\hat{A}e^{\hat{T}}$ and $\hat{X}^B_{\omega_1}$ and $\hat{Y}^B_{\omega_1}$ are the first-order right and left hand perturbed amplitudes corresponding to perturbation operator B respectively. The LRF expression above can be re-written in terms of frequency-dependent first-order perturbed densities $D^{B^{\omega_1}(1)}_{pq}$,

$$\begin{aligned}\langle\langle A;B\rangle\rangle_{\omega_1} &= \frac{1}{2}\hat{P}(A,B)[\sum_{pq} A_{pq}\langle 0|\ \hat{Y}^B_{\omega_1}, \overline{a^\dagger_p a_q}]|0\rangle + \langle 0|\ (1+\hat{\Lambda})|[\overline{a^\dagger_p a_q}, \hat{X}^B_{\omega_1}]|0\rangle] \\ &= \frac{1}{2}\hat{P}(A,B)\big[\sum_{pq} A_{pq}[D^{B^{\omega_1}}_{pq}]^{(1)}\big]\end{aligned} \tag{5.2}$$

where $a^\dagger_p$ and a_q are creation and annihilation operators respectively. In spin orbitals, the virtual-virtual block of this density looks like,

$$D^{B^{\omega_1}(1)}_{ab} = \frac{1}{2}\sum_{ijc}[\lambda^{ij}_{ac}X^{bc}_{ij}\ + Y^{ij}_{ac}t^{bc}_{ij}] + \sum_{i}[\lambda^{i}_{a}X^{b}_{i}\ + Y^{i}_{a}t^{b}_{i}] \tag{5.3}$$

where X and Y are the right and left hand first order perturbed amplitudes associated with perturbation B at frequency ω_1. These amplitudes can be obtained by solving a linear system of equations,

$$\begin{aligned}\sum_{\nu}(\bar{H}-\omega I)_{\mu\nu}X^B_\nu &= -\bar{B}_\mu \\ \sum_{\nu} Y^B_\nu(\bar{H}+\omega I)_{\nu\mu} &= -\sum_{\nu} X^B_\nu F'_{\nu\mu} - \bar{B}'_\mu\end{aligned} \tag{5.4}$$

where,

$$\begin{aligned}(\bar{H}\pm\omega I)_{\mu\nu} &= \langle\mu|\big[(\bar{H}\pm\omega I),\tau_\nu\big]|0\rangle \\ F'_{\nu\mu} &= \langle 0|(1+\hat{\Lambda})|\big[\big[\bar{H},\tau_\nu\big],\tau_\mu\big]|0\rangle \\ \bar{B}_\mu &= \langle\mu|\bar{B}|0\rangle \\ \bar{B}'_\mu &= \langle 0|(1+\hat{\Lambda})|\big[\bar{B},\tau_\mu\big]|0\rangle.\end{aligned} \tag{5.5}$$

Here τ_μ, τ_ν are operators which generate excited determinats $|\mu\rangle$ and $|\nu\rangle$ by acting on the reference wavefunction $|0\rangle$. Once we solve for X_ν^B and Y_ν^B amplitudes, the first-order perturbed density can be built from eq.(5.3) to construct the CC-LRF. Elements of the dynamic polarizability ($\boldsymbol{\alpha}$) and optical rotation ($\boldsymbol{\beta}$) tensors can be obtained from the LRF with appropriate perturbation operators. For example,

$$\begin{aligned} \alpha_{xy}(\omega) &= -\langle\langle \mu_x; \mu_y \rangle\rangle_{\omega_1} \\ \beta_{xy}(\omega) &= \mathrm{Im}\langle\langle \mu_x; m_y \rangle\rangle_{\omega_1} \end{aligned} \tag{5.6}$$

where $\boldsymbol{\mu} = \sum_i q_i \boldsymbol{r_i}$, $\boldsymbol{m} = \sum_i \frac{q_i}{2m_i} \boldsymbol{r_i} \times \boldsymbol{p_i}$ and "Im" signifies that $\beta_{xy}(\omega)$ equals the imaginary part of the corresponding LRF.

5.2.2 Ground State PNOs

The first step in any local correlation approach is the induction of sparsity in the occupied space. Standard techniques like Boys-Foster, Pipek-Mezey[9] accomplish this by producing localized MOs or LMOs. The PNOs for a given pair of LMOs ij can then be defined by a unitary rotation of the virtual orbitals,

$$|\bar{\boldsymbol{a}}^{ij}\rangle = \sum_a |a\rangle \boldsymbol{Q}_{a\bar{a}}^{ij} \tag{5.7}$$

where the transformation matrix $\boldsymbol{Q}^{ij}_{a\bar{a}}$ is the eigenvector of the pair ij's contribution to the virtual-virtual block of the one electron density matrix (1-RDM) i.e $\boldsymbol{D} = \sum_{ij}[\boldsymbol{D}^{ij}]$.

$$\boldsymbol{D}^{ij}\boldsymbol{Q}^{ij} = \boldsymbol{Q}^{ij}\boldsymbol{n}^{ij} \tag{5.8}$$

The eigenvalues $\boldsymbol{n}^{ij}$ are referred to as "occupation numbers" (ONs) and can be seen as a metric for estimating the importance of the corresponding PNO for describing electron correlation effects for the pair ij. For CCSD ground state calculations, approximate pair densities are usually formed from the MP2 amplitudes,

$$\boldsymbol{D}^{ij} = \frac{2}{1+\delta_{ij}}(\boldsymbol{T}^{ij}\tilde{\boldsymbol{T}}^{ij\dagger} + \boldsymbol{T}^{ij\dagger}\tilde{\boldsymbol{T}}^{ij}) \tag{5.9}$$

where,

$$\begin{aligned} \tilde{\boldsymbol{T}}^{ij} &= 2\boldsymbol{T}^{ij} - \boldsymbol{T}^{ij\dagger} \\ T^{ij}_{ab} &= \frac{\langle ab|ij\rangle}{f_{ii} + f_{jj} - \epsilon_a - \epsilon_b}. \end{aligned} \tag{5.10}$$

Here, indices i, j, k and a, b, c have been used for occupied and virtual orbitals respectively. The integrals $\langle ab|ij\rangle$ are in physicist notation, f_{ii} and f_{jj} are the i^{th} and j^{th} diagonal elements of the Fock matrix in the LMO basis and ϵ_a, ϵ_b are the orbital energies of the canonical virtual orbitals a and b respectively. The PNOs with ONs smaller than a given threshold (usually in $10^{-6} - 10^{-8}$ range) are then neglected as they have minimal contributions to the total correlation energy. Finally, the canonical CCSD equations are reformulated or refac-

tored in terms of these truncated PNO transformations. It should be noted that the virtual spaces of different pairs of LMOs are non-orthogonal to each other and the transformation of amplitudes from one pair to another requires a overlap metric given by,

$$\boldsymbol{S}^{ij,kl} = \boldsymbol{Q}^{ij\dagger}\boldsymbol{Q}^{kl} \tag{5.11}$$

5.2.3 Perturbed PNOs

It was shown from our earlier work that the regular LPNO-CCSD-LR approach has very slow convergence towards the full canonical result both for dynamic polarizabilities and specific rotations. This is unsurprising since the sparsity patterns in the perturbed and unperturbed amplitudes are usually very different from each other. Thus, the pair densities should be able to capture the response of the ground state amplitudes. Recent reduced scaling works on EOM-CC2/CCSD excitation energies employ PNO-MP2 and PNO-CIS(D) densities for ground and excited state calculations respectively[24, 32]. However, for caluclating response properties using CC-LR theory, one needs to express both unperturbed and perturbed amplitudes in the same PNO basis in order to match the results obtained from finite field procedures. Due to this constraint, two different schemes could be explored where a) PNOs are defined from perturbed densities, and b) effective PNOs are obtained by a union of truncated PNOs defined from MP2 and perturbed densities. It should be noted that one can't just add ground state and perturbed densities together to define an effective density as they are not in the same units. We have implemented scheme a) in this work and call it PNO++.

This approach can be justified due to the fact that our target is not total energies but the derivative of the total energies in the presence of external fields. Furthermore, it can be shown that on replacing the CC ground state amplitudes with those of MP2 in CC-LR theory one introduces minimal errors for both polarizabilities and specific rotations.[44] Hence, even though PNO++ can't be expected to work as well as the LPNO approach for ground state calculations, it can capture the response of the wavefunction very efficiently and hence should perform a lot better for these kinds of properties. The PNO++ approach involves creation of a perturbation specific density for each ij pair. This is an extension of our work on natural orbitals where we showed that second-order perturbed densities can be used quite efficiently for calculating response properties[44]. For a given perturbation A, the PNO++ density is constructed by replacing the MP2 T_{ab}^{ij} amplitudes by the corresponding perturbed amplitudes X_{ab}^{ij}.

$$\boldsymbol{D}^{A;ij} = \frac{2}{1+\delta_{ij}}(\boldsymbol{X}^{ij}\tilde{\boldsymbol{X}}^{ij\dagger} + \boldsymbol{X}^{ij\dagger}\tilde{\boldsymbol{X}}^{ij}) \tag{5.12}$$

Rewriting the first part of eq.(5.4),

$$X_{\mu}^{A} = -\sum_{\nu} \left(\bar{H} - \omega I\right)^{-1}{}_{\mu\nu}\bar{A}_{\nu} \tag{5.13}$$

one can see that an obvious guess for X_{ab}^{ij} amplitudes could be constructed as

$$X_{ab}^{ij} = \frac{\bar{A}_{ab}^{ij}}{\bar{H}_{ii} + \bar{H}_{jj} - \bar{H}_{aa} - \bar{H}_{bb}} \tag{5.14}$$

since the leading contribution to the inverse of the diagonally dominant $(\bar{H} - \omega I)$ matrix would come from the inverse of its diagonal elements, i.e. $\bar{H}_{ii} + \bar{H}_{jj} - \bar{H}_{aa} - \bar{H}_{bb}$. Also, $\bar{A}$ has been approximated by using MP2 amplitudes for the similarity transformation,

$$\bar{A}_{ab}^{ij} = P_{ij}^{ab}\Bigg[\sum_{e} t_{eb}^{ij}[A_e^a - t_a^m A_e^m] - \sum_{m} t_{ab}^{mj}[A_i^m - t_e^i A_e^m]\Bigg]$$
$$P_{ij}^{ab} f_{ij}^{ab} = f_{ij}^{ab} + f_{ji}^{ba} \tag{5.15}$$

Furthermore, we have taken ω_1 as zero so that we can use the same density for response calculations at multiple frequencies. This can be justified as the sparsity pattern of the perturbed amplitudes should more or less stay the same at the frequencies we are interested in. In this approach, the weak pair approximation can also be employed by using a pair-pseudoresponse metric,

$$e_{ab}^{A} = \sum_{ij} \bar{A}_{ab}^{ij} \tilde{\boldsymbol{X}}_{ab}^{ij}. \tag{5.16}$$

All the pairs whose pseudoresponses are below a given threshold can be considered as weak pairs and neglected.

5.3 Computational Details

The ultimate goal of this work is to be able to carry out CCSD response calculations of large solvated molecular clusters for which one would need a production level CCSD-PNO++-LR code. As can be seen from eq (5.4), such a code would involve reconstruction of $\bar{H}$ elements in every iteration of the response equations. However, before investing a lot of time and effort in this regard, we use a simulation code in this work to test if the PNO++ approach can offer a more compact virtual space for calculating these properties. We use linear (P)-$(H_2)_n$ helices as our test cases as these are ideal systems for demonstrating the efficiency of the local correlation approaches. Dynamic polarizabilities and specific rotations calculations are carried out within the CCSD-LR formalism with the aug-cc-pVDZ (aDZ)[20, 38, 92] basis set at 589 nm using Psi4 and Psi4Numpy software packages[60, 83]. Furthermore, the electric dipole operator μ is represented in length gauge (LG) for polarizabilities while specific rotations employ both LG and modified velocity gauge (MVG) representations. Also, we have chosen electric dipole based perturbed pair density for defining our PNO space: $\boldsymbol{D}^{\mu;ij} = \sum_q \frac{1}{3}[\boldsymbol{D}^{\mu_q;ij}]$, where $q \equiv [x, y, z]$.

One of the advantages of the simulation code is that it requires minimal changes in the canonical CCLR code. In this procedure, the residual of the CC amplitude equations, (R^{ij}, R^i) is transformed from the canonical MO basis to the PNO basis in every iteration,

$$\begin{aligned} \boldsymbol{R}^{ij} &= \boldsymbol{Q}^{ij\dagger} R^{ij} \boldsymbol{Q}^{ij} \\ \boldsymbol{R}^{ii} &= \boldsymbol{Q}^{ii\dagger} R^{i} \boldsymbol{Q}^{ii}. \end{aligned} \tag{5.17}$$

One can can continue to work in the PNO basis but since the virtual-virtual block of the Fock matrix is not diagonal in this basis, the convergence of the amplitude equations is expected to be slower. Thus, its common to use a semicanonical PNO basis which diagonalizes $\boldsymbol{F}^{ij}_{vir}$,

$$\begin{aligned} \boldsymbol{U}^{ij\dagger} \boldsymbol{F}^{ij}_{vir} \boldsymbol{U}^{ij} &= \boldsymbol{\Lambda}^{ij} \\ \bar{\boldsymbol{R}}^{ij} &= \boldsymbol{U}^{ij\dagger} \boldsymbol{R}^{ij} \boldsymbol{U}^{ij} \\ \bar{\boldsymbol{R}}^{ii} &= \boldsymbol{U}^{ii\dagger} \boldsymbol{R}^{ii} \boldsymbol{U}^{ii} \end{aligned} \tag{5.18}$$

where $\boldsymbol{\Lambda}^{ij}$ is the diagonal matrix containing orbital energies ($\boldsymbol{\epsilon}^{ij}_a$, $\boldsymbol{\epsilon}^{ij}_b$, ..). Subsequently, the preconditioner is applied to the residual to calculate the increment,

$$\begin{aligned} \bar{\boldsymbol{\Delta}}^{ij} &= \frac{\bar{\boldsymbol{R}}^{ij}}{F_{ii} + F_{jj} - \boldsymbol{\epsilon}^{ij}_a - \boldsymbol{\epsilon}^{ij}_b} \\ \bar{\boldsymbol{\Delta}}^{i} &= \frac{\bar{\boldsymbol{R}}^{ii}}{F_{ii} - \boldsymbol{\epsilon}^{ii}_a}. \end{aligned} \tag{5.19}$$

The increment is transformed back to the canonical basis,

$$\begin{aligned} \Delta^{ij} &= \boldsymbol{Q}^{ij} \boldsymbol{U}^{ij} \bar{\boldsymbol{\Delta}}^{ij} \boldsymbol{U}^{ij\dagger} \boldsymbol{Q}^{ij\dagger} \\ \Delta^{ii} &= \boldsymbol{Q}^{ii} \boldsymbol{U}^{ii} \bar{\boldsymbol{\Delta}}^{ii} \boldsymbol{U}^{ii\dagger} \boldsymbol{Q}^{ii\dagger} \end{aligned} \tag{5.20}$$

and added to the amplitudes of the previous iteration $(n-1)$,

$$\begin{aligned} t^{ij}(n) &= t^{ij}(n-1) + \Delta^{ij} \\ t^{i}(n) &= t^{i}(n-1) + \Delta^{i}. \end{aligned} \tag{5.21}$$

It should be noted that this procedure is applied for filtering the non-local parts of $\hat{T}$, $\hat{\Lambda}$, X^A_ω and Y^A_ω amplitudes.

5.4 Results and Discussions

Through our earlier works[44, 45], we have demonstrated the poor performances of the NOs based on the ground state MP2 density in describing the response of the CC wavefunction. This behaviour is not unexpected since the diffuse orbitals which are crucial to the description of the low lying Rydberg states and hence to the response properties, have very low contributions to the ground state correlation energy and will always be removed first when ground state densities are used for generating the NOs. By the same logic, the ground state based PNOs can't be expected to perform well for calculating response properties. Consequently, we devised a simple strategy where we use a hybrid virtual space consisting of virtual MOs (VMOs) and ground state PNOs. Specifically, we identify the most diffuse VMOs on the basis of their spatial extents[44] by choosing an (empirical) cutoff and construct the MP2 pair specific density in the remaining virtual space. Thus, in this modified PNO approach (PNO(M)) every pair of LMOs, in addition to their PNOs, possess the same set of VMOs. From now on, we call the LPNO approach as the PNO approach for the sake

of convenience. Fig. 5.1 compares the performance of both PNO(M) amd PNO approaches

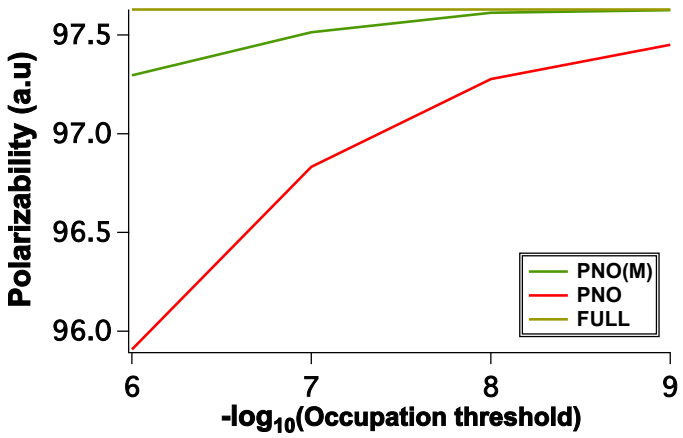

Figure 5.1: CCSD/aDZ polarizabilities of $(H_2)_7$ in both PNO and PNO(M) approaches as a function of -log(occupation threshold).

for calculating CCSD dynamic polarizabilities of $(H_2)_7$ molecule at 589 nm. It can be seen that the PNO(M) scheme converges to the full result much faster than the PNO method. A cutoff of 10^{-6} in the PNO(M) approach gives almost the same accuracy as a cutoff of 10^{-9} for the PNO approach. Similar trends can be seen for specific rotation as well for the same system (see Fig. 5.2), where even at a very high cutoff of 10^{-4}, the PNO(M) approach has almost converged to the full canonical result. On the other hand, the PNO approach even at a tight cutoff of 10^{-9} doesn't reproduce the canonical value. Furthermore, on account of fortuitous cancellation of errors in the PNO approach, a cutoff of 10^{-7} gives much more accurate results than a tighter cutoff of 10^{-9}. However, in the PNO(M) approach, evey

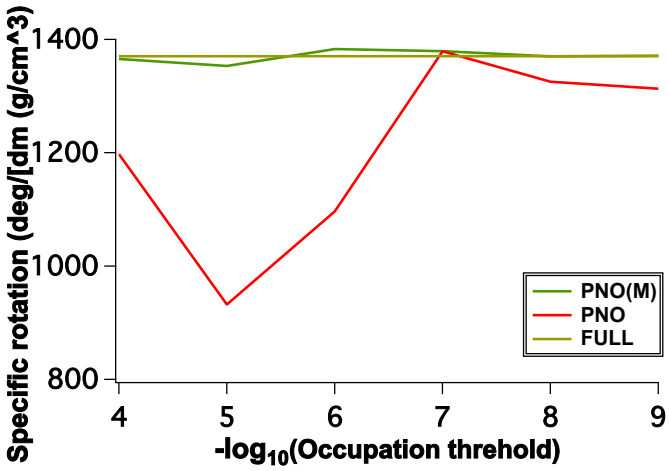

Figure 5.2: CCSD/aDZ/MVG Specific rotations of $(H_2)_7$ in both PNO and PNO(M) approaches as a function of -log(occupation threshold)

pair of LMOs now becomes "important" as it always possesses a fixed number of VMOs. Thus, the computational expenses are significantly higher in such an approach. Also, the selection of the diffuse space is not straightforward as the criterion of spatial extents is not robust. Hence, we look at the PNO++ approach to see if it can naturally identify and retain the PNOs which are important for response properties. Fig. 5.3 compares the performances of the PNO and PNO++ approaches for calculating dynamic polarizabilities of the $(H_2)_n$ helices. The T_2 ratio as shown in the figure can be seen as a measure of the % of the wavefunction retained in these calculations. Thus, a T_2 ratio of 1 would give the full canonical result. The PNO++ approach can be seen to significantly outperform the regular PNO approach for all the test cases. A T_2 ratio as small as 0.2 in the PNO++ approach is

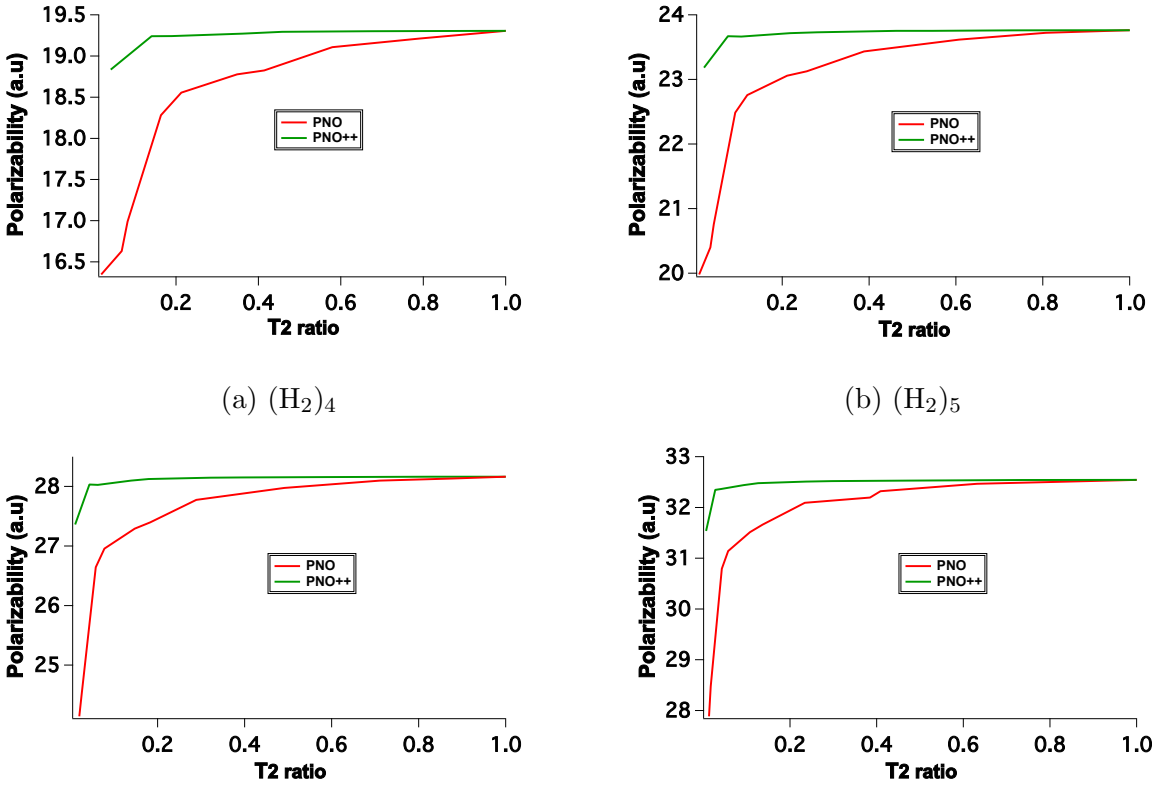

(a) $(H_2)_4$ (b) $(H_2)_5$

(c) $(H_2)_6$ (d) $(H_2)_7$

Figure 5.3: CCSD/aDZ polarizabilities of $(H_2)_n$ helices, $n = 4 - 7$ in both PNO and PNO++ schemes as a function of T_2 ratio.

able to reproduce polarizabilities very close to the full canonical values. The PNO approach on the other hand requires T_2 ratios in the range of 0.9 ($(H_2)_4$) to 0.7 ($(H_2)_7$) for results of similar accuracy. It can be seen that the truncation errors in specific rotations (fig. 5.4) for both PNO and PNO++ approaches are higher compared to polarizabilities, which is not unexpected since specific rotations are much more sensitive to the wavefunction truncation. An aggressive truncation of the virtual space in the PNO approach could even lead to opposite sign specific rotations. Indeed, just like polarizabilities, the convergence of the specific rotation values computed using the PNO++ approach, is much faster towards the canonical result and a T_2 ratio close to 0.2 yields an error of less than 10% ($(H_2)_4$) for all the test cases.

5.5 Conclusions

We propose a new scheme by the name of PNO++ which can be seen as an extension of the PNO approach for calculating CC linear response properties. The pair specific densities constructed in this approach strongly resemble in structure with the CC linear response functions and preliminary results on linear chain hydrogen helices seem to indicate that both dynamic polarizabilities and specific rotation values converge to the canonical result much faster in the PNO++ approach. Thus, this approach provides a very compact virtual space for simulating these response properties. However, calculations on two and three dimensional structures involving different forms of second-order perturbed densities need to be carried

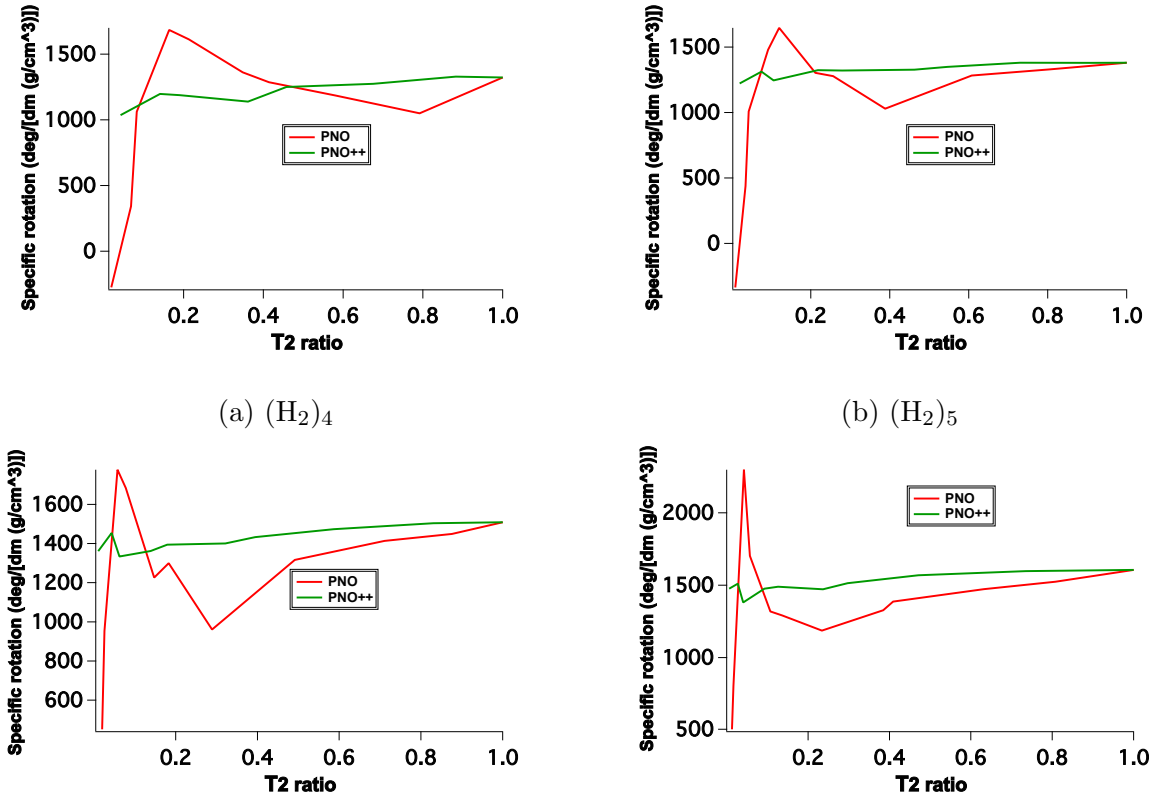

(a) $(H_2)_4$

(b) $(H_2)_5$

(c) $(H_2)_6$

(d) $(H_2)_7$

Figure 5.4: CCSD/aDZ specific rotations of $(H_2)_n$ helices, $n = 4 - 7$ in both PNO and PNO++ schemes as a function of T_2 ratio.

out in order to make PNO++ a truly black-box method. Furthermore, the validity of the weak pair approximations, needs to be investigated within the PNO++ formalism to ensure that this scheme retains the reduced-scaling behaviour of the original PNO method.

Chapter 6

Conclusions

Reduced-scaling techniques have extended the application of accurate coupled cluster (CC) methods to molecules with hundreds of heavy atoms[57, 58]. However, efforts towards extension of these schemes to simulate linear response properties have been fairly limited[25, 28, 43, 51, 70, 71]. McAlexander and Crawford[50] recently compared the performances of reduced-scaling methods based on projected atomic orbitals (PAOs)[65, 73, 74], orbital specific virtuals (OSVs)[93] and pair natural orbitals (PNOs)[2, 21, 56, 58] for calculating optical rotations using the coupled cluster linear response theory[40], where they found the PNOs to be the most compact representation of the virtual space. However, very tight cutoffs needed to be employed in order to match the canonical results.

In our search for an optimal virtual space for response calculations, we investigated the performance of the frozen virtual natural orbital (FVNO) scheme, (Chapter 3) which had been applied quite successfully to bring down the computational costs of CC calculations

involving energies, geometry optimizations, ionization energies, etc.[18, 19, 46, 84, 88, 89], for calculating dynamic polarizabilities of small chiral compounds[45]. It was found that the virtual natural orbitals (VNOs) obtained from the ground state MP2 density (GSMP2D) are not suitable for calculating polarizabilities (and hence optical rotations) in the absence of orbital relaxation effects as the shift in their values with respect to the full canonical result grew almost linearly with the number of truncated VNOs. However, since the introduction of orbital relaxation can introduce spurious or unphysical poles in the linear response function, it is not included in the CC linear response calculations. On a closer inspection, we found that all the diffuse VNOs had very low occupation numbers (ONs) and thus were removed first in this scheme resulting in large errors. It should be noted that these diffuse orbitals are absolutely essential for calculating chiroptical properties as many chiral molecules possess low lying Rydeberg type excited states. We also employed a CC2[12] based correction for the external truncated space which was able to reduce the errors drastically, but such an approach could not lead to any computational savings. Finally, we constructed a first order perturbed density by taking the derivative of the GSMP2D with respect to an external electric field, with the hope that the occupation numbers (ONs) generated using this density would be a better metric for estimating the importance of a VNO for describing the response of the wavefunction. However, this approach offered only marginal improvement in the errors. On the other hand, truncating canonical molecular orbitals (CMOs) with high orbital energies resulted in very small errors (less than 2% after removing 50% of the virtual space) due to intrinsic cancellation of errors.

On the basis of the above findings, we tried out a modified FVNO scheme, FVNO(M) in Chapter 4, where the virtual CMOs (VCMOs) were sorted according to their diffusivity which was measured by the values of their orbital spatial extents (OSEs) and GSMP2D was built only in the space of non-diffuse (under a given OSE cutoff) orbitals. In other words, the diffuse part of the virtual space remains unaffected by the FVNO procedure. Pilot studies on H_2O_2 molecule showed that the FVNO(M) method yielded minimal errors compared to the original scheme for polarizabilities, optical rotations, rotational strengths, excitation energies, etc. However, more systematic studies are needed to make it a truly black-box method. We also looked at the perturbed density model in more details by first constructing the (full) CCSD first order perturbed density. It was found that the diagonal elements of this density matrix are always zeros irrespective of the perturbation. Clearly, the VNOs obtained by the diagonalization of such densities don't carry any useful information. Ideally, the structure of the perturbed density should be able to mimic these (linear response) properties which are second order in the perturbation. Hence, we proposed a new approach called FVNO++, where a second-order perturbed density is constructed and then diagonalized to define the virtual space. Pilot studies on H_2O_2 molecule and chiral linear chain hydrogen helices ((P)-$(H_2)_n$) using the FVNO++ approach have shown quite promising results for both polarizabilities and optical rotations. The major advantage of this approach over FVNO(M) is that ONs are a much more robust truncation criterion compared to the OSEs.

We extended the above analyses to the PNO domain in Chapter 5 as the the PNOs can be seen as an extension of the concept of natural orbitals. Consequently, the PNO(M) method

was designed where all the diffuse VCMOs were retained and every pair of occupied orbitals inherited this global virtual space. Just as before, PNO(M) significantly accelerates the convergence of these properties towards the full canonical result. However, this means that every occupied pair becomes a strong pair and hence can't be neglected, which has an adverse affect on the reduced scaling capabilities of the PNO scheme. Along the lines of FVNO++, PNO++ approach was formulated where the structure of the pair specific densities resemble with the contributions of a given pair to the response functions. Preliminary results on chiral linear chain hydrogen helices indicate a performance similar to the PNO(M) approach for both polarizabilities and optical rotations. However, calculations on two and three dimensional structures involving different forms of second-order perturbed densities need to be carried out in order to make PNO++ a truly robust method.

Encouraged by the performances of these methods, we plan to use them in conjunction with density-fitted CC linear response codes[26] to target larger systems like solvated molecular clusters. We assume that a larger solvent shell around the solute molecule would require comparitively smaller number of snapshots for the optical rotations to converge to the experimental value. Thus, we can significantly lower down the computational costs involved in CC calculations of optical rotations of solvated molecules.

Appendix A

Publication List

1. **A. Kumar** and T. D. Crawford. Perturbed Natural Orbitals for Coupled-Cluster Linear-Response Theory. **2018**, *manuscript in preparation*.

2. **A. Kumar** and T. D. Crawford. Perturbed Pair Natural Orbitals for Coupled-Cluster Linear-Response Theory. **2018**, *manuscript in preparation*.

3. D. G. A. Smith, L. A. Burns, D. A. Sirianni, D. R. Nascimento, **A. Kumar**, A. M. James, J. B. Schriber, T. Zhang, B. Zhang, A. S. Abbott, E. J. Berquist, M. H. Lechner, L. A. Cunha, A. G. Heide, J. M. Waldrop, T. Y. Takeshita, A. Alenaizan, D. Neuhauser, R. A. King, A. C. Simmonett, J. M. Turney, H. F. Schaefer, F. A. Evangelista, A. E. DePrince, T. D. Crawford, K. Patkowski and C. D. Sherrill. Psi4NumPy: An Interactive Quantum Chemistry Programming Environment for Reference Implementations and Rapid Development. *J. Chem. Theory Comput.*, **2018**, doi: 10.1021/acs.jctc.8b00286.

4. R. M. Parrish, L. A. Burns, D. G. A. Smith, A. C. Simmonett, A. E. DePrince, E. G.

Hohenstein, U. Bozkaya, A. Y. Sokolov, R. D. Remigio, R. M. Richard, J. F. Gonthier, A. M. James, H. R. McAlexander, **A. Kumar**, M. Saitow, X. Wang, B. P. Pritchard, P. Verma, H. F. Schaefer, K. Patkowski, R. A. King, E. F. Valeev, F. A. Evangelista, J. M. Turney, T. D. Crawford, and C. D. Sherrill. Psi4 1.1: An open-source electronic structure program emphasizing automation, advanced libraries, and interoperability. *J. Chem. Theory Comput.*, **2017**, *13*(7), pp 3185-3197.

5. **A. Kumar** and T. D. Crawford, *J. Phys. Chem. A*, Frozen Virtual Natural Orbitals for Coupled-Cluster Linear-Response Theory. **2017**, *121*(3), pp 708-716.

6. T. D. Crawford, **A. Kumar**, K. P. Hannon, S. Höfener and L. Visscher. Frozen-Density Embedding Potentials and Chiroptical Properties. *J. Chem. Theory Comput.*, **2015**, *11*(11), pp 5305-5315.

7. J. Friedrich, H. R. McAlexander, **A. Kumar** and T. D. Crawford. Incremental evaluation of coupled cluster dipole polarizabilities. *Phys. Chem. Chem. Phys.*, **2015**, 17, pp 14284-14296.

Appendix B

Supporting Information for "Frozen Virtual Natural Orbitals for Coupled Cluster Linear-Response Theory"

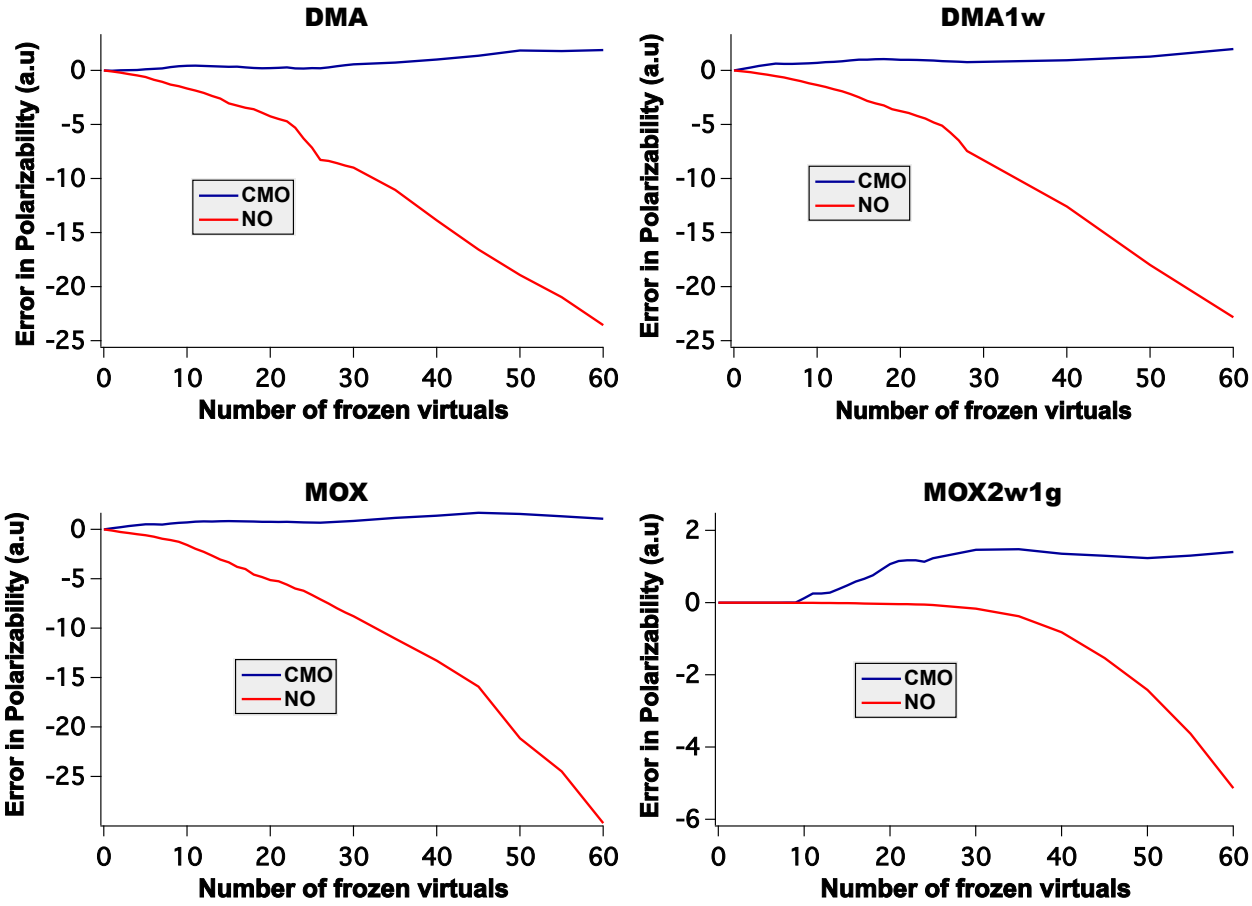

Figure 6.1: Errors in the CCSD/aDZ dynamic polarizability (589 nm) in both CMO and NO bases as a function of number of virtual orbitals removed for four additional test cases: (*P*)-dimethylallene (DMA), (*P*)-dimethylallene and one water molecule (DMA1w), (*S*)-Methyloxirane (MOX), and (*S*)-Methyloxirane and two water molecules with one of the water molecules removed leaving only its basis functions.

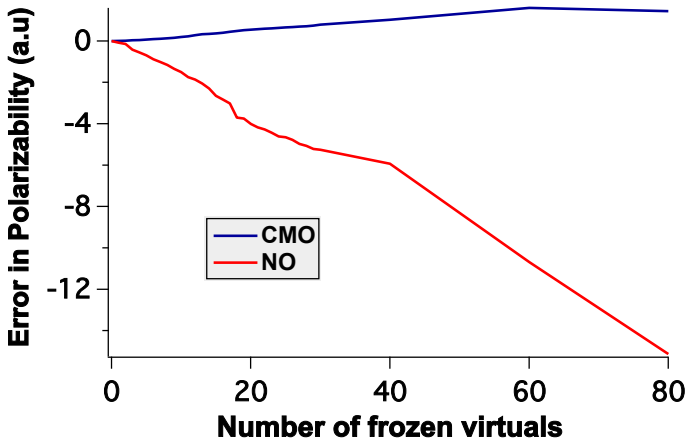

Figure 6.2: Errors in the CCSD/aTZ dynamic polarizability (589 nm) of H_2O_2 in in both CMO and NO bases as a function of number of virtual orbitals removed.

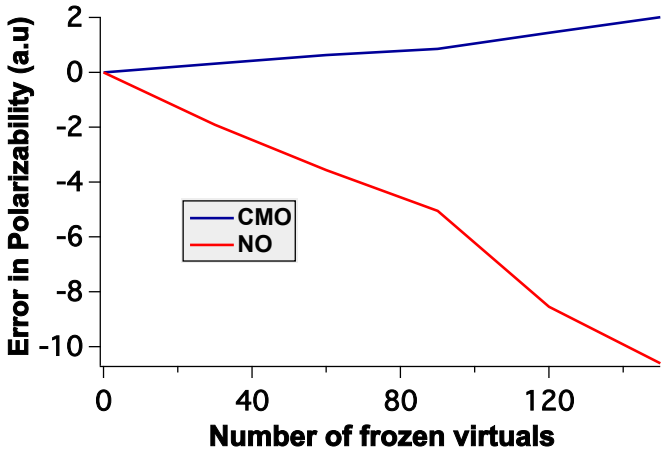

Figure 6.3: Errors in the CCSD/aQZ dynamic polarizability (589 nm) of H_2O_2 in in both CMO and NO bases as a function of number of virtual orbitals removed.

Table 6.1: B3LYP/aug-cc-pVDZ optimized geometry (Å) of hydrogen peroxide.

Atomic symbol	X	Y	Z
O	-0.028962160801	-0.694396279686	-0.049338350190
O	0.028962160801	0.694396279686	-0.049338350190
H	0.350498145881	-0.910645626300	0.783035421467
H	-0.350498145881	0.910645626300	0.783035421467

Table 6.2: B3LYP/aug-cc-pVDZ optimized geometry (Å) of (*P*)-dimethylallene.

Atomic symbol	X	Y	Z
C	0.00000000	0.00000000	0.00000000
C	-0.87382800	0.87178900	0.87038800
C	-0.87382800	2.18536200	0.87080500
C	-0.87382800	3.49893500	0.87038800
H	-0.19165900	4.01714100	1.55371200
C	-1.74765600	4.37072400	0.00000000
H	-2.39264800	3.76601200	-0.64911100
H	-2.38616500	5.02111900	0.61760600
H	-1.13340200	5.02895100	-0.63367100
H	-1.55599700	0.35358300	1.55371200
H	0.64499200	0.60471200	-0.64911100
H	0.63850900	-0.65039500	0.61760600
H	-0.61425400	-0.65822700	-0.63367100

Table 6.3: B3LYP/aug-cc-pVDZ optimized geometry (Å) of (*P*)-dimethylallene and one water molecule.

Atomic symbol	X	Y	Z
C	0.00000000	0.00000000	0.00000000
C	-1.46444400	-0.36643000	0.02694600
C	-2.44105800	0.44524100	0.36174100
C	-3.41923100	1.26314500	0.68806000
H	-3.71780300	1.32103000	1.74107500
C	-4.16801100	2.15536700	-0.27447800
H	-3.80129000	2.02991300	-1.30007100
H	-5.24434000	1.92768500	-0.25838400
H	-4.05435400	3.21167600	0.01259000
H	-1.72145400	-1.39204600	-0.25890200
H	0.15629600	1.04448300	0.29557800
H	0.57342800	-0.64609200	0.68212100
H	0.41596400	-0.14458000	-1.00872300
O	-5.05428200	-1.67323100	-0.06746500
H	-4.46520000	-0.94134100	0.17201000
H	-5.19373900	-2.15473700	0.75630300

Table 6.4: B3LYP/aug-cc-pVDZ optimized geometry (Å) of (*S*)-methyloxirane.

Atomic symbol	X	Y	Z
C	14.60000000	14.52999999	15.13000000
O	14.60000000	14.52999999	16.53000000
C	15.85999999	14.52999999	15.84999999
C	14.51999999	15.70999999	14.30000000
H	13.57999999	15.70999999	13.75000000
H	14.58000000	16.60000000	14.91999999
H	15.35000000	15.70999999	13.58999999
H	14.08999999	13.64000000	14.76999999
H	16.43000000	13.64000000	15.59000000
H	16.43000000	15.41999999	15.59000000

Table 6.5: B3LYP/aug-cc-pVDZ optimized geometry (Å) of (*S*)-methyloxirane and two water molecules. The water molecule that has been removed leaving only its basis functions is indicated by the "Gh" notation.

Atomic symbol	X	Y	Z
C	14.60000000	14.52999999	15.13000000
O	14.60000000	14.52999999	16.53000000
C	15.85999999	14.52999999	15.84999999
C	14.51999999	15.70999999	14.30000000
H	13.57999999	15.70999999	13.75000000
H	14.58000000	16.60000000	14.91999999
H	15.35000000	15.70999999	13.58999999
H	14.08999999	13.64000000	14.76999999
H	16.43000000	13.64000000	15.59000000
H	16.43000000	15.41999999	15.59000000
O	11.04999999	14.87999999	13.42000000
H	11.06999999	14.67000000	14.34999999
H	11.77999999	15.49000000	13.28999999
Gh(O)	18.57999999	15.27999999	15.68999999
Gh(H)	18.51000000	14.46000000	15.22000000
Gh(H)	19.39000000	15.19999999	16.19999999

Bibliography

[1] M. L. Abrams and C. D. Sherrill. Natural Orbitals as Substitutes for Optimized Orbitals in Complete Active Space Wavefunctions. *Chem. Phys. Lett.*, 395:227–232, 2004.

[2] R. Ahlrichs, H. Lischka, V. Staemmler, and W. Kutzelnigg. PNO-CI (Pair Natural Orbital Configuration Interaction) and CEPA-PNO (Coupled Cluster Pair Approxiomation with Pair Natural Orbitals) Calculations of Molecular Systems. I. Outline of the Method for Closed-Shell States. *J. Chem. Phys.*, 62(4):1225–1234, 1975.

[3] F. Aiga and R. Itoh. Calculation of Frequency-Dependent Polarizability and Hyperpolarizabilities by the Second-Order Møller-Plesset Perturbation Theory. *Chem. Phys. Lett.*, 251:372–380, 1996.

[4] T. L. Barr and E. R. Davidson. Nature of the Configuration-Interaction Method in *Ab Initio* Calculations. I. Ne Ground State. *Phys. Rev. A*, 1(3):644–658, 1970.

[5] P. Baudin and K. Kristensen. Correlated natural transition orbital framework for low-scaling excitation energy calculations (CorNFLEx). *J. Chem. Phys.*, 146(21):214114, 2017.

[6] A. D. Becke. Density-functional thermochemistry. III. The role of exact exchange. *J. Chem. Phys.*, 98(7):5648–5652, April 1993.

[7] C. F. Bender and E. R. Davidson. Studies in Configuration Interaction: The First-Row Diatomic Hydrides. *Phys. Rev.*, 183(1):23–30, 1969.

[8] M. Born and J. R. Oppenheimer. Zur Quantentheorie der Molekeln [On the Quantum Theory of Molecules]. *Annalen der Physik (in German)*, 389(20):457–484, 1927.

[9] J. W. Boughton and P. Pulay. Comparison of the Boys and Pipek-Mezey localizations in the local correlation approach and automatic virtual basis selection. *J. Comput. Chem.*, 14(6):736–740, June 1993.

[10] J. R. Cheeseman, M. J. Frisch, F. J. Devlin, and P. J. Stephens. Hartree-Fock and density functional theory *ab initio* calculation of optical rotation using GIAOS: Basis set dependence. *J. Phys. Chem. A*, 104:1039–1046, November 1999.

[11] O. Christiansen, P. Jørgensen, and C. Hättig. Response Functions from Fourier Component Variational Perturbation Theory Applied to a Time-Averaged Quasienergy. *Int. J. Quantum Chem.*, 68:1–52, 1998.

[12] O. Christiansen, H. Koch, and P. Jørgensen. The Second-Order Approximate Coupled Cluster Singles and Doubles Model CC2. *Chem. Phys. Lett.*, 243(5-6):409–418, September 1995.

[13] T. D. Crawford. *Ab initio* calculation of molecular chiroptical properties. *Theor. Chem. Acc.*, 115:227–245, December 2006.

[14] T. D. Crawford. Reduced-Scaling Coupled-Cluster Theory for Response Properties of Large Molecules. In P. Carsky, J. Pittner, and J. Paldus, editors, *Recent Progress in Coupled Cluster Methods: Theory and Applications*, volume 11 of *Challenges and Advances in Computational Chemistry and Physics*, chapter 2, pages 37–55. Springer, Berlin, 2010.

[15] T. D. Crawford and R. A. King. Locally correlated equation-of-motion coupled cluster theory for the excited states of large molecules. *Chem. Phys. Lett.*, 366:611–622, 2002.

[16] T. D. Crawford and H. F. Schaefer. An Introduction to Coupled Cluster Theory for Computational Chemists, volume = 14, year = 2000. *Reviews in Computational Chemistry*, pages 33–136.

[17] T. D. Crawford and H. F. Schaefer. An Introduction to Coupled Cluster Theory for Computational Chemists. In K. B. Lipkowitz and D. B. Boyd, editors, *Reviews in Computational Chemistry*, volume 14, chapter 2, pages 33–136. VCH Publishers, New York, 2000.

[18] A. E. DePrince and C. D. Sherrill. Accuracy and Efficiency of Coupled-Cluster Theory Using Density Fitting/Cholesky Decomposition, Frozen Natural Orbitals, and a t_1-Transformed Hamiltonian. *J. Chem. Theory. Comp.*, 9:2687–2696, 2013.

[19] A. E. DePrince and C. D. Sherrill. Accurate Noncovalent Interaction Energies Using Truncated Basis Sets Based on Frozen Natural Orbitals. *J. Chem. Theory Comput.*, 9:293–299, 2013.

[20] T. H. Dunning. Gaussian basis sets for use in correlated molecular calculations. I. The atoms boron through neon. *J. Chem. Phys.*, 90(2):1007, 1989.

[21] C. Edmiston and M. Krauss. Pseudonatural Orbitals as a Basis for the Superposition of Configurations. I. He_2^+. *J. Chem. Phys.*, 45(5):1833–1839, 1966.

[22] J. T. Fermann, C. D. Sherrill, T. D. Crawford, and H. F. Schaefer. Benchmark Studies of Electron Correlation in Six-Electron Systems. *J. Chem. Phys.*, 100:8132–8139, 1994.

[23] R.P. Feynman. Forces in Molecules. *Physical review*, 56:340–343, 1939.

[24] M. S. Frank and C. Hättig. A pair natural orbital based implementation of CCSD excitation energies within the framework of linear response theory. *J. Chem. Phys.*, 148(13):134102, 2018.

[25] J. Friedrich, H. R. McAlexander, A. Kumar, and T. D. Crawford. Incremental Evaluation of Coupled Cluster Dipole Polarizabilities. *Phys. Chem. Chem. Phys.*, 17:14284–14296, 2015.

[26] D. H. Friese, N. O. C. Winter, P. Balzerowski, R. Schwan, and C. Hättig. Large scale polarizability calculations using the approximate coupled cluster model CC2 and

MP2 combined with the resolution-of-the-identity approximation. *J. Chem. Phys.*, 136(17):174106, 2012.

[27] J. Gauss. The Coupled-Cluster Method, year = 1998. In P.v.R. Schleyer, N. L. Allinger, T. Clark, J. Gasteiger, P. A. Kollman, H. F. Schaefer III, and P. R. Schreiner, editors, *Encyclopedia of Computational Chemistry*, pages 615–636. John Wiley and Sons, Chichester.

[28] J. Gauss and H.-J. Werner. NMR chemical shift calculations within local correlation methods: the GIAO-LMP2 approach. *Phys. Chem. Chem. Phys.*, 2:2083–2090, March 2000.

[29] Claudia H. and H.-J. Werner. Local treatment of electron correlation in coupled cluster theory. *J. Chem. Phys.*, 104(16):6286–6297, April 1996.

[30] C. Hättig and B. A. Hess. Correlated Frequency-Dependent Polarizabilities and Dispersion Coefficients in the Time-Dependent Second-Order Møller-Plesset Approximation. *Chem. Phys. Lett.*, 233:359–370, 1995.

[31] T. Helgaker, S. Coriani, P. Jørgensen, K. Kristensen, J. Olsen, and K. Ruud. Recent Advances in Wave Function-Based Methods of Molecular -Property Calculations. *Chem. Rev.*, 112:543–631, 2012.

[32] B. Helmich and C. Hättig. A pair natural orbital implementation of the coupled cluster model CC2 for excitation energies. *J. Chem. Phys.*, 139(8):084114, 2013.

[33] G. Hetzer, M. Schütz, H. Stoll, and H.-J. Werner. Low-order scaling local correlation methods. II: Splitting the Coulomb operator in linear scaling local second-order Møller-Plesset perturbation theory. *J. Chem. Phys.*, 113(21):9443–9455, December 2000.

[34] S. Höfener and W. Klopper. Natural transition orbitals for the calculation of correlation and excitation energies. *Chemical Physics Letters*, 679:52 – 59, 2017.

[35] H. J. A. Jensen, P. Jørgensen, H. Ågren, and J. Olsen. Second-Order Møller–Plesset Perturbation Theory as a Configuration and Orbital Generator in Multiconfiguration Self-Consistent Field Calculations. *J. Chem. Phys.*, 88(6):3834–3839, 1988.

[36] P. Jørgensen and J. Simons. *Second Quantization-Based Methods in Quantum Chemistry*. Academic Press, New York, 1981.

[37] Sir William Thomson Lord Kelvin. In *The Molecular Tactics of a Crystal*.

[38] R. A. Kendall, T. H. Dunning, and R. J. Harrison. Electron Affinities of the First-Row Atoms Revisited. Systematic Basis Sets and Wave Functions. *J. Chem. Phys.*, 96(9):6796–6806, 1992.

[39] R. Kobayashi, H. Koch, and P. Jørgensen. Calculation of frequency-dependent polarizabilities using coupled-cluster response theory. *Chem. Phys. Lett.*, 219:30–35, March 1994.

[40] H. Koch and P. Jørgensen. Coupled cluster response functions. *J. Chem. Phys.*, 93(5):3333–3344, September 1990.

[41] H. Koch, R. Kobayashi, and P. Jørgensen. Brueckner Coupled Cluster Response Functions. *Int. J. Quantum Chem.*, 49:835, 1994.

[42] R. K. Kondru, P. Wibf, and D. N. Beratan. Structural and conformational dependence of optical rotation angles. *J. Phys. Chem. A*, 103(33):6603–6611, 1999.

[43] T. Korona, K. Pflüger, and H.-J. Werner. The Effect of Local Approximations in Coupled-Cluster Wave Functions on Dipole Moments and Static Dipole Polarizabilities. *Phys. Chem. Chem. Phys*, 6:2059–2065, 2004.

[44] A. Kumar and T. D. Crawford. *manuscript in preparation.*

[45] A. Kumar and T. D. Crawford. Frozen Virtual Natural Orbitals for Coupled-Cluster Linear-Response Theory. *J. Phys. Chem. A*, 121(3):708–716, 2017. PMID: 28045265.

[46] A. Landau, K. Khistyaev, S. Dolgikh, and A. I. Krylov. Frozen Natural Orbitals for Ionized States Within Equation-of-Motion Coupled-Cluster Formalism. *J. Chem. Phys.*, 132:014109, 2010.

[47] C. Lee, W. Yang, and R. G. Parr. Development of the Colle-Salvetti Correlation-Energy Formula Into a Functional of the Electron Density. *Phys. Rev. B.*, 37:785–789, 1988.

[48] P. O. Lowdin. Quantum Theory of Many-Particle Systems. I. Physical Interpretations by Means of Density Matrices, Natural Spin-Orbitals, and Convergence Problems in the Method of Configurational Interaction. *Physical review*, 97(6):1474, March 1955.

[49] T. J. Mach and T. D. Crawford. Computing Optical Rotation via an N-Body Approach. *Theor. Chem. Acc.*, 133:1449, 2014.

[50] H. R. McAlexander and T. D. Crawford. A Comparison of Three Approaches to the Reduced-Scaling Coupled Cluster Treatment of Non-Resonant Molecular Response Properties. *J. Chem. Theory Comp.*, 12(1):209–222, 2016.

[51] H. R. McAlexander, T. J. Mach, and T. D. Crawford. Localized Optimized Orbitals, Coupled Cluster Theory, and Chiroptical Response Properties. *Phys. Chem. Chem. Phys.*, 14(21):7830–7836, 2012.

[52] B. Mennucci, J. Tomasi, R. Cammi, J. R. Cheeseman, M. J. Frisch, F. J. Devlin, S. Gabriel, and P. J. Stephens. Polarizable continuum model (PCM) calculations of solvent effects on optical rotations of chiral molecules. *J. Phys. Chem. A*, 106(25):6102–6113, May 2002.

[53] E. Merzbacher. *Quantum Mechanics,2nd ed.,*. Wiley, New York.

[54] D. Mester, P. R. Nagy, and M. Kállay. Reduced-cost linear-response CC2 method based on natural orbitals and natural auxiliary functions. *J. Chem. Phys.*, 146(19):194102, 2017.

[55] D. Mester, P. R. Nagy, and M. Kállay. Reduced-cost second-order algebraic-diagrammatic construction method for excitation energies and transition moments. *J. Chem. Phys.*, 148(9):094111, 2018.

[56] W. Meyer. PNOCI studies of electron correlation ffects. I. Configuration expansion by means of nonorthogonal orbitals, and application to the ground state and ionized states of methane. *J. Chem. Phys.*, 58(3):1017–1035, February 1973.

[57] F. Neese, A. Hansen, and D. G. Liakos. Efficient and accurate approximations to the local coupled cluster singles and doubles method using a truncated pair natural orbtial basis. *J. Chem. Phys.*, 131(064103):064103–1 – 064103–15, August 2009.

[58] F. Neese, F. Wennmohs, and A. Hansen. Efficient and Accurate Local Approximations to Coupled-Electron Pair Approaches: An Attempt to Revive the Pair Natural Orbital Method. *J. Chem. Phys.*, 130(114108):114108–1 – 114108–18, 2009.

[59] J. Olsen and P. Jørgensen. Linear and nonlinear response functions for an exact state and for an MCSCF state. *J. Chem. Phys.*, 82:3235, 1985.

[60] R. M. Parrish, L. A. Burns, D. G. A. Smith, A. C. Simmonett, A. E. DePrince, E. G. Hohenstein, U. Bozkaya, A. Y. Sokolov, R. D. Remigio, R. M. Richard, J. F. Gonthier, A. M. James, H. R. McAlexander, A. Kumar, M. Saitow, X. Wang, B. P. Pritchard, P. Verma, H. F. Schaefer, K. Patkowski, R. A. King, E. F. Valeev, F. A. Evangelista, J. M. Turney, T. D. Crawford, and C. D. Sherrill. Psi4 1.1: An Open-Source Electronic Structure Program Emphasizing Automation, Advanced Libraries, and Interoperability. *J. Chem. Theory Comput.*, 13(7):3185–3197, 2017. PMID: 28489372.

[61] T. B. Pedersen, B. Fernández, and H. Koch. Gauge Invariant Coupled Cluster Response Theory Using Optimized Nonorthogonal Orbitals. *J. Chem. Phys.*, 114(16):6983–6993,

2001.

[62] T. B. Pedersen and H. Koch. Coupled cluster response functions revisited. *J. Chem. Phys.*, 106(19):8059–8072, May 1997.

[63] C. Peng, M. C. Clement, and E. F. Valeev. Exploration of Reduced Scaling Formulation of Equation of Motion Coupled-Cluster Singles and Doubles Based on State-Averaged Pair Natural Orbitals. *ArXiv e-prints*, February 2018.

[64] P. L. Polavarapu. *Ab initio* molecular optical rotations and absolute configurations. *Mol. Phys.*, 91(3):551–554, November 1997.

[65] P. Pulay. Localizability of dynamic electron correlation. *Chem. Phys. Lett.*, 100(2):151–154, June 1983.

[66] G. D. Purvis and R. J. Bartlett. A Full Coupled-Cluster Singles and Doubles Model: The Inclusion of Disconnected Triples. *J. Chem. Phys.*, 76:1910–1918, 1982.

[67] J. E. Rice and N. C. Handy. The Calculation of Frequency-Dependent Polarizabilities and Pseudo-Energy Derivatives. *J. Chem. Phys.*, 94(7):4959–4971, 1991.

[68] C. Riplinger, P. Pinski, U. Becker, E. F. Valeev, and F. Neese. Sparse Maps — A Systematic Infrastructure for Reduced-Scaling Electronic Structure Methods. II. Linear Scaling Domain Based Pair Natural Orbital Coupled Cluster Theory. *J. Chem. Phys.*, 144:024109, 2016.

[69] L Rosenfeld. Quantenmechanische Theorie der naturlichen optischen Aktivitat von Flussigkeiten und Gasen. *Z Physik*, 52:161–174, 1929.

[70] N. J. Russ and T. D. Crawford. Local correlation in coupled cluster calculations of molecular response properties. *Chem. Phys. Lett.*, 400:104–111, November 2004.

[71] N. J. Russ and T. D. Crawford. Local correlation domains for coupled cluster theory: Optical rotations and magnetic-field perturbations. *Phys. Chem. Chem. Phys.*, 10:3345–3352, May 2008.

[72] K. Ruud, P. J. Stephens, F. J. Devlin, P. R. Taylor, J. R. Cheeseman, and M. J. Frisch. Coupled-cluster calculations of optical rotation. *Chem. Phys. Lett.*, 373:606–614, March 2003.

[73] S. Saebø and P. Pulay. Fourth-order Møller-Plesset perturbation theory in the local correlation treatment. I. Method. *J. Chem. Phys.*, 86(2):914–922, January 1986.

[74] S. Saebø and P. Pulay. Local treatment of electron correlation. *Annual Reviews in Physical Chemistry*, 44:213–236, 1993.

[75] E. Schrødinger. AN UNDULATORY THEORY OF THE MECHANICS OF ATOMS AND MOLECULES. *Physical review*, 28(6):1049–1070, December 1926.

[76] M Schütz. Low-order scaling local correlation methods. III. Linear scaling local perturbative triples correction (T). *J. Chem. Phys.*, 113(22):9986–10001, December 2000.

[77] M. Schütz and F. Manby. Linear scaling local coupled cluster theory with density fitting. Part I: 4-external integrals. *Phys. Chem. Chem. Phys.*, 5:3349–3358, July 2003.

[78] M. Schütz and H.-J. Werner. Low-order scaling local correlation methods. IV. Linear scaling local coupled-cluster (LCCSD). *J. Chem. Phys.*, 114(2):661–681, January 2001.

[79] R. Send, V. R. I. Kaila, and D. Sundholm. Reduction of the virtual space for coupled-cluster excitation energies of large molecules and embedded systems. *J. Chem. Phys.*, 134(21):214114, 2011.

[80] I. Shavitt and R. J. Bartlett. *Many-Body Methods in Chemistry and Physics: MBPT and Coupled-Cluster Theory.* Cambridge University Press, Cambridge, 2009.

[81] J. Shen, Z. Kou, E. Xu, and S. Li. The coupled cluster singles, doubles, and a hybrid treatment of connected triples based on the split virtual orbitals. *J. Chem. Phys.*, 136:044101–1 – 044101–9, January 2012.

[82] C. D. Sherrill and H. F. Schaefer. The Configuration Interaction Method: Advances in Highly Correlated Approaches. *Adv. Quantum Chem.*, 34:143–269, 1999.

[83] D. G. A. Smith, L. A. Burns, D. A. Sirianni, D. R. Nascimento, A. Kumar, A. M. James, J. B. Schriber, T. Zhang, B. Zhang, A. S. Abbott, E. J. Berquist, M. H. Lechner, L. A. Cunha, A. G. Heide, J. M. Waldrop, T. Y. Takeshita, A. Alenaizan, D. Neuhauser, R. A. King, A. C. Simmonett, J. M. Turney, H. F. Schaefer, F. A. Evangelista, A. E. DePrince, T. D. Crawford, K. Patkowski, and C. D. Sherrill. Psi4NumPy: An Interactive

Quantum Chemistry Programming Environment for Reference Implementations and Rapid Development. *J. Chem. Theory Comput.*, 2018, doi: 10.1021/acs.jctc.8b00286.

[84] C. Sosa, J. Geertsen, G. W. Trucks, R. J. Bartlett, and J. A. Franz. Selection of the Reduced Virtual Space for Correlated Calculations. An Application to the Energy and Dipole Moment of H_2O. *Chem. Phys. Lett.*, 159(2,3):148–154, 1989.

[85] P. J. Stephens, F. J. Devlin, C. F. Chabalowski, and M. J. Frisch. *Ab initio* Calculation of Vibrational Absorption and Circular Dichroism Spectra Using Density Functional Theory. *J. Phys. Chem.*, 98(45):11623–11627, 1994.

[86] P. J. Stephens, F. J. Devlin, J. R. Cheeseman, and M. J. Frisch. Calculation of optical rotation using density functional theory. *J. Phys. Chem. A*, 105:5356–5371, May 2001.

[87] Attila Szabo and Neil S. Ostlund. *Modern Quantum Chemistry: Introduction to Advanced Electronic Structure Theory*. Dover Publications, Inc., Mineola, New York, 1996.

[88] A. G. Taube and R. J. Bartlett. Frozen Natural Orbitals: Systematic Basis Set Truncation for Coupled-Cluster Theory. *Coll. Czech. Chem. Commun.*, 70(6):837–850, 2005.

[89] A. G. Taube and R. J. Bartlett. Frozen Natural Orbital Coupled-Cluster Theory: Forces and Application to Decomposition of Nitroethane. *J. Chem. Phys.*, 128:164101, 2008.

[90] J. M. Turney, A. C. Simmonett, R. M. Parrish, E. G. Hohenstein, F. A. Evangelista, J. T. Fermann, B. J. Mintz, L. A. Burns, J. J. Wilke, M. L. Abrams, N. J. Russ, M. L. Leininger, C. L. Janssen, E. T. Seidl, W. D. Allen, H. F. Schaefer, R. A. King, E. F.

Valeev, C. D. Sherrill, and T. D. Crawford. Psi4: An Open-Source Ab Initio Electronic Structure Program. *WIREs. Comput. Mol. Sci.*, 2:556–565, 2012.

[91] G.C. Wick. The Evaluation of the Collision Matrix. *Physical review*, 80(2):268–272, October 1950.

[92] D. E. Woon and T. H. Dunning. Gaussian Basis Sets for Use in Correlated Molecular Calculations. IV. Calculation of Static Electrical Response Properties. *J. Chem. Phys.*, 100(4):2975–2988, 1994.

[93] J. Yang, G. K.-L. Chan, F. R. Manby, M. Schütz, and H.-J. Werner. The orbital-specific-virtual local coupled cluster singles and doubles method. *J. Chem. Phys.*, 136(144105):144105–1 – 144105–16, April 2012.